UNIVERSITA' DEGLI STUDI DI PAVIA

Ph.D. SCHOOL IN ELECTRONICS, COMPUTER SCIENCE AND ELECTRICAL ENGINEERING

CYCLE XXXI

2018

NOVEL CLASSES OF BANDPASS FILTERS IN SUBSTRATE INTEGRATED WAVEGUIDE TECHNOLOGY

DOCTORAL THESIS OF

LORENZO SILVESTRI

TUTOR:

PROFESSOR MAURIZIO BOZZI

Introduction

The evolution of the Internet of Things (IoT), Wireless Sensor Network (WSN) and the emerging market of the fifth generation mobile (5G) is leading the microwave community towards new challenges, created by growing demands for interconnected components. IoT and WSN are groups of autonomous spatially distributed elements (sensors or tags) that communicate between each other for a specific purpose: to track an object or being, measuring their vitals by responding to requests relating to the physical parameters of their surrounding environment. The use of these components spans across many occupational fields and, for both the academic and the industrial fields, they present new and exciting possibilities. However, with these new possibilities comes the responsibility to develop technologies that are socially conscious. To achieve this, technologies must be inclusive in the circular economy and adopt, where possible, methods that are not damaging to the ecosystem. In IoT, for example, the wide distribution of "things" requires easily manufactured and disposable elements to be mass produced at a low cost, further amplifying the need to adopt an environmentally responsible approach. Thus, the success of a particular technology lies in not only meeting complex technical requirements but, also, satisfying a "green" standard. Furthermore, the deployment of complete wireless systems and sensor nodes requires the implementation of a technology with an efficient scale of integration.

In this scenario, the Substrate Integrated Waveguide (SIW) technology could become an important player by being an optimal trade-off between highly efficient yet bulky metallic waveguide components and low cost yet easily embeddable planar components. In addition, from the System-in-Package (SiP), adopted in the design of RF circuits, the System-on-Substrate (SoS) paradigm can be achieved with this technology. Design flexibility, performance improvement (at a low cost) and the possibility to choose "green" substrates (such as paper) are the three potentialities of SIW technology that suggest this technology could be a key component in the success of the IoT, WSN and, related 5G, markets.

For these reasons, this Doctoral Thesis examines the potentialities of Substrate Integrated Waveguide (SIW) technology applied, in particular, to microwave bandpass filter design. The application of these components scopes across many fields - from base stations to satellite communications. The decision to realize these components based on the SIW technology is expounded with the previous motivations.

The Thesis is organized as follows:

– Chapter 1 is devoted to a critical Introduction of the SIW technology. In addition, a selection of bandpass filters, that have inspired the work of this thesis, are proposed with a focus on size and loss reduction.

– Chapter 2 describes the study of a new class of SIW filters based on the periodical perforation of the dielectric substrate: the local effective permittivity, reduced by the perforation of the substrate, creates waveguide sections below cut-off, defining an iris-type like filter design. A comparison between the proposed filter and the iris-type is shown to highlight the advantages of the perforated structure. In order to reduce the size of this structure the Half-mode and Folded Half-mode SIW filters have been designed, realized and measured. In addition, with the Folded Half-mode topology another critical parameter of these filters is improved: in fact, the out-of-band rejection is improved with the introduction of transmission zeros.

– Chapter 3 introduces a new class of dual-mode air-filled SIW cavity filters. This structure combines the advantages of an air-filled and a dual-mode structure, namely low loss and size reduction. A theoretical model, based on an equivalent transmission line, relates the filter characteristics to the variation of a few

geometrical parameters. From this analysis, doublets, that are building blocks for the design of higher order filters, are deeply investigated. A five-pole filter, obtained cascading doublets through a non resonating node, is designed to extend the study to higher order filters. In order to validate the theoretical studies, the prototypes of doublets and a five-pole filter are manufactured and measured.

– In Chapter 4, a further study, based on the dual-mode air-filled SIW cavity (Chapter 3) is presented. In particular, this topology, in contrast to the previous structure, is realized considering a complementary geometry, obtained by removing the lateral dielectric portions of the substrate – instead of the central portion of the SIW cavity. This new structure gives a degree of freedom related to the possibility to locate the transmission zeros both below or above the pass-band of the filter. This structure is compared with a homogeneous cavity, able to realize a similar filtering response, highlighting the advantage of the proposed filter. Different cases are shown to describe the control of the transmission zeros and the extension to higher order filter (four-pole) is presented. Prototypes are measured and compared to the simulations to confirm the theoretical studies.

– A novel class of mushroom shaped resonator SIW filter is described in Chapter 5. With this topology is possible to obtain the maximum number of transmission zeros, equal to the number of resonators, in an in-line configuration, for an improved selectivity. In addition, the overall length, compared to the classical in-line filters with inductive obstacles, is smaller. The singlet is studied in detail, describing the method of obtaining and controlling a filtering response. Doublets (starting from singlet) and higher order filters (starting from doublet) are reported. Simulations and measurements are compared as in the previous Chapters.

In the Conclusions, the results of the work are briefly summarized with an overview of the improvements achieved.

Table of contents

Table of figures

Chapter 1

INTRODUCTION

This Chapter is devoted to a critical Introduction of the Substrate Integrated Waveguide (SIW) technology applied, in particular, to filter design. The SIW technology is beneficial when developing filter topologies that are typically difficult to realize. With SIW, costs remain low whilst performance rates are relatively high. Today scale expansion of 3D printers has made realizing complex geometrical structures easier, offering a new prospective in SIW filter design ([62], [63] and [64]] In addition, from an industrial point of view, the technology's adaptability - such as the possibility to choose different substrates and, as consequence, to the different fabrication processes - can be considered a plus. This is important, in particular, for the growth of IoT [66] and WSN [65], both of which demand low-cost, relatively high performance and highly embeddable components. Moreover, this technology is suitable for realizing "green" microwave components by using eco-compatible substrate, such as paper [54], demonstrating a valuable design flexibility. On the other hand, size and losses can be two detrimental disadvantages of this technology: some solutions to overcome these limitations, in filter design, have been discussed in literature and are here presented. More specifically, the topologies, that have been significant for the theoretical ideas, and have somewhat inspired the realization of the four new classes of filters (described in the following Chapters), are analyzed. All the presented filters were realized on commercial dielectric substrates, to show the design rules and the feasibility of the theoretical studies.

1 SUBSTRATE INTEGRATED WAVEGUIDE TECHNOLOGY

Substrate Integrated Waveguide (SIW) implements a waveguide-like structure in a planar structure. The metallized lateral vias of the dielectric substrate, connecting the top and bottom metal planes, represent the lateral walls of the classical rectangular waveguide as in Fig. 1(*a*). In 1994 in [46] SIW appears for the first time in literature and then in 1998 under the name of post-wall or laminated waveguide [47]. The SIW combines traits of the planar technology and the classical rectangular waveguide, bridging the gap between the two technologies. The planar technology is advantageous as its fully embeddable circuits can be realized at a low-cost [3]. Furthermore, the technology is lightweight and compact, increasing its versatility and applicability [2]. The planar circuit fabrication processes - such as the planar circuit board (PCB) or the low-temperature cofired ceramic (LTCC) [2] - can be used with well-known standards. The ability to use established procedures is beneficial as it heightens the predictability of results and facilitates the mass production and distribution of the technology. However, high losses and a non-shielded structure limit the use of this technology in high performance demanding frameworks. Waveguide technology, on the other hand, offers a solution for challenging high performance systems as the technology is capable of producing low losses even under high power stimulation. This technology's entirely shielded structure reduces the spurious interference between components within the complex systems. However, the technology is limited by its bulky, expensive and not fully integrable structure. Evidently, the strength of one approach is the limitation of the other – and vice versa. Throughout the development of SIW technology, different components, either passive

or active, have been proposed [4]. The majority of the H-plane waveguide circuits have also been designed and tested in SIW technology. One of the strongest advantages of this method is the possibility to achieve the System-on-Substrate (SoS) [48] paradigm, because of the high scale of integration of this technology [4], extending the concept of System in Package (SiP).

The main geometrical parameters of this structure are shown in Fig. 1.

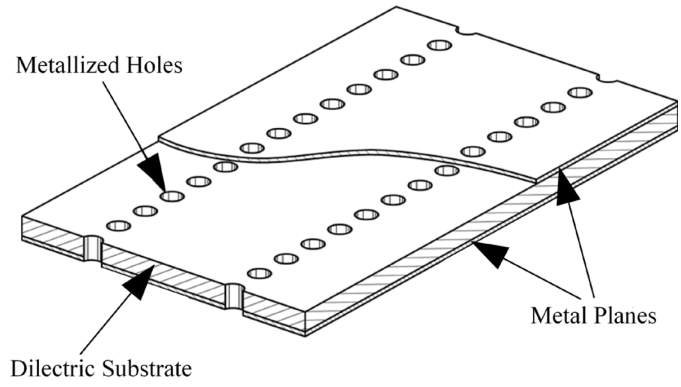

(*a*)

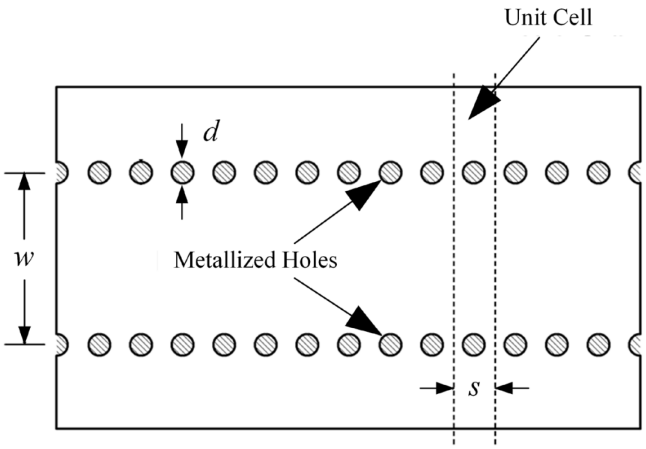

(*b*)

Fig. 1. SIW transmission line: (*a*) geometrical structure; (*b*) scheme with the geometrical dimensions (top view). [49]

The top and bottom metal planes cover the dielectric substrate of thickness h. The lateral metallized vias (diameter d) are spaced with value s. The SIW shows propagation characteristics similar to the rectangular waveguide. SIW modes coincide with a subset of the guided modes of the rectangular waveguide, in fact, the TM modes and the TE_{np} modes with $p \neq 0$ are not supported because of the longitudinal component of the surface current. The mono-modal bandwidth of the SIW is limited, as in the case of the rectangular waveguide, to one-octave. The width of the SIW is reduced respect to the hollow rectangular waveguide of a factor $\varepsilon_r^{-1/2}$. Considering the similarities with the rectangular waveguide structure, an equivalent rectangular waveguide width w_{EFF}, showing the same propagation characteristics of the SIW, is defined. Different relations have been developed from empirical consideration, increasing in order of precision from (1) to (3) [1], [4]. In particular, these relations help for a first dimensioning of the structure.

The relation (1) is valid when $s < 4d$ and $d < w/8$

$$w_{EFF} = w - \frac{d^2}{0.95s} \tag{1}$$

(with geometrical parameters as in Fig. 1). The precision is in the order of ± 5% on the w_{EFF}: particular attention should be paid when the use is related to the design of cavity filters because the frequency shift can be important respect to the narrowband. In the relation (2) the values $s<3d$ and $d<w/5$ should be considered. The accuracy of this relation is higher because d/w is taken into account with higher precision than in (1).

$$w_{EFF} = w - 1.08\frac{d^2}{s} + 0.1\frac{d^2}{w} \tag{2}$$

A more accurate relation (3), has been defined as

$$w = \frac{2w_{EFF}}{\pi}\cot^{-1}\left(\frac{\pi s}{4w_{EFF}}\ln\frac{s}{2d}\right) \tag{3}$$

In this way, using these relations, different electromagnetic tools, synthesis programs and analysis equations - developed specifically for the rectangular waveguide components - can be directly applied in the SIW circuit analysis. The graph in Fig. 2 [5] displays the regions of interest for a SIW structure. The graph gives a comprehensive view of the different effects of the dimensioning and spacing of the vias. The longitudinal distance between the metallized vias, s, is defined in order to reduce the radiation losses and the bandgap phenomena. A golden rule is $s<2.5d$ but normally $s=2d$ is used [6]. It should be noted that, when a spacing between vias is too small (small s), an issue occurs in the mechanical rigidity of the structure. The post's diameter, d, can be equal to the substrate thickness - even if this is not a necessary restriction. Normally, the vias are mechanically drilled and chemically electroplated or plasma deposited metallized, though a conductive paste can also be used. In the realized prototypes of this Thesis, the conductive paste has been used to simplify the fabrication process. Moreover, the operational frequency of the proposed and realized filters is not too high, leading to post diameters that are reasonable to be metallized with the conductive paste.

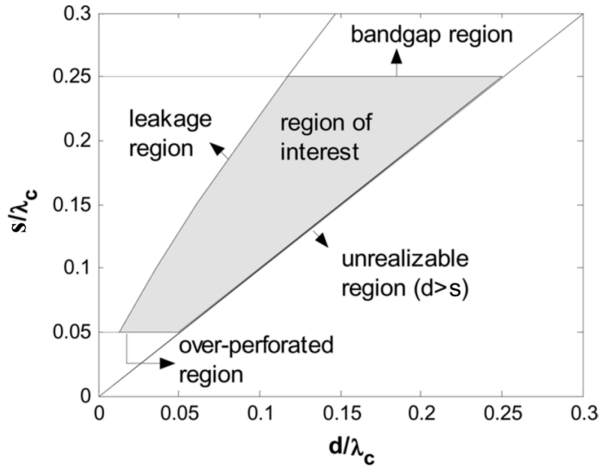

Fig. 2. Regions of operation in the SIW technology. [6]

Different transitions have been designed from planar to SIW technologies (Fig. 3). They are very important in order to connect different components realized with the two technologies. In particular, in Fig. 3(a), the tapered microstrip to SIW has been shown. The dimensions of the taper has been studied in [51]. Transitions based on multilayer microstrip-to-SIW have been implemented in order to connect components realized on a

thin microstrip to the one designed on a thicker SIW. In Fig. 3(*b*) and Fig. 3(*c*), different transitions based on the coplanar are shown with the use of current probe or 90° bend. When thick dielectric substrates need to be used the coplanar transition is a better choice for the conductor losses reduction. Conversely, when the request is to connect components between the classical waveguide technology and SIW, the transition proposed in [52] is a possible choice.

One of the problems in the design of components, adopting this technology, is related to the loss. Therefore, the loss minimization is one of the key point in the success of this technology even at high frequency. In particular, three different varieties of loss can be taken into consideration and they have been extensively explained and modelled in [50]:

- Conductor losses
- Dielectric losses
- Radiation losses

Conductor and dielectric losses have the same behavior as in a dielectric filled rectangular waveguide. In particular, conductor losses are related to the finite conductivity of the metal planes (top and bottom) and the lateral vias. This contribution plays an important role at high frequency (above 30 GHz) when the roughness of the metal surface becomes an important parameter in circuit design. Instead, the dielectric losses depend on the dielectric substrate used. It is explained in Par 3.3 that a method to reduce the dielectric loss is the use of the so-called Air-filled SIW. In this case the dimensions of the components are increased because of the effective permittivity but the losses are noticeably reduced. The radiation losses are due to the leakage through the via gaps but are strongly diminished by following the expression $s/d<2.5$.

The second issue, related to the design of microwave filters and components in SIW technology, is the footprint. Considering a classical waveguide component, the dimensions are reduced, as previously noticed, but for an industrially desirable technology: the smaller the components, the better. Starting from this consideration different topologies have been implemented to reduce the overall size of the SIW components, namely the Substrate Integrated Folded Waveguide (SIFW), the Half-Mode Substrate Integrated Waveguide (HMSIW) and the Folded Half-Mode Substrate Integrated Waveguide (FHMSIW). The application of these structures in filter design is explained in Par 3.4.

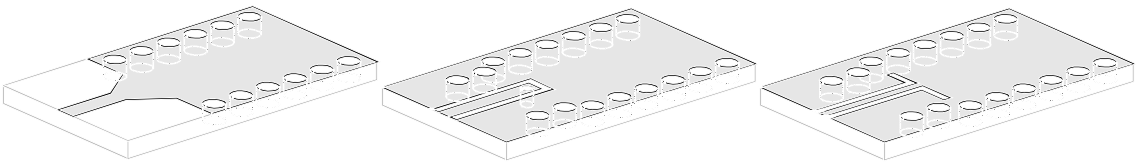

(*a*) (*b*) (*c*)

Fig. 3. Different planar-to-SIW transitions: (*a*) microstrip-to-SIW; (*b*) coplanar-to-SIW, with a current probe; (*c*) coplanar-to-SIW transition, with a 90° bend. [4]

2 RESONATORS IN SIW TECHNOLOGY

Resonators are building blocks able to define the filtering function of a filter. The shape and the geometrical parameters of the structure determine the field distribution and the stored energies. Fig. 4 displays the different technologies used to realize, in filter design, the microwave resonators. It highlights the differences in cost, relative insertion loss and size and, in addition, the unloaded quality factor (Q_u) is presented. The variations of Q_u are functions of the technologies, the materials used and the excitations. Considering that the same cavity can support different modes (field distribution), different Q_u factors can be obtained.

In particular, microstrip circuits are ideal for cost and size minimization, but they are vulnerable to extremely high losses (related to the dielectric substrate used) and radiation. Radiation losses are problematic, in a complex complete system design, because of the possible interference between the different components. The fabrication processes of planar circuits are well-known, and this helps to realize low-cost components. However, when performances are the main goal in filter design, waveguide and super conductors should be considered. Adopting the metallic waveguide structure, the bulky, expensive and non-embeddable limitations of the technology become apparent. In fact, the fabrication processes to realize these components are expensive. Furthermore, the connections between different circuital components - to realize a complex system - need transitions, incrementing the losses and the overall complexity of the structure. The technical difficulty in realizing some specific couplings limits the number of topologies that can be obtained in filter design.

A technology that can be considered revolutionary in filter design, especially in the satellite communication field, uses dielectric resonators. These resonators were firstly defined by R. D. Ritchmyer in 1930 [9] but only in the late 1960s did they find their application in filter design. At first, the technological problems, related to the temperature stability, limited their use. Later on, in the 1980s, with the increased demand for satellite communication and the progress offered by the use of ceramic substrate (with high permittivity-low temperature coefficient and high quality factor) they became a more popular choice for filter design [8]. The size reduction is one of the main characteristics of the dielectric resonators because the footprint is inversely proportional to the permittivity of the material. The Q_u factor is mainly limited by the dielectric losses inside the resonator. These resonators can be considered a good option when high performance components are required but they are limited by a bulky structure and expensive realization processes.

The SIW technology stands in the middle between the planar (microstrip/stripline) and non-planar (dielectric resonators and waveguide) technologies: the Q_u factors can reach high values in the order of 1000 - with a moderate size (function of the permittivity of the substrate) and a low-cost structure. It should be noted that the cost is higher respect to the microstrip structure because slots or vias should be drilled and then metallized.

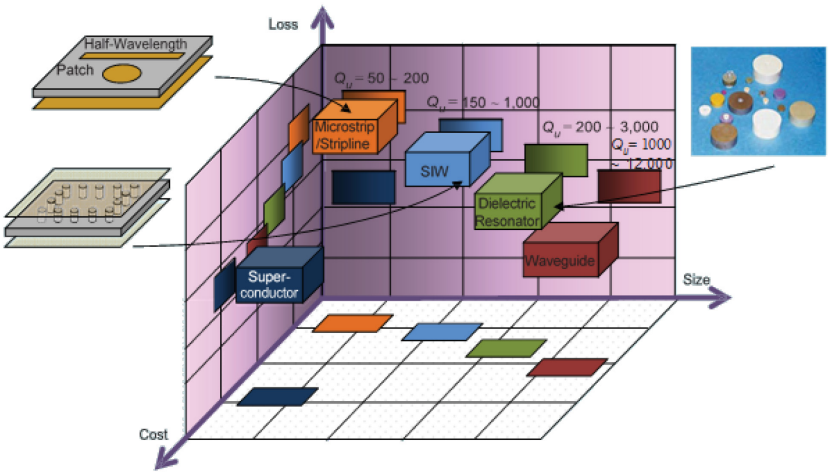

Fig. 4. Different technologies to implement resonators. [6]

The Q_u is a sum of different components: the dielectric loss quality factor, the conduction quality factor and the quality factor related to the radiation leakage through the metallized vias. As previously explained, respecting the conditions $s/d<2.5$, the radiation losses can be, dramatically, reduced. Dielectric loss produce the largest loss contribution and so, a proper selection of the substrate is needed. For general PCB dielectric substrates, the Q_u of a SIW cavity resonator can vary between 150 and 1000 [6]. Considering low loss dielectric substrates, such as quartz and processed metallic surfaces, such as gold-plating, higher values can be reached [6]. A different way to reduce these losses and higher the Q_u is related with the use of Air-filled SIW as in [13]-[15] and [18] (and explained in Par. 3.3).

3 BANDPASS FILTER DESIGN IN SIW TECHNOLOGY

Starting from the different resonator technologies, filters can be designed. The choice of the technology is related to the design requests according to performance, cost, size and environment (of usage). By playing with the shape and the geometrical parameters of the resonators, used as building blocks to create filters, various topologies have been studied and realized in the past years. In particular, bandpass filters are used in multiple contexts and for various applications, rejecting signals at frequencies out of the pass-band, meanwhile allowing signals with frequencies in the pass-band to pass through. The use spans from microwave transmitters or receivers to multiplexers [34]. In receivers they are used to reject unwanted out-of-band interference. In addition, the sensitivity of the front-end noise bandwidth is set by this element. Meanwhile, in transmitters they reduce the spurii and eliminate the transmitter noise. For modern communication systems the requirements are very stringent, in particular for insertion loss, footprint, stopband and selectivity. In this context, the bandpass filters built in SIW technology have been considered for its characteristics – as previously explained – able to meet most of the requirements addressing with different possible configurations.

The similarities between classic rectangular waveguide and SIW structure, as shown in Par 1, give way to a wide number of solutions, adopted in the previous technology, with the SIW structure [4]. Different filter designs, with different topologies, spanning from subgigahertz to subterahertz, adopting different materials (from 3D printed substrates to "green" substrates), have been design and realized. Furthermore, SIW technology gives some advantages in realizing topologies that are difficult to be realized with the classical waveguide structure and open up a new direction in filtering solutions. The following subsections discuss a progression of various filter topologies which have inspired the research of this thesis.

3.1 Direct-coupled resonators

Considering the parallels in filter design between SIW and classical rectangular waveguide, the direct-coupled resonators with inductive irises can be easily borrowed in SIW.

Among all the filters realized with the SIW technology, one of the first prototype realized was presented in [2]. Mapping the SIW into a rectangular waveguide structure the standard filter theory can be used. Generally speaking, inductive post filters have been designed with posts with different diameters all centered. This needs the use of different diameter drills and increases the fabrication costs. For this reason, from the centered inductive post filter, an offset inductive post with same diameters has been designed, thus simplifying the whole fabrication process (Fig. 5). A three-pole Chebyshev filter at 28GHz (1GHz bandwidth, on RT/Duroid 5880 with tgδ=0.0009 at 10 GHz and ε_r=2.2) has been designed, realized and measured showing 1dB IL [2].

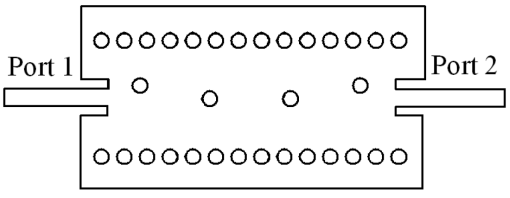

Fig. 5. Offset inductive post SIW filter. [4]

In order to properly compare the results of filters realized in classical waveguide and in SIW technologies, the results of [10] are proposed. Starting from a classical waveguide inductive iris-type bandpass filter [12], a

SIW bandpass filter can be obtained (Fig. 7(*b*)) in the Ku-band for satellite applications. In this case, the non-symmetric irises have been implemented for easier fabrication. The non-symmetrical iris-type filter is an evolution of the common and well-known centered iris-window (Fig. 6), used as impedance inverters, defining, instead, the uniform waveguides as half-wavelength resonators. The filter design includes a lowpass prototype with a subsequent bandpass transformation. A well-known straightforward procedure to design a waveguide filter includes the use of the K-inverter [16][11] (as explained in Chapter 2). From the calculations of the normalized inverted parameters for a Chebyshev design [11], the waveguide filter (Fig. 7(*a*)) has been designed. The SIW filter has been obtained from the waveguide filter by simply scaling down all the dimensions of the value of the permittivity according to the substrate used (Rogers RO4003c, $tg\delta = 0.0027$ at 10 GHz and $\varepsilon_r = 3.55$). Afterwards the dimensions have been slightly optimized in order to obtain an identical filtering response. The SIW filter has been fed with a microstrip line (50 Ω): the microstrip-to-SIW transition has been designed to guarantee a 17 dB in-band return loss. In the results [10], the main advantages and disadvantages of these two methodologies are highlighted. The insertion losses are 0.8 dB and 3.3 dB for the waveguide and SIW structure respectively. The difference is due to the dielectric substrate losses, substrate roughness and a small leakage [10]. On the other hand, the use of a dielectric substrate in the SIW structure scales down all the lengths of the waveguide structure and so reduces the overall dimensions. In this specific case, the overall footprint of the waveguide iris-type filter is reduced by a factor of almost seven, using the SIW structure. The higher *Q* of the waveguide structure reflects a sharper cut-off, however increases the group-delay.

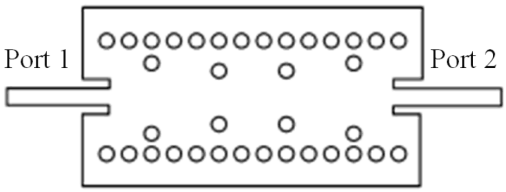

Fig. 6. Iris-type symmetric SIW filter. [4]

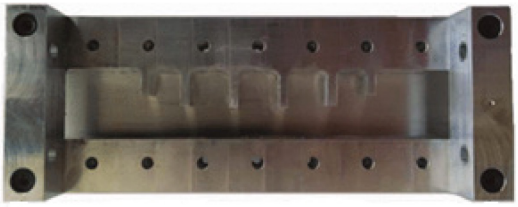

(*a*)

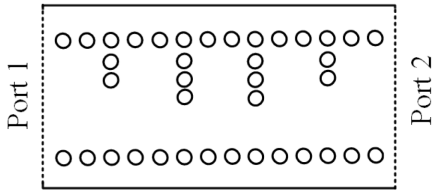

(*b*)

Fig. 7. Iris-type asymmetric filter: (*a*) classical metallic waveguide filter [10]; (*b*) SIW filter.

3.2 Rectangular and Circular cavities SIW filter

Subsequently, the evolution in SIW filter design is connected to the use of rectangular SIW and circular cavities. Generally speaking, direct coupled SIW filters do not present steep attenuation slopes. Incrementing the number of resonators, the out-of-band can be improved whilst incrementing the insertion loss and filter size. Starting from basic rectangular cavities, more complex structures can be defined in SIW filter design such as in [61] with the design of triangular cavities. More specifically, adopting SIW equilateral triangle cavities, an hexagonal-shape six-cavity filter can be obtained as shown in Fig. 8.

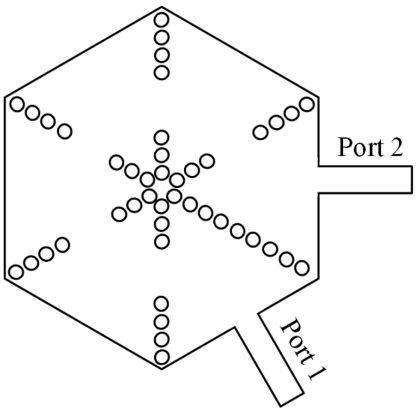

Fig. 8. Hexagonal-shape six-cavity SIW filter.

Indeed, the real advantage related with the use of the rectangular/circular shaped cavities relies in the ability to introduce transmission zeroes to improve the out-of-band performances by adopting the cross-coupling between cavities (Fig. 9) as in [43], [44] and [38].

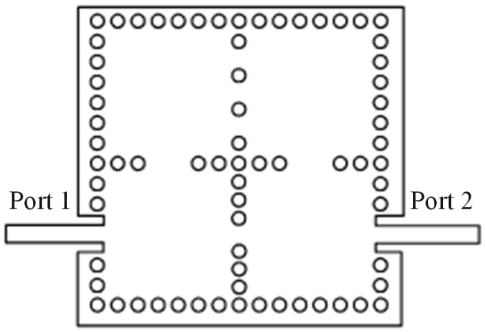

Fig. 9. Cross-coupled rectangular cavities SIW filter. [4]

Circular cavities have been used in SIW filter design as in [39]-[42] (Fig. 10) due to the high versatility of this structure. In particular, in [37] has been shown how, by varying a relatively simple geometrical parameter, such as the input-output angle variation, the out-of-band rejection can be improved. Normally the SIW cavity are fed with an inline input-output with a good out-of-band rejection at the lower side of the band. On the other hand, varying the angle between the input-output feeding line gives the opportunity to place transmission zeros to improve the performance in the upper side of the passband.

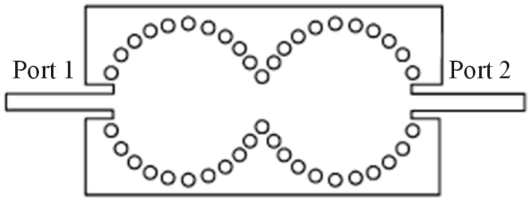

Fig. 10. Circular-cavities SIW filter. [4]

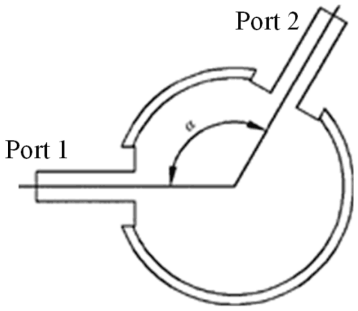

Fig. 11. Circular cavity with input-output angle α. [37]

Beginning with α=180° (cavities cascaded in line as in Fig. 10) no transmission zeros are present; decreasing this value, the upper side of the bandwidth is improved and, when α < 90° the transmission zero moves closer to the passband. The coupling coefficient is not affected by the angle of the input-output lines because of the axial symmetry of the fundamental mode in the circular cavity. A single resonator can be used as a building block for the design of higher order filters. In particular, a cavity with a specific angle α introduces a transmission zero. Different filters have been designed and fabricated to highlight the differences, in the frequency response (upper side of the passband), related to the angle input-output feeding lines variation.

3.3 Air-filled SIW technology applied to filter design

As previously explained, the major limitation of SIW technology in high-performance systems is related to the intrinsic dielectric losses. In particular, one of the first attempts to reduce the dielectric losses has been presented in [45]. In this paper, a modified PCB-based SIW, realized with a multilayer technology and air-cut in the middle of the structure, has been described. In [13] and [14] air-filled SIW structures have been presented to limit the losses and increment the power handling capability. The structure is a sandwich of three different layers. The top and bottom layers are metal covers and the middle layer is substituted with air. The lateral walls of the SIW can be realized with different methods. In the first method, the vias are still embedded in the dielectric substrate and therefore they can be realized using the traditional PCB techniques, reducing the overall costs. The performance is not dramatically affected because the fundamental TE_{10} mode is mainly located in the center of the waveguide. The second method, otherwise, at a higher cost, utilizes continuous metallized walls. However, the former is often favored because of its ease of fabrication and its mechanical strength.

Considering a comparison between the transmission losses of an Air-filled SIW and a Dielectric-filled SIW, it can be noted that they can be reduced (with the use of Air-filled SIW) by a mean value of 0.068 and 0.104 dB/cm compared to Rogers RT/Duroid 5880 and 6002-filled SIWs (Rogers 5880, tgδ=0.0009 at 10 GHz and ε_r=2.2; Rogers 6002, tgδ=0.0012 at 10 GHz and ε_r=2.94), respectively, at Ka-band [13]. This structure results in a better power handling capability.

Considering that the Air-filled to Dielectric filled variation is quite abrupt, a transition is needed as described in [18] and [13] (Fig. 12). Therefore, this structure has been used for the design of different components, such as the 90° hybrid coupler, T-junction [13] or bandpass filters.

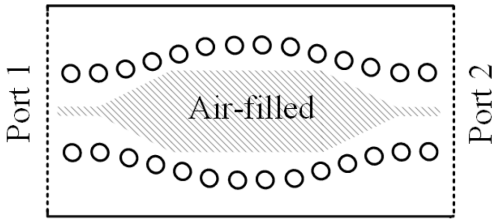

Fig. 12. Transition from the dielectric filled to the air filled SIW. (inspired by [15] and [18])

In particular, in [15] an Air-Filled SIW (AFSIW) inductive-post bandpass filter has been presented in Ka-band. This technology realizes higher *Q*-factor filters for an increased selectivity. In this specific case, the theoretical study of the filter is presented using the circuital model [16] (single post) from the asymmetrical structure to the symmetrical structure as shown in Fig. 13 [17]. In this study, the aforementioned transition between the Dielectric-filled and the Air-filled sections is used (Fig. 13) but, it has been re-designed for the specific occasion in order to obtain a -15dB RL in the entire Ka-band [15]. Meanwhile, the transition Conductor-Backed Co-Planar Waveguide (CBCPW) [53] to SIW is used to feed the structure. In order to compare the Dielectric-filled and the Air-filled structures (in this case for filter design), also a Dielectric-filled symmetrical inductive post bandpass filter with the same filtering characteristics has been designed based on Rogers RT/Duroid 6002. The decision to compare the symmetrical inductive Air-filled post filter to the Dielectric-filled filter is due to two specific benefits: the suppression of the TE_{n0} modes (with n even) and the ability to place the first and last pair of posts closer to the load impedance [15]. A TRL calibration has been necessary for the correct comparison between the filters in order to de-embed the transitions. Alternatively, the use of the Air-filled structure, in this specific case, helped to reduce the losses by a factor of 3 [15]. However, by adopting an air-filled structure, the footprint of the filter is increased. Unlike the waveguide structure, the air-filled SIW maintains the advantages of a low-cost planar structure. This example demonstrates how the use of an Air-filled structure reduces the losses and tackles one of the main limitations of the SIW technology for high-performance systems.

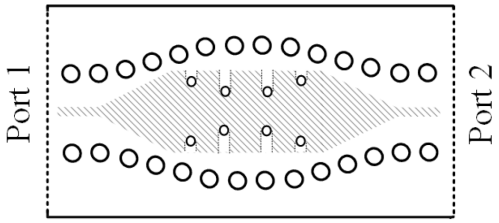

Fig. 13. Air-filled iris-type band pass SIW filter. (inspired by [15] and [18])

3.4 Size reduction solutions adopted in filter design

The structure previously mentioned helped reducing the intrinsic losses of the SIW technology. Other topologies have been, instead, implemented to reduce the overall footprint of the filters, namely Folded (SIFW) [19],[23],[24], Half-Mode SIW (HMSIW) [20],[26], Quarter Mode SIW (QMSIW) [21] and Eight Mode SIW [22].

Originating from the Folded Waveguide, the Folded SIW (SIFW) [23] has been designed: the structure consists of two substrate layers, folded around a metal septum of width w_s. The TE_{10} mode, folded round the central metal conductor, resembles the classic waveguide mode. Carefully selecting the width of the waveguide, the thickness and the width of the metal septum, w_s, the same propagation characteristics of a

rectangular waveguide can be obtained. The use of a dual-layer substrate reduces the width of the waveguide by almost $(9\varepsilon_r)^{-1/2}$. The SIFW have been designed with a horizontal symmetry plane or a vertical symmetry plane as described in [25]. By using this structure, filters can be designed in order to reduce the overall footprint, maintaining the advantages of the SIW technology as in [19]. The filter in Fig. 14 shows a two layer structure in which the central metal septum has been shaped in order to modify the resonance frequency of the cavity modes. Because of the field distribution, the insets affect the modes with the first odd modal index (e.g. TM_{110}, referring to the z axix of Fig. 14). The modes with the first even modal index are unaltered. In [19] the variation of the geometrical parameters of the insets and metal septum are considered in order to control the shift of the resonance frequencies of the modes, defining the bandwidth of the filter (with TM_1 and TM_2 that correspond to the unaltered cavity modes TM_{110} and TM_{120}, respectively). The folded structure is fed by using a stripline that naturally presents an odd symmetry distribution in respect to the metal septum. Taking this approach, only the modes with this symmetry are excited. The other modes are not excited thus incrementing the reject band (up to 10GHz, Fig. 15). The filter has been realized on Taconic TLX-9 ($tg\delta=0.0012$ at 10 GHz and $\varepsilon_r=2.45$) with a 10% relative bandwidth at central frequency of 4.5 GHz (Fig. 15). The dimensions of the filter are quite compact resulting in $0.45\lambda_0$ x $0.24\lambda_0$ (λ_0 is the wavelength in vacuum at 4.5GHz).

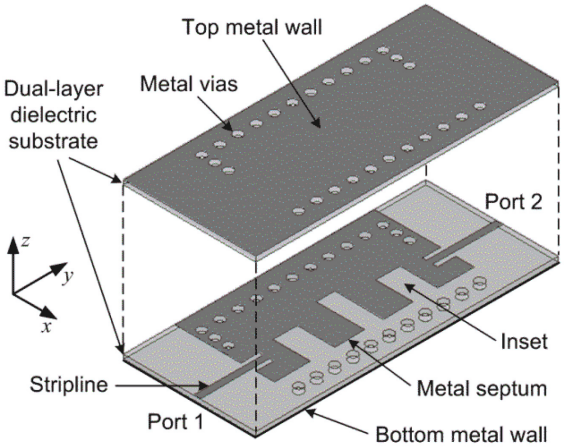

Fig. 14. Geometrical structure of the SIFW filter. [19]

A different structure able to reduce the size of the SIW structure is the Half-Mode SIW (HMSIW). The structure is realized from the SIW structure, by removing half of the top metal wall. The low aspect ratio of the open boundary defines an equivalent magnetic wall supporting only the modes with the first odd modal index. This characteristic leads to a broader single-mode bandwidth and helps in designing wider bandwidth filters [27].

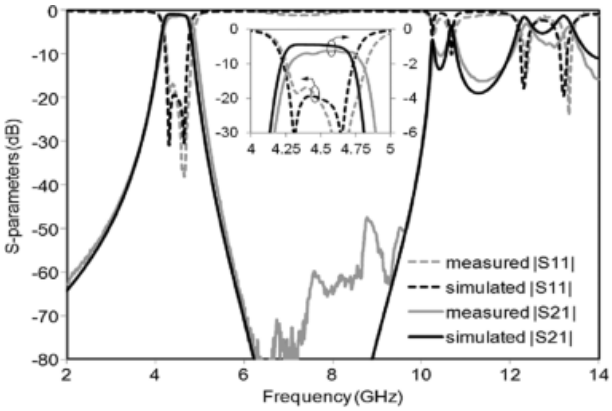

Fig. 15. Realized and measured bandpass filter prototype. [19]

With this configuration, radiation losses are present but limited, while maintaining a low aspect ratio of the open end. In [26] the comparison between the HMSIW and SIFW is presented: an analogous study, as in [19], based on the resonant frequencies of the cavity modes. The structure has then been realized with the HMSIW technology as in Fig. 16, with a microstrip line feeding (50 Ω).

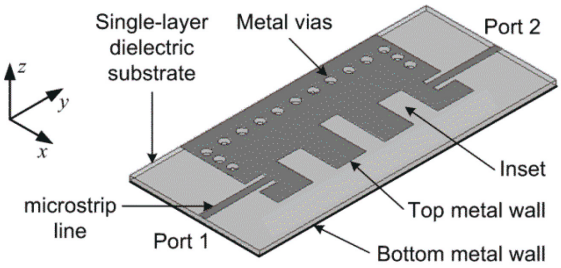

Fig. 16. HMSIW bandpass filter. [26]

As reported in [26], the comparison between the two structures shows almost identical: pass bandwidths; out-of-band rejections; insertion losses and sizes. On the contrary, the HMSIW structure involves an easier fabrication and the use of a selected subset of modes that lead to a simpler cavity design.

In the size reduction framework, Quarter-Mode filters (QMSIW) are able to significantly reduce the footprint. This structure was first presented in [28] and in [29] in which a two-pole and one transmission zero has been designed. Different QMSIW topologies have been implemented since then as in [30] and [31]. The structure consists of a quarter of a SIW cavity (cut along the symmetry planes), thus achieving a 75% size-reduction respect to the full SIW cavity with dimension W (Fig. 17). It can also be created beginning with the HMSIW and bisecting this structure with an ulterior fictitious magnetic wall [28]. As in the HMSIW structure, the open boundary, due to the low aspect ratio, can be represented as equivalent magnetic walls. For this reason, the modes supported are the TM_{mnp}-to-z with p=0. The TM_{110} is the first mode of the cavity and is plotted in Fig. 17 [21]. The higher order modes are the TM_{nm} with n, m odd values. In this case, after the TM_{110} mode comes the TM_{130} or TM_{310}.

Considering the single contributions to the Q factor in relation with the SIW cavity, it should be noted that: Q_d (dielectric) is slightly larger because of the fringing fields at the open boundaries; Q_c (conduction) is slightly smaller due to the current flowing near the sharp edges. The Q_{rad} (radiation) can be approximated with $Q_{rad} \approx Q_d$ [21]. Moreover, taking in consideration the size-reduction, the conductor losses do not increase significantly respect to other compact structures.

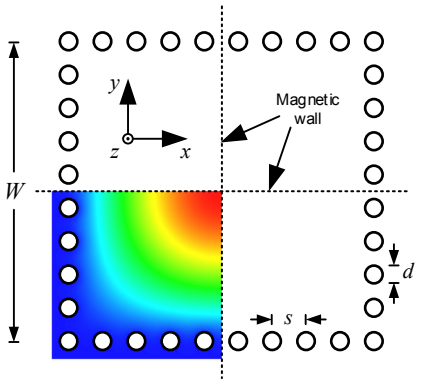

Fig. 17. TM_{110} in the remaining quarter portion of the entire cavity. [21]

The Q factor is reduced (unlike with the SIW cavity) hence not allowing high-performance narrow bandwidth filters but, on the contrary, due to stronger internal couplings between the cavities, broadband bandpass filters can be achieved [28]. It has been shown in [21] that, in general, this limitation can be overcome by controlling the coupling and the feeding mechanisms. Using this approach, a strong or a weak internal coupling can be obtained, thus allowing the design of narrow or broadband filters, respectively. In order to control the internal coupling between neighborhood cavities, two different feeding line positions have been analysed in [21]: the side-coupled and the corner-coupled QMSIW cavities. In Fig. 18 by laterally shifting the resonators the coupling can be controlled. Furthermore, the microstrip line can be moved along the open side, playing on the coupling between the microstrip and the resonator. In this way, two different filters, narrowband (FBW=1.7%) and broadband (FBW=17%), centered at 4 GHz can be designed. Otherwise, the control of the coupling can be obtained by overlapping the corners of the QMSIW resonators as in Fig. 19. Increasing the overlap, the coupling window's width grows, as does the bandwidth of the filter (from FBW 2.6% up to 16% in the proposed prototypes). In addition, the overlap helps to reduce the overall size of the filter by up to 40%. In conclusion, the QMSIW structure dimishes the footprint of the filter, with a greater design flexibility than the HMSIW. However, the radiation losses are sligtly increased and, for this reason, a low operation frequency is preferrable for the design of bandpass filters.

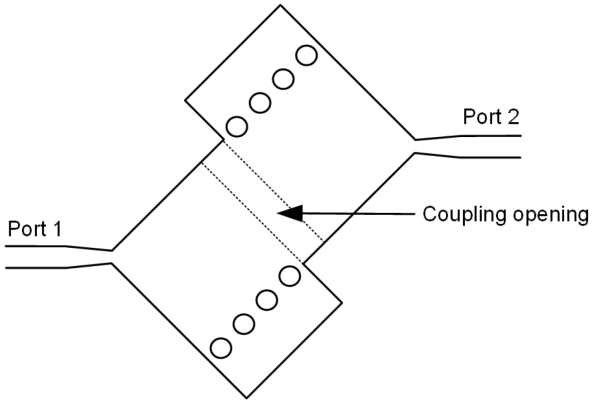

Fig. 18. Side coupling of the two QMSIW cavities. [21]

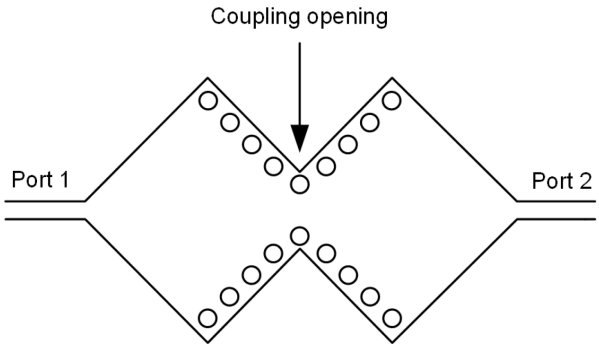

Fig. 19. Corner coupling of the two QMSIW cavities. [21]

A different structure used to reduce the size of the filter is related to the use of Dual-Mode resonators. A Dual-Mode resonator consists of a physical cavity in which mode degeneracy is employed. The degenerate modes can exist separately, orthogonally polarized, until they are coupled by perturbing the field. Dual-mode filters are often implemented by using circular waveguides with two degenerate TE_{111} modes [32], [33]. The polarizations of the two modes are orthogonal. Similarly, the rectangular waveguide can be used with the degeneracy of the TE_{101} and the TE_{011} modes [34], [35]. With these concepts in mind, other structures have

been designed and realized also in SIW technology. Considering, instead, the use of TM modes in relation with TE modes the occupation of the volume of the cavity can be more efficient with the creation of triple or quadruple mode cavity but with a poor temperature stability [59], [32]. Another advantage of the Dual-Mode cavities is the ability to produce transmission zeroes through nonresonating modes, as in [32]. Generally speaking, in the TE dual mode filters, realized with a proper coupling of the resonant modes of adjacent cavities, the maximum number of transmission zeros is limited by the number of resonators. Considering, instead, the rectangular TM dual-mode cavity, the number of transmission zeros is maximum, because both the resonant and non resonanating mode are implemented [60]. In this way, considering N^{th} (the order of the filter), the number of transmission zeroes that can be obtained is N [36]. In Chapter 3 and 4 dual-mode SIW cavities have been used together with the perforation of portions of the substrate (Par 3.3). It is shown that this structures are able to introduce transmission zeros and it is demonstrated how to control them.

4 PRACTICAL CONSIDERATIONS

In SIW filter design a key consideration is the choice of the substrate used. This is valid in particular for bandpass filters because they are more sensistive to mechanical and thermal issues [55]. The dielectric substrate is important because it affects different parameters in filter design such as: size, insertion loss, cost, tolerance, mechanical stability and power handling [55]. In addition, with the choice of one substrate, a specific fabrication method is favored. As, of these parameters, tolerance of fabrication and environment of usage are the least considered, and arguably most particular, during the design phase, they will be the focus of the following subsection.

4.1 Fabrication errors and environment of usage

In filter design, post-tuning (needed to compensate for the errors introduced by fabrication intollerances) is undesirable as it introduces extra fabrication costs. For this reason, the filter's robustness to intollerances is an important parameter. A Monte Carlo analysis can be performed on different geometrical parameters to highlight the sensitivity of the filter. In particular, presented in Chapter 2, this analysis illustrates a comparison between the periodically perforated SIW filter in respect to the iris-type filter (well documented in literature). Generally speaking, the errors occur with a misallignment or a radius variation of the via holes or in a discrepancy, between simulation and used substrate, in the dielectric permittivity. It is important to notice that, even if tolerances can represent a problem during the fabrication process, the SIW technology is more robust respect to microstrip or coplanar structures because the field distribution is more uniform [55]. For this reason, this techonology is a better choice for less precise fabrication processes (that, normally, are related to low-cost processes). The component's surrounding environment is another important factor for the choice of the substrate. In particular, if the components are disposable they should meet "green" requirements [49], such the use of paper substrates [54]. In addition, thermal stability is another parameter that should be considered when the variations in temperature are significant. A fluctuation in temperature can vary the physical dimentions of the filter, as well as in the permittivity. For this reason, the thermal properties of a substrate can be an important deciding factor. A common choice is to use dielectric materials that maintain their size during temperature variations. In these cases, materials with low coefficient thermal expansion (CTE) can be used [56]. On the other hand, different methods are present in literature to compensate, a posteriori, the variation. A shape memory alloy actuator is one of the methods proposed in [58]. In [57] a new self-compensation of the resonant frequency is proposed. In this study, the design of the size and the permittivity of the cavity rely on the use of specific CTEs.

Variation in temperature is not the only factor that can generate error in an open environment. Moisture and humidity can influence the properties of the components. Moreover, in a complex system a shielded component is required to minimize possible spurious interference. Its structure makes SIW the perfect cansidate to overcome these issues.

To summarize, substrate choice is not only dictated by cost-performance but, also, by the environment of operation and the fabrication process.

REFERENCES

[1] D. Deslandes, and K. Wu, "Integrated Microstrip and Rectangular Waveguide in Planar Form," *IEEE Microwave and Wireless Components Letters*, Vol. 11, No. 2, pp. 68–70, Nov. 2001.

[2] D. Deslandes, and K. Wu, "Single-Substrate Integration Techniques for Planar Circuits and Waveguide Filters," *IEEE Trans. Microwave Theory Tech*., Vol. 51, pp. 593-596, Feb, 2003.

[3] R. Garg, I. Bahl, M. Bozzi, "Microstrip Lines and Slotlines" (Third Edition) Artech House, May 2013.

[4] M. Bozzi, A. Georgiadis, and K. Wu, "Review of Substrate Integrated Waveguide (SIW) Circuits and Antennas," *IET Microwave Antennas and Propagation*, Vol. 5, No. 8, pp. 909–920, June 2011.

[5] Y. Cassivi, et al., "Dispersion Characteristics of Substrate Integrated Rectangular Waveguide," *IEEE Microwave Wireless Comp. Lett.*, Vol. 12, No. 9, pp. 333–335, 2002.

[6] X.-P. Chen, and K. Wu, "Substrate Integrated Waveguide Filter: Basic Design Rules and Fundamental Structure Features," *IEEE Microwave Magazine*, Vol. 15, No. 5, pp. 108-116, July-Aug. 2014.

[7] F. Xu, and K. Wu, "Guided–Wave and Leakage Characteristics of Substrate Integrated Waveguide," *IEEE Trans. Microwave Theory Tech*., Vol. 53, No. 1, pp. 66–73, 2005.

[8] C. Wang and K. A. Zaki, "Dielectric resonators and filters," *IEEE Microwave Magazine*, vol. 8, no. 5, pp. 115-127, Oct. 2007.

[9] R.D. Richtmeyer, "Dielectric Resonator," *J. Appl. Phys*., vol. 10, pp. 391, June 1939.

[10] F. Rautschke, D. Maassen, O. Konc and G. Boeck, "Comparison of conventional and substrate integrated waveguide filters for satellite communication," *2016 IEEE MTT-S International Wireless Symposium (IWS)*, Shanghai, 2016, pp. 1-4

[11] G. Matthaei, E. Jones, and L. Young, "Microwave Filters, Impedance matching networks, and coupling structures", Norwell, Artech House, 1985, pp. 521.

[12] L. Yechou, A. Tribak, M. Kacim, J. Zbitou and A. Mediavilla, "Ku-band waveguide band-pass filter with iris radius," *2014 International Conference on Multimedia Computing and Systems (ICMCS)*, Marrakech, 2014, pp. 1435-143.

[13] F. Parment, A. Ghiotto, T.P. Vuong, J.M. Duchamp, and K. Wu, "Airfilled substrate integrated waveguide for low loss and high power handling millimeter-wave substrate integrated circuits," *IEEE Trans. Microw. Theory Techn.*, vol. 63, no. 4, pp. 1-11, Apr. 2015.

[14] F. Parment, A. Ghiotto, T.P. Vuong, J.M. Duchamp, K. Wu, "Air-filled SIW transmission line and phase shifter for high performances and lowcost U-band integrated circuits and systems ," *8th IEEE Global Symposium on Millimeter-Waves*, Montreal, 25-27 May. 2015.

[15] F. Parment, A. Ghiotto, T. Vuong, J. Duchamp and K. Wu, "Low-loss Air-filled Substrate Integrated Waveguide (SIW) band-pass filter with inductive posts," *2015 European Microwave Conference (EuMC)*, Paris, 2015, pp. 761-764.

[16] N. Marcuvitz, "Waveguide Handbook", Peter Peregninus Ltd., 1985.

[17] H. Gruenberg, "Symmetrical placed inductive posts in rectangular wave guide," *Radio and Electrical Engineering Division National Research of Canada*, Ottawa, Dec. 1951.

[18] F. Parment, A. Ghiotto, T. P. Vuong, J. M. Duchamp, K. Wu, "Broadband transition from dielectric-filled to Air-filled substrate integrated waveguide for low loss and high power handling millimeterwave substrate integrated circuits," *Proc. IEEE MTT-S Int. Microw. Symp.*, pp. 1-4, Jun. 2014.

[19] R. Moro, S. Moscato, M. Bozzi and L. Perregrini, "Substrate Integrated Folded Waveguide Filter with Out-of-Band Rejection Controlled by Resonant-Mode Suppression," in *IEEE Microwave and Wireless Components Letters*, vol. 25, no. 4, pp. 214-216, April 2015.

[20] N. Delmonte, L. Silvestri, M. Bozzi, and L. Perregrini, "Compact Half-Mode SIW Cavity Filters Designed by Exploiting Resonant Mode Control," *International Journal of RF and Microwave Computer-Aided Engineering*, vol. 26, no. 1, pp. 72–79, Jan. 2016.

[21] S. Moscato, C. Tomassoni, M. Bozzi, and L. Perregrini, "Quarter-Mode Cavity Filters in Substrate Integrated Waveguide Technology," *IEEE Trans. Microw. Theory Techn.,* vol. 64, no. 8, pp. 2538-2547, Aug. 2016.

[22] P. Li, H. Chu, and R. S. Chen, "Design of Compact Bandpass Filters Using Quarter-Mode and Eighth-Mode SIW Cavities," *IEEE Trans. Compon. Packag. Manuf. Technol*., vol. 7, no. 6, pp. 956-963, June 2017.

[23] N. Grigoropoulos, B. S. Izquierdo, and P. R. Young, "Substrate Integrated Folded Waveguides (SIFW) and Filters*," IEEE Microw. Wireless Compon. Lett.*, vol. 15, no. 12, pp. 829–831, Dec. 2005.

[24] S. K. Alotaibi and J. S. Hong, "Novel substrate integrated folded waveguide filter," *Microw. Optical Technol. Lett.,* vol. 50, no. 4, pp. 1111–1114, Apr. 2008.

[25] N. Nguyen-Trong, T. Kaufmann, L. Hall and C. Fumeaux, "Variational Analysis of Folded Substrate-Integrated Waveguides," in *IEEE Microwave and Wireless Components Letters*, vol. 25, no. 6, pp. 352-354, June 2015.

[26] S. Moscato, N. Delmonte, L. Silvestri, M. Bozzi and L. Perregrini, "Half-mode versus folded SIW filters: Modeling and design," *2015 IEEE MTT-S International Conference on Numerical Electromagnetic and Multiphysics Modeling and Optimization (NEMO)*, Ottawa, ON, 2015, pp. 1-3.

[27] Rui-Sen Chen, Sai Wai Wong, Zai-Cheng Guo, Kai Wang and Qin-Xin Chu, "Wideband bandpass filter based on substrate integrated waveguide (SIW) and half-mode substrate integrated waveguide (HMSIW) cavities," *2015 IEEE International Wireless Symposium (IWS 2015)*, Shenzhen, 2015, pp. 1-4.

[28] Z. Zhang, N. Yang, and K. Wu, "5-GHz bandpass filter demonstration using quarter-mode substrate integrated waveguide cavity for wireless systems*," Proc. IEEE Radio Wireless Symp.*, San Diego, CA, USA, Jan. 2009, pp. 95–98.

[29] M. Z. U. Rehman, Z. Baharudin, M. A. Zakariya, M. H. M. Khir, and M. T. Khan, "Microwave bandpass filter using QMSIW," *Proc. IEEE Int. RF Microw. Conf.*, Penang, Malaysia, Dec. 2013, pp. 172–175.

[30] C. Jin and Z. Shen, "Compact triple-mode filter based on quarter-mode substrate integrated waveguide," *IEEE Trans. Microw. Theory Techn*., vol. 62, no. 1, pp. 37–45, Jan. 2014.

[31] X. Zhang, C. Ma, and F. Wang, "Design of compact dual-passband LTCC filter exploiting stacked QMSIW and EMSIW," *Electron. Lett*., vol. 51, no. 12, pp. 912–914, 2015.

[32] S. Bastioli, C. Tomassoni and R. Sorrentino, "TM dual-mode pseudoelliptic filters using nonresonating modes," *2010 IEEE MTT-S International Microwave Symposium*, Anaheim, CA, 2010, pp. 880-883.

[33] A. E. Williams, "A four-cavity elliptic waveguide filter," *IEEE Trans. Microwave Theory Tech.,* (1970 Symposium Issue), vol. MIT-18, pp. 1109-1114, Dec. 1970.

[34] A. E. Atia and A. E. Williams, "New Types of Waveguide Bandpass Filters for Satellite Transponders", *COM SAT Technical Review*, Vol. 1, No.1, Fall 1971.

[35] A. E. Williams and A. E. Atia, "Dual-Mode Canonical Waveguide Filters," in *IEEE Transactions on Microwave Theory and Techniques*, vol. 25, no. 12, pp. 1021-1026, Dec. 1977.

[36] S. Bastioli, L. Marcaccioli, C. Tomassoni, R. Sorrentino, "Ultracompact highly-selective dual-mode pseudoelliptic filters," *IET Electronics Letters*, vol. 46, No.2, pp. 147-149, Jan. 2010.

[37] H.J. Tang, W. Hong, Z.C. Hao, J.X. Chen, K.Wu, "Optimal design of compact millimetre-wave SIW circular cavity filters," *Electron. Lett.,* 2005, 41, (19), pp. 1068–1069.

[38] Chen, X.-P., Wu, K.: "Substrate integrated waveguide cross-coupled filter with negative coupling structure", *IEEE Trans. Microw. Theory Tech*., 2008, 56, (1), pp. 142– 149.

[39] H.J. Tang, W. Hong, Z.C. Hao, J.X. Chen and K. Wu, "Optimal design of compact millimetre-wave SIW circular cavity filters," *Electron. Lett.,* Vol. 41, pp. 1068-1069, Sep. 2005.

[40] H.J. Tang, W. Hong, J.X. Chen, G.Q. Luo, K. Wu, "Development of millimeter-wave planar diplexers based on complementary characters of dual-mode substrate integrated waveguide filters with circular and elliptic cavities," *IEEE Trans. Microwave Theory Tech.,* Vol. 55, pp. 776-782, April. 2007.

[41] B.Potelon, J.C.Bohorquez, J.F.Favennec, C. Quendo, E.Rius, C.Person, "Design of Ku-band filter based on substrate-integrated circular cavities (SICCs)," *IEEE MTT-S International Microwave Symposium Digest*, pp. 1237-1240, June 2006.

[42] Qi-Fu Wei, Zheng-Fan Li, Lin-Sheng Wu, and Lin Li, "A novel multilayered crosscoupled substrateintegrated waveguide (SIW) circular cavity filter in LTCC," *Microwave and Optical Techn Lett.*, Vol. 51, pp. 1686-1689, July 2009.

[43] Xiaoping Chen, Wei Hong, T. Cui, Jixin Chen and Ke Wu, "Substrate integrated waveguide (SIW) linear phase filter," in *IEEE Microwave and Wireless Components Letters*, vol. 15, no. 11, pp. 787-789, Nov. 2005.

[44] F. Zhu, W. Hong, J. Chen and K. Wu, "Cross-Coupled Substrate Integrated Waveguide Filters With Improved Stopband Performance," in *IEEE Microwave and Wireless Components Letters*, vol. 22, no. 12, pp. 633-635, Dec. 2012.

[45] N. Ranjkesh and M. Shahabadi, "Reduction of dielectric losses in substrate integrated waveguide," *Electron. Lett.*, vol. 42, no. 21, pp. 1230–1231, Oct. 2006.

[46] Hirokawa, J., M. Ando, "Single–Layer Feed Waveguide Consisting of Posts for Plane TEM Wave Excitation in Parallel Plates," *IEEE Tran. Ant. Propagat.*, Vol. 46, No. 5, 1998, pp. 625–630.

[47] Hiroshi, U., T. Takeshi, and M. Fujii, "Development of a 'Laminated Waveguide'," *IEEE Trans. Microwave Theory Tech.,* Vol. 46, No. 12, 1998, pp. 2438–2443.

[48] Wu, K., "Towards System–on–Substrate Approach for Future Millimeter–Wave and Photonic Wireless Applications," *Proc. Asia–Pacific Microwave Conference 2006*, Yokohama, Japan, Dec. 12–15, 2006, pp. 1895–1900.

[49] Ph.D thesis, Riccardo, M., "Substrate Integrated Waveguide components based on eco-friendly materials," 2011, Università degli studi di Pavia.

[50] M. Bozzi, L. Perregrini, and K. Wu, "Modeling of Losses in Substrate Integrated Waveguide by Boundary Integral-Resonant Mode Expansion Method," *IEEE International Microwave Symposium (IMS 2008) Digest*, pp. 515–518, Atlanta, GA, 2008.

[51] D. Deslandes, "Design equations for tapered microstrip-to-Substrate Integrated Waveguide transitions," *IEEE MTT-S Inter. Microwave Symposium Digest 2010*, pp. 704–707, Anaheim, CA, USA, May 23-28, 2010.

[52] L. Xia, R. Xu, B. Yan, J. Li, Y. Guo, and J. Wang, "Broadband transition between Air-filled waveguide and substrate integrated waveguide," *Electronics Letters*, Vol. 42 , No. 24, pp. 1403–1405, Nov. 2006.

[53] X. Chen and K. Wu, "Low-loss ultra-wideband transition between conductor-backed coplanar waveguide and substrate integrated waveguide," *2009 IEEE MTT-S International Microwave Symposium Digest*, Boston, MA, 2009, pp. 349-352.

[54] S. Moscato, N. Delmonte, L. Silvestri, M. Pasian, M. Bozzi and L. Perregrini, "Compact substrate integrated waveguide (SIW) components on paper substrate," *2015 European Microwave Conference (EuMC)*, Paris, 2015, pp. 24-27.

[55] X. Chen and K. Wu, "Substrate Integrated Waveguide Filters: Practical Aspects and Design Considerations," in *IEEE Microwave Magazine*, vol. 15, no. 7, pp. 75-83, Nov.-Dec. 2014.

[56] S. Lundquist, M. Yu, D. Smith, and W. Fitzpatrick, " Ku-band temperature compensated high power multiplexers," *in 20th AIAA Int. Commun. Satellite Syst. Conf. & Exhibit*, May 2002, pp. 12–15.

[57] T. Djerafi, K. Wu and D. Deslandes, "A Temperature-Compensation Technique for Substrate Integrated Waveguide Cavities and Filters," in *IEEE Transactions on Microwave Theory and Techniques*, vol. 60, no. 8, pp. 2448-2455, Aug. 2012.

[58] B. F. Keats, R. B. Gorbet, and R. R. Mansour, "Design and testing of SMA temperature compensated cavity resonators," in *IEEE Trans. Microw. Theory Tech.*, vol. 51, no. 12, pp. 2284–2289, Dec. 2003

[59] W. C. Tang and S. K. Chaudhuri, "A true elliptic function filter using triple mode degenerate cavities," in *IEEE Trans. Microw. Theory Tech.*, vol. MTT-34, no. 11, pp. 1449–1454, Nov. 1984

[60] U. Rosenberg, S. Amari, and J. Bornemann, "Inline -mode filters with high design flexibility by utilizing bypass couplings of nonresonating modes," *IEEE Trans. Microw. Theory Tech.*, vol. 51, no. 6, pp. 1735–1742, Jun. 2000.

[61] Y. L. Zhang, W. Hong, K. Wu, J. X. Chen, and Z. C. Hao, "Development of Compact Bandpass Filters with SIW Triangular Cavities," *APMC Proceedings*, 2005.

[62] E. Massoni *et al*., "3-D Printed Substrate Integrated Slab Waveguide for Single-Mode Bandwidth Enhancement," in *IEEE Microwave and Wireless Components Letters*, vol. 27, no. 6, pp. 536-538, June 2017.

[63] S. Moscato *et al*., "Exploiting 3D printed substrate for microfluidic SIW sensor," *2015 European Microwave Conference (EuMC)*, Paris, 2015, pp. 28-31.

[64] W. Su *et al*., "3D printed wearable flexible SIW and microfluidics sensors for Internet of Things and smart health applications," *2017 IEEE MTT-S International Microwave Symposium (IMS)*, Honololu, HI, 2017, pp. 544-547.

[65] M. Bozzi and R. Moro, "Low-cost fabrication, eco-friendly materials, and easy integration: The new technological paradigm for the future wireless sensor networks," *2013 European Microwave Conference*, Nuremberg, 2013, pp. 858-861.

[66] Farooq *et al.*, "A Review on Internet of Things (IoT)," in *International Journal of Computer Applications*. 2015, n. 113, pp. 1-7.

[67] Shi *et al.*, "Review of Key Technologies of 5G Wireless Communication System," in *MATEC Web of Conferences*.

Chapter 2

NOVEL CLASS OF BANDPASS FILTERS BASED ON THE PERIODIC PERFORATION OF THE DIELECTRIC SUBSTRATE [1][2][3]

In this chapter, the investigation of a novel class of bandpass SIW filters based on a periodic perforation of the dielectric substrate is described.

At first, this investigation has been anticipated in [4]. In [1], a preliminary study has been proposed and, then, in two conference papers [2] and [3] the concept has been ulterior extended, adding flexibility to the design. The structure has been studied starting from the classical waveguide iris-type filter theory. In particular, the dielectric perforation of the substrate (Fig. 20(*a*)) helps to reduce the local effective dielectric permittivity ([8] and [9]), creating waveguide sections below cutoff (Fig. 20(*b*)) thus creating immittance inverters.

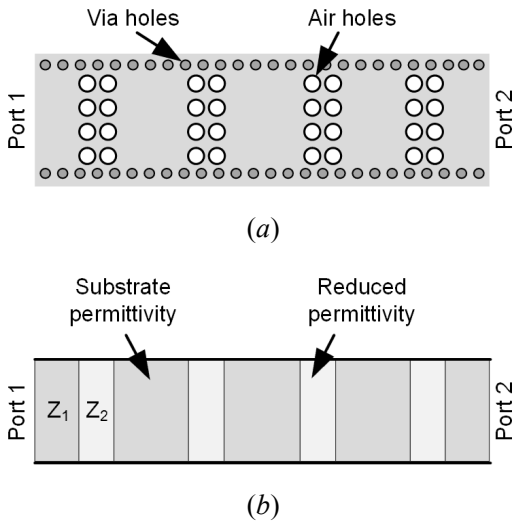

Fig. 20. SIW filter with periodic perforations: (*a*) physical geometry of the filter; (*b*) equivalent structure based on alternate sections with substrate permittivity and reduced permittivity (perforated areas). [1], [2]

The design properties of the immittance inverters have been described, including also an outline of the fine control guidelines for the coupling. Interestingly, the resonator retains a particularly short physical length (around $\lambda_g/6$ in the previously demonstrated examples). On the contrary, the dimensions of the coupling elements are not as compact, because they are realized with perforated waveguide sections. These structures exhibit a better out-of-band performance, respect to the iris-type filters, and lower sensitivity to fabrication inaccuracies with an analogous frequency response. This feature of the perforated SIW filters leads to new manufacturing possibilities, by adopting low-cost fabrication techniques, such as the punching technique [5]. The dimension of the filter can be reduce by adopting a Half-mode structure [11][12]. A prototype has been designed starting from the full-mode filter design. In order to overcome the higher insertion loss of the half mode structure, the Folded half-mode filter has been introduced [13], able to maintain the compact dimensions

whilst reducing the radiation losses. In addition, the introduction of transmission zero plays and important role in the out-of-band rejection performances. The results of this work have been presented in [1], [2] and [3].

1 OPERATION PRINCIPLE OF THE FILTER

In order to introduce a circuital model of Fig. 20, the evanescent waveguide section can be represented as an impedance inverter (plus two transmission lines) and the propagating waveguide sections connecting two evanescent sections as dispersive transmission lines (Fig. 21).

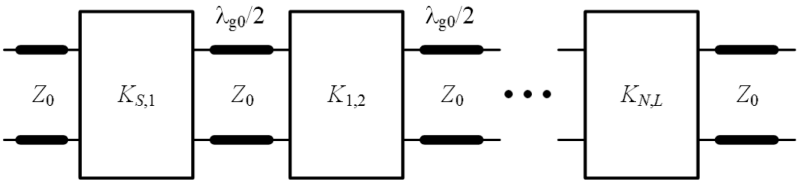

Fig. 21. Equivalent circuit of an in-line N-pole filter. [3]

The normalized impedance inverter $K_{i,j}^{(\mathrm{Nor})} = K_{i,j}/Z_0$ can be evaluated directly from the coupling matrix elements.

$$K_{S,1}^{(\mathrm{Nor})} = M_{S,1}\sqrt{\frac{\pi}{2} FBW_{\lambda_g}} \tag{4}$$

$$K_{N,L}^{(\mathrm{Nor})} = M_{N,L}\sqrt{\frac{\pi}{2} FBW_{\lambda_g}} \tag{5}$$

$$K_{i,j}^{(\mathrm{Nor})} = M_{i,j}\frac{\pi}{2} FBW_{\lambda_g} \tag{6}$$

where subscripts *S* and *L* stand for source and load, while indices *i* and *j* refer to the *i*-th and *j*-th resonator, respectively, and *N* is the total number of resonators. The fractional bandwidth is calculated by using the waveguide wavelength to account for dispersion

$$FBW_{\lambda_g} = \frac{\lambda_{g2} - \lambda_{g1}}{\lambda_{g0}} \tag{7}$$

being λ_{g1} and λ_{g2} the waveguide wavelengths at the lower and higher pass-band edge, respectively, while λ_{g0} is the waveguide wavelength at the central frequency:

$$\lambda_{g0} = \sqrt{\lambda_{g1}\lambda_{g2}} \tag{8}$$

1.1 Synthesis of the immittance inverter

The section with reduced permittivity ε_{r1} (Fig. 22(*a*)) acts as an immittance inverter with two transmission line sections (Fig. 22(*b*)). This equivalence is shown by evaluating the reflection coefficient of the evanescent waveguide section. The propagation constant ε_0 of the input and output waveguides is real, whereas the one of the evanescent waveguide ε_1 is purely imaginary.

$$\beta_0 = \sqrt{\left(\frac{2\pi}{\lambda}\right)^2 \varepsilon_{r0} - \left(\frac{\pi}{a}\right)^2} \tag{9}$$

$$\beta_1 = -j\gamma_1 = \sqrt{\left(\frac{2\pi}{\lambda}\right)^2 \varepsilon_{r1} - \left(\frac{\pi}{a}\right)^2} \tag{10}$$

Analogously, the characteristic impedance Z_0 (in the propagating waveguide section) is real, whereas Z_1 (in the evanescent waveguide section) is imaginary

$$Z_0 = \frac{\omega\mu}{\beta_0} \tag{11}$$

$$Z_1 = \frac{\omega\mu}{\beta_1} = \frac{\omega\mu}{-j\gamma_1} \tag{12}$$

The input impedance Z_{in} can be expressed as

$$Z_{in} = Z_1 \frac{Z_0 + jZ_1 \tan(\beta_1 l)}{Z_1 + jZ_0 \tan(\beta_1 l)} \tag{13}$$

where l is the length of the evanescent waveguide section. This allows the evaluation of the reflection coefficient Γ

$$\Gamma = S_{11} = \frac{Z_{in} - Z_0}{Z_{in} + Z_0} = \frac{Z_1 \dfrac{Z_0 + jZ_1 \tan(\beta_1 l)}{Z_1 + jZ_0 \tan(\beta_1 l)} - Z_0}{Z_1 \dfrac{Z_0 + jZ_1 \tan(\beta_1 l)}{Z_1 + jZ_0 \tan(\beta_1 l)} + Z_0} = \frac{j\left(Z_1^2 - Z_0^2\right)\tan(\beta_1 l)}{2Z_0 Z_1 + j\left(Z_1^2 + Z_0^2\right)\tan(\beta_1 l)} =$$

$$= -\frac{\left(\gamma_1^2 + \beta_0^2\right)\tanh(\gamma_1 l)}{2j\gamma_1\beta_0 + \left(\gamma_1^2 - \beta_0^2\right)\tanh(\gamma_1 l)} = -\frac{\left(\gamma_1^2 + \beta_0^2\right)\tanh(\gamma_1 l)}{\sqrt{4(\gamma_1\beta_0)^2 + \left(\left(\gamma_1^2 - \beta_0^2\right)\right)^2 \tanh^2(\gamma_1 l)}} e^{-j\arctan\left(\frac{2\gamma_1\beta_0}{\left(\left(\gamma_1^2 - \beta_0^2\right)\tanh(\gamma_1 l)\right)}\right)} \tag{14}$$

Starting from a ABCD matrix of an impedance inverter

$$\begin{bmatrix} A & B \\ C & D \end{bmatrix} = \begin{bmatrix} 0 & jK \\ j/K & 0 \end{bmatrix}$$

it can be demonstrated [3], that the evanescent waveguide section can be represented by an impedance inverter and two transmission line sections, as shown in Fig. 22(*b*) [3]. In fact, the normalized inverter of value

$$K^{(\mathrm{Nor})} = \frac{K}{Z_0} = \sqrt{\frac{1+S_{11}^{(\mathrm{Ampl})}}{1-S_{11}^{(\mathrm{Ampl})}}} \tag{15}$$

with

$$S_{11}^{(\mathrm{Ampl})} = -\frac{\left(\gamma_1^2+\beta_0^2\right)\tanh(\gamma_1 l)}{\sqrt{4(\gamma_1\beta_0)^2+\left(\gamma_1^2-\beta_0^2\right)^2\tanh^2(\gamma_1 l)}} \tag{16}$$

that accounts for the return loss amplitude of the evanescent waveguide section, while the transmission line sections at the inverter ports with length

$$\Lambda = \frac{1}{2\beta_0}\arctan\left(\frac{2\gamma_1\beta_0}{\left(\gamma_1^2-\beta_0^2\right)\tanh(\gamma_1 l)}\right) \tag{17}$$

takes into account the return loss phase. In conclusion, (15) and (17) provide analytical formulas for the design of the impedance inverter in Fig. 22(*b*).

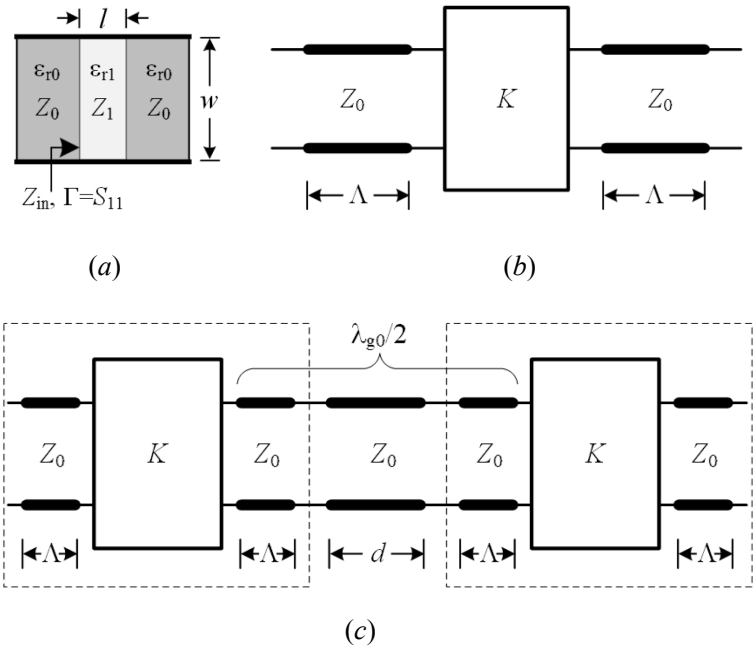

Fig. 22. Evanescent waveguide section: (*a*) geometrical parameters of the evanescent waveguide section; (*b*) representation as an inverter and two transmission line sections; (*c*) resonator by two inverters. [3]

1.2 Implementation of the evanescent waveguide section

Perforation in the dielectric substrate helps to reduce the dielectric constant, thus realizing evanescent waveguide sections as shown in Fig. 23(*a*). Considering both the permittivity of the dielectric substrate and the air, the subsequent effective dielectric constant ε_{eff} assumes an intermediate value between the two. With reference to Fig. 22(*a*), the desired impedance inverter value can be obtained by applying (14) and considering $\varepsilon_{r1} = \varepsilon_{eff}$. As an example, considering a waveguide width w = 16.8 mm, dielectric constant ε_r = 10, and holes with radius r = 0.85 mm and side-by-side distance Δ = 0.25 mm, the effective dielectric constant is ε_{eff} = 5. Considering this effective dielectric constant and using (15) and (17), an estimation of the equivalent K-inverter and of the transmission line lengths Λ can be found (Fig. 22(*b*)). The lengths of the evanescent perforated waveguide sections considered in (15) and (17) are related to the number of hole columns (1.7 mm, 3.65 mm, 5.6 mm, 7.55 mm, 9.5 mm, 11.45 mm). In TABLE I, such results are compared to full-wave HFSS analysis results, showing a good agreement. It should be noted that a limitation of this structure is the length of the evanescent waveguide section, as the length depends on the discrete value of the number of hole columns. Generally, in filter design, a discrete value is not sufficient and a wider selection of K-inverter values is necessary. As shown in Fig. 23(*b*), this limitation can be surmounted simply by removing the top and bottom hole rows. The field distribution is weaker in the lateral positions, where the rows are removed, and this slightly changes the K-inverter value. However, this is sufficient to create enough room for the holes to move, increasing gap a (Fig. 23(*c*)). The coarse selection of the K-inverter can be obtained with the number of hole columns. A more precise value can be selected with a proper choice of gap a. In Fig. 23(*d*) the K-inverter values related to perforated evanescent waveguide sections having a number of hole columns ranging from 1 to 6 are plotted as a function of the gap a. As aforementioned, by exploiting the further degree of freedom of the gap a, all possible K-inverter values in the range from 0.34 to 0.91 are possible. If Values lower than 0.34 are necessary, more than 6 hole columns should be used. Instead, if values larger than 0.91 are necessary, a variation of the hole radius or a distance increase between close holes. Finally, in Fig. 23(*e*) the diagram for the evaluation of the transmission line lengths Λ to be added to the K-inverter ports is shown.

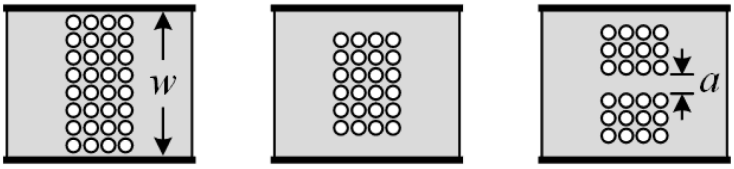

(*a*) (*b*) (*c*)

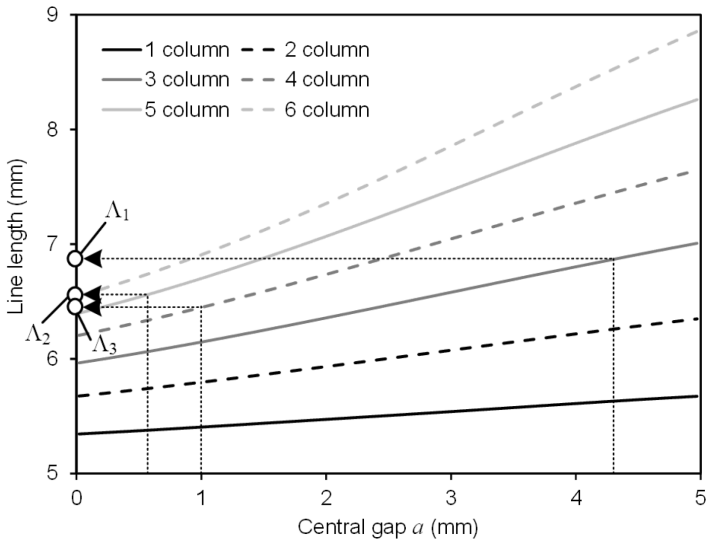

(*d*)

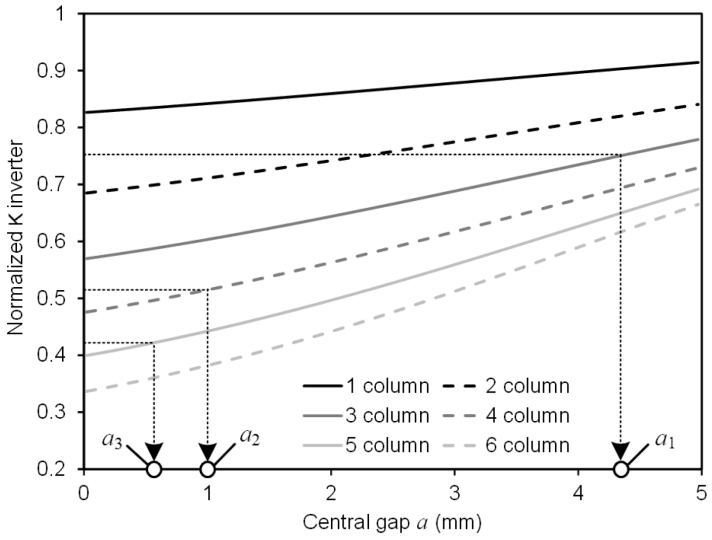

(*e*)

Fig. 23. Model of the evanescent waveguide section: (*a*), (*b*), (*c*) three possible realizations of the evanescent waveguide section; (*d*) $K^{(Nor)}$ versus *a* (*w* = 16.8 mm, ε_r = 10, radius of the holes *r* = 0.85 mm, and distance between adjacent holes Δ = 0.25 mm); (e) line length Λ versus the central gap *a*. [3]

TABLE I
VALUES OF THE IMPEDANCE INVERTER (IN MM)

	Normalized K-inverter		Transmission line length Λ	
Number of hole columns	Full-wave (HFSS)	Equation (ε_{eff}=5)	Full-wave (HFSS)	Equation (ε_{eff}=5)
1	0.8231	0.8467	5.332	5.552
2	0.6791	0.7000	5.648	5.864
3	0.5622	0.5814	5.923	6.139
4	0.4673	0.4843	6.150	6.368
5	0.3901	0.4049	6.330	6.551
6	0.3268	0.3398	6.468	6.693

2 FILTER BASED ON THE PERIODIC PERFORATION OF THE DIELECTRIC SUBSTRATE

The in-line filter with the following coupling matrix (f_0 = 3.65 GHz, *FBW*=0.16) is here considered.

$$\begin{bmatrix} 0 & 1.1 & 0 & 0 & 0 & 0 \\ 1.1 & 0 & 1 & 0 & 0 & 0 \\ 0 & 1 & 0 & 0.76 & 0 & 0 \\ 0 & 0 & 0.76 & 0 & 1 & 0 \\ 0 & 0 & 0 & 1 & 0 & 1.1 \\ 0 & 0 & 0 & 0 & 1.1 & 0 \end{bmatrix}$$

By using (15)-(17), the normalized K-inverters are found: $K_{S,1}^{(\mathrm{Nor})} = K_{4,L}^{(\mathrm{Nor})} = 0.75, K_{1,2}^{(\mathrm{Nor})} = K_{3,4}^{(\mathrm{Nor})} = 0.515,$ $K_{2,3}^{(\mathrm{Nor})} = 0.425$. The design procedure consists in the use of (15)-(17) to find the lengths l of the evanescent waveguide sections by using the effective dielectric constant of the perforated waveguide (in this case $\varepsilon_{\mathrm{eff}} = 5$). The resulting lengths are $l_1 = 2.9$ mm, $l_2 = 6.9$ mm and $l_3 = 9.0$ mm. Such lengths can be approximated by a number of hole columns equal 2, 4 and 5 respectively. This corresponds, for the structure of Fig. 23*b*, to normalized K-inverters of value 0.69, 0.48, and 0.41, respectively. With a full-wave simulator the fine tuning of K-inverter values is attainable with an appropriate choice of the gap a. Note that the starting value of the K-inverters should be lower than the desired one, as gap a only allows the increase this value. This means that distances l_1, l_2, and l_3 should be rounded to the higher integer.

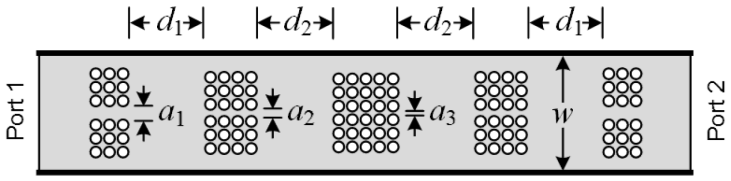

(*a*)

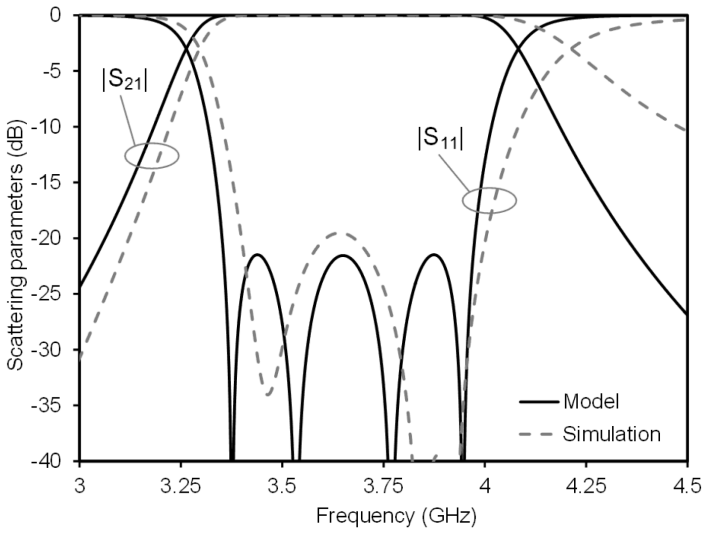

(*b*)

Fig. 24. Perforated four-pole filter: (*a*) geometry of the filter (dimensions in mm: d_1=7.15, d_2=7.44, a_1=4.32, a_2=1, a_3=0.63, and w=16.8); (*b*) |S| Parameters (comparison between model and HFSS simulation). [3]

A faster design procedure is possible by exploiting the diagram of Fig. 23(*d*), to directly find the number of hole columns and the gap a. The K-inverter value 0.75 can be obtained by using 2 or 3 columns, the value 0.515 with 4, 5 or 6 columns, while the value 0.425 with 5 or 6 columns. In this example, K_{S1} has been realized by using 3 columns and $a_1 = a_5 = 4.32$ mm, K_{12} by using 4 columns and $a_2 = a_4 = 1$ mm, K_{23} by using 4 columns

and a_3 = 0.63 mm. By using the diagram of Fig. 23(*e*) it is possible to find the length of the transmission lines to be added to the K-inverter: Λ_1 = 6.87 mm, Λ_2 = 6.45 mm, and Λ_3 = 6.58 mm. Such lengths are then subtracted to the resonator ($\lambda_g/2$ = 20.47 mm), leading to physical resonator of length $d_1 = d_4$ = 20.47–6.87–6.45 = 7.15 mm and $d_2 = d_3$ = 20.47–6.45–6.58 = 7.44 mm (Fig. 24(*a*). In Fig. 24(*b*), the scattering parameters of the designed filter are compared to the coupling matrix response, showing a very good agreement despite the filter has not been optimized.

This structure shows a reduced resonators length (about $\lambda_g/6$ in this example) due to the presence of transmission line sections in the impedance inverter representing the evanescent waveguide sections. In an iris filter the same phenomenon appears but with a limited reduction in resonators length.

3 FABRICATION AND MEASUREMENTS

From the filter synthesis, the geometry of the prototype has been obtained. Originally, in filter synthesis, the equivalent rectangular waveguide was adopted. This structure has been replaced by the SIW structure [6], adopting metallised vias, with d = 1 mm and s = 1.5 mm [7]. In addition, tapered microstrip to SIW transitions are used to measure the filter. The final dimensions of the filter, shown in (Fig. 25(*a*)), require a light full-wave optimization (based on the commercial electromagnetic solver HFSS).

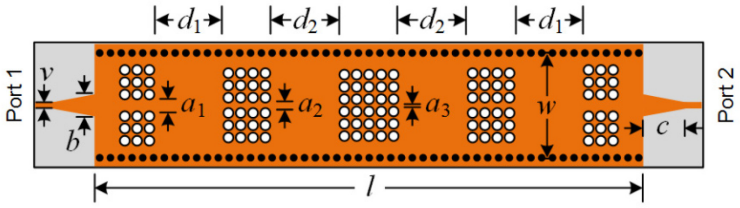

(*a*)

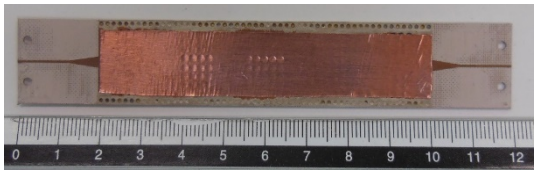

(*b*)

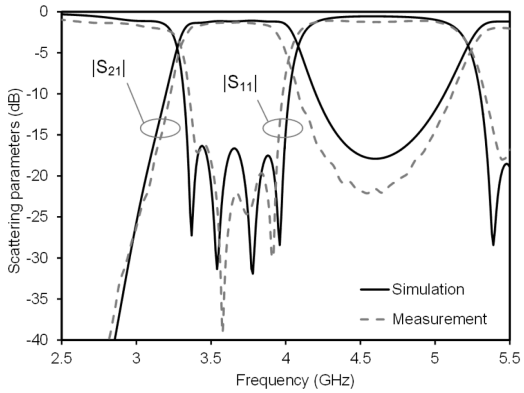

(*c*)

Fig. 25. Prototype of the four-pole filter based on perforated SIW structure: (*a*) geometry of the filter (dimensions in mm: v=0.6, b=2.6, d_1=10, d_2=7.95, a_1=4, a_2=0.55, a_3=0.25, w=17.8, c=7, and l=81); (*b*) photograph of the prototype; (*c*) scattering parameters of the four-pole filter (HFSS simulation compared with measured data). [1], [2] and [3]

A commercial dielectric substrate Taconic CER-10 (thickness 0.64 mm, $\varepsilon_r = 10.0$, $\tan\delta = 0.0035$) has been adopted for the realization of the filter. The metal layer was shaped with a mechanic LPKF E33 milling machine, used also to drill the via holes. The holes, constituting the side walls of the SIW structure, were then metalized with a LPKF ProConduct paste. The prototype is shown in Fig. 25(*b*). In this first attempt the filter has been measured as the structure in Fig. 25(*b*). Covering both side with copper tapes, the air holes have been closed. The prototype has been measured using an Anritsu Universal Test Fixtures (UTF) 3680 and an Anritsu 37347C vector network analyzer (VNA) without de-embedding to eliminate the impact of the connectors and transitions. In Fig. 25(*c*) the comparison between simulations and measurements is reported.

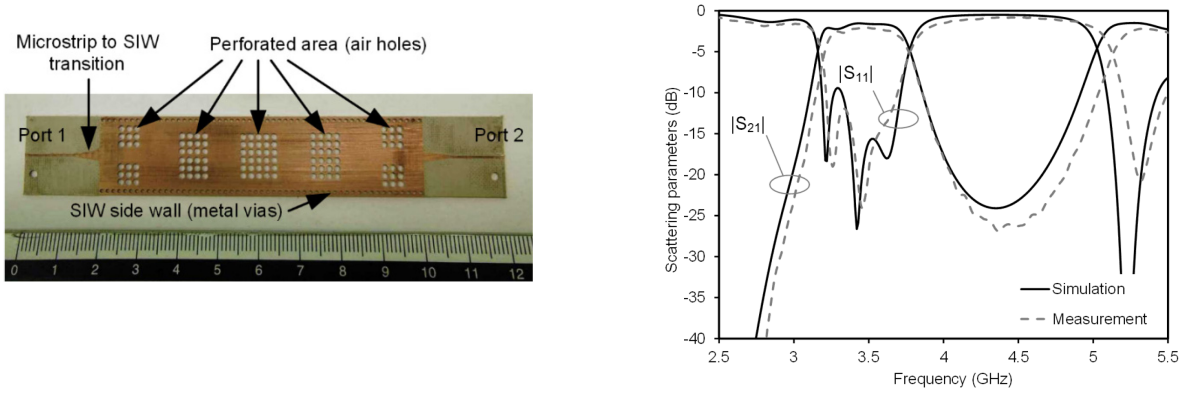

(*a*) (*b*)

Fig. 26. Prototype of the four-pole filter based on perforated SIW structure: (*a*) photograph of the prototype [1], [2] and [3]; (*b*) scattering parameters of the four-pole filter (HFSS simulation compared with measured data).

This demonstrates a measured insertion loss (IL) equal to 1.31 dB at $f_0 = 3.65$ GHz and a bandwidth (BW) of 630 MHz defined at 10 dB input matching. Simulations, as displayed in Fig. 25(*c*), are slightly different with 1.15 dB IL and BW of 660 MHz.

In order to identify the different contributions of losses, simulations have been performed showing 0.77 dB for the SIW filter loss: consisting of 0.47 dB of dielectric loss and 0.30 dB of conductor loss. Almost no radiation loss occurs (0 dB) with transition contributes equivalent to 0.19 dB (each). The overall footprint of the filter is $l \times w = 1442$ mm^2. The same structure has been tested also without covering the holes as in Fig. 26(*a*) (same dimensions as Fig. 25(*b*)). In this case the final structure results simplified but with some disadvantages. The first relies in the variation of the effective dielectric permittivity, due to the strong capacitive effect between the rim of the top aperture and of the bottom aperture, that strongly limits the field from entering the holes. In addition, the structure is not shielded anymore. For these reasons the first solution should be adopted for the design of this class of filters.

4 FULL-MODE AND IRIS-TYPE SIW FILTER COMPARISON

In order to highlight the advantages of the proposed structure, the filter of Fig. 25 is compared with an inductive iris filter with similar filtering characteristics (same central frequency f_0, number of poles, pass bandwidth, and input matching level). Furthermore, the same dielectric substrate has been used. The iris-type filter was optimized using HFSS, and the final geometry is shown in Fig. 27(*a*). The simulation results of the iris-type filter and of the perforated filter of Fig. 25 are compared in Fig. 27(*b*). A better performance can be noted in the out-of-band rejection for the perforated filter (spurious band at $1.45\,f_0 = 5.22$ GHz in the perforated filter and at $1.32\,f_0 = 4.77$ GHz in the iris filter) with an almost identical insertion loss for both filters. On the

contrary, the iris filter shows a more compact footprint, being 24% smaller than the perforated filter (1091 mm^2 compared with 1442 mm^2).

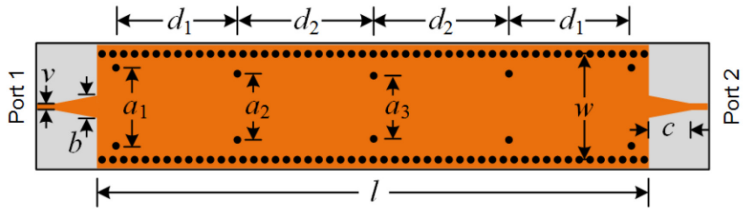

(*a*)

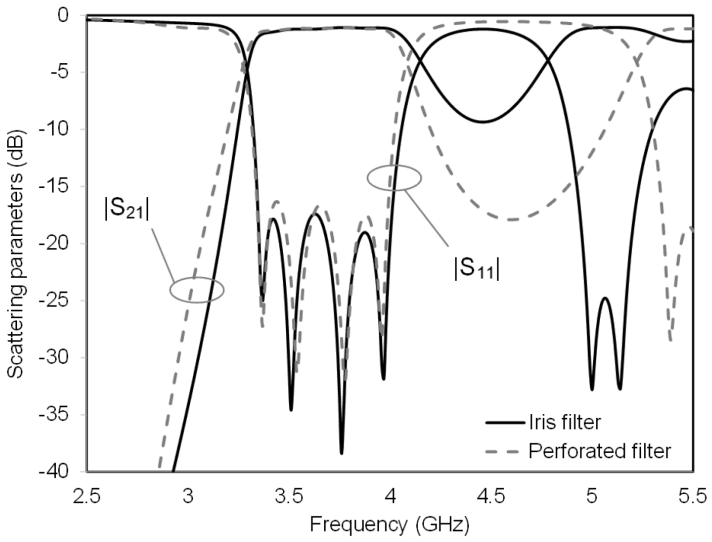

(*b*)

Fig. 27. Performance comparison between the perforated SIW filter and a classical iris-type SIW filter: (*a*) geometry of the iris-type SIW filter (dimensions in mm: v=0.6, b=3.03, d_1=15.25, d_2=15.1, a_1=13.3, a_2=12.1, a_3=11.4, w=17.425, c=9.5, and l=62.7); (*b*) scattering parameters of the perforated SIW filter and the iris-type SIW filter (HFSS simulation). [3]

The advantages of the perforated filter are not only limited to a better out-of-band rejection but, most importantly, are also related to its tolerance of fabrication inaccuracies. A Mont Carlo analysis, running 2000 HFSS simulations, was conducted to examine the strength of tolerance. The positions were independently altered for each of the iris posts, using a maximum displacement of 50 μm from the original position. For the perforated filter, a similar analysis has been carried out. In this analysis, the perforated area positions were transformed using a maximum displacement of 50 μm. When adopting a manufacturing by punching method [5], the most detrimental error can in the misalignment of the iris posts - not the individual holes; therefore the distance between each hole was not modified.

Comparing the two filters, Fig. 28 highlights the limited range of the scattering parameters in the perforated filter's passband (Fig. 28(*b*)), in respect to the inductive iris filter (Fig. 28(*a*)), thus confirming the robustness of the prosed filter to fabrication intolerances.

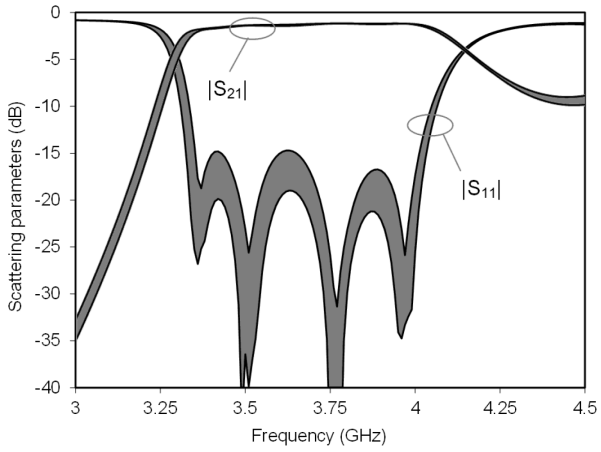

(*a*)

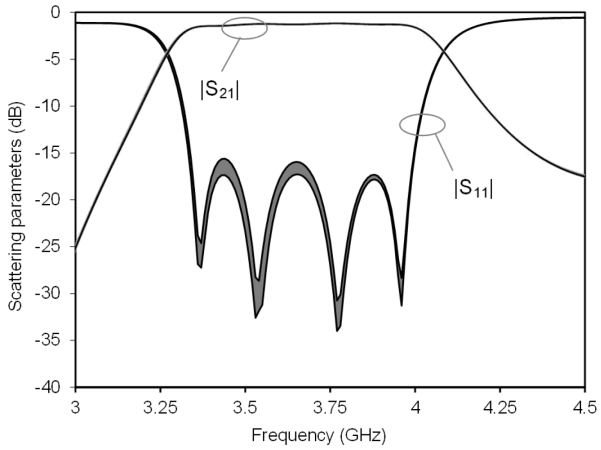

(*b*)

Fig. 28. Sensitivity analysis of the iris-type SIW filter and the perforated SIW filter: (*a*) spread of the scattering parameters of the iris-type SIW filter; (*b*) spread of the scattering parameters of the perforated SIW filter (HFSS simulation). [3]

5 PERFORATED HALF-MODE SIW FILTER

The same filter concept was applied to the half-mode SIW structure, in order to minimize the filter footprint. As explained in the introduction, by removing half of the top metal layer of the SIW full-mode a half-mode SIW can be obtained. For this fact, the half-mode SIW filter is adapted from the previous design with a further HFSS re-optimization. The geometry of the filter and the final dimensions are shown in Fig. 29(*a*). By using a fabrication process identical to that of the full-mode structure, a half-mode prototype has been realized. The realised prototype (Fig. 29(*b*)) has been measured covering the holes at the top/bottom for the reasons explained in the previous paragraph. The photograph in (Fig. 29(*b*)) shows the filter before the covering. In Fig. 29(*c*) the comparison of simulated and measured scattering parameters is presented. This demonstrates a measured insertion loss (IL) equal to 2.15 dB at f_0 = 3.65 GHz and a bandwidth (BW) of 760 MHz defined at 10 dB input matching. Simulations are slightly different with 2.4 dB IL and BW of 730 MHz.

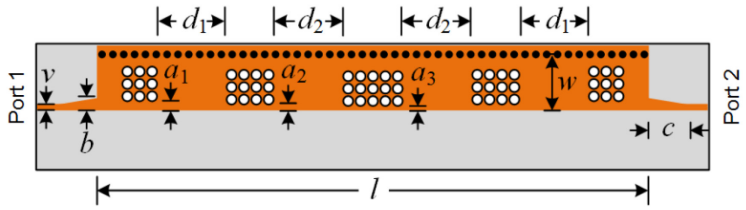

(*a*)

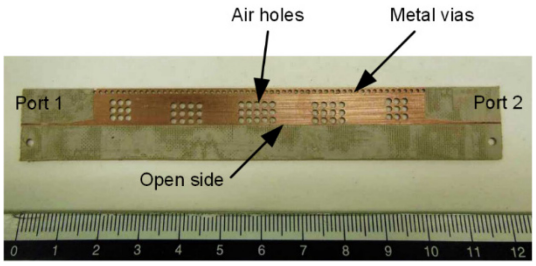

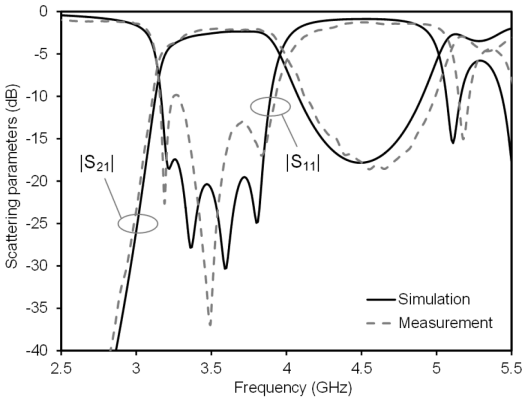

(*b*)(*c*)

Fig. 29. Prototype of the four-pole filter based on perforated half-mode SIW structure: (*a*) geometry of the filter (dimensions in mm: v=0.6, b=1.6, d_1=9.6, d_2=8.35, a_1=1, a_2=0.2, a_3=0.4, w=8.3, c=7, and l=83); (*b*) photograph of the prototype; (*c*) scattering parameters of the four-pole filter (HFSS simulation compared with measured data). [1], [2] and [3]

TABLE II
RESONANCE FREQUENCY AND QUALITY FACTOR OF THE PERFORATED HALF-MODE SIW CAVITY

	No radiation		Radiation	
	Frequency (GHz)	Quality Factor	Frequency (GHz)	Quality Factor
Mode 1	3.30	187	3.19	61
Mode 2	3.44	186	3.28	103
Mode 3	3.70	185	3.55	146
Mode 4	4.00	198	3.90	184

Furthermore, in this particular example, the extents of each various losses have been examined through simulations. Each transition contributes with a loss of 0.48 dB, Considering a SIW filter loss equal to 1.44 dB, 0.38 dB is attributed to dielectric loss, 0.43 dB to conductor loss, and 0.63 dB to radiation loss. In this case, the radiation losses are not negligible respect to the full-mode SIW filter but, on the other side, the footprint, with an area $l \times w$=690 mm^2 , is significantly diminished. It can be noted that, in a lower portion of the pass band, as reported in Fig. 29(*c*), the insertion loss is larger in both the measured and simulated results. To provide a physical insight of this phenomenon, a modal analysis has been performed.

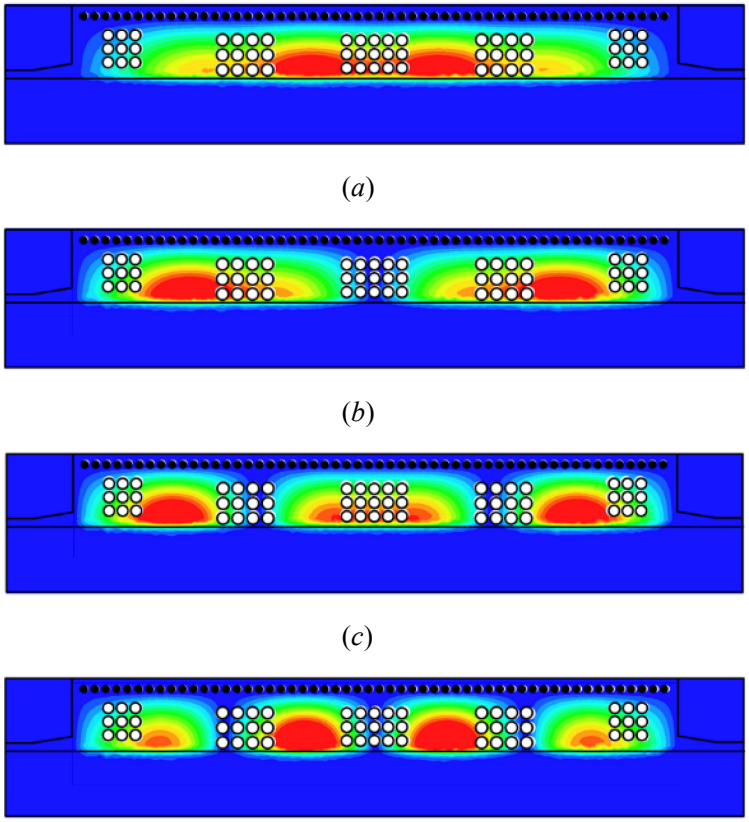

Fig. 30. Amplitude of the electric modal field of the first resonant modes of the perforated half-mode SIW cavity: (*a*) first mode; (*b*) second mode; (*c*) third mode; (*d*) fourth mode. [3]

In fact, the filter structure can be considered as a cavity resonator, supporting four resonant modes in the pass band of the filter. With the HFSS eigenvalue solver the mode spectrum was calculated. The eigenvalue analysis has been performed under two different boundary conditions of the air box surrounding the cavity: with perfect electric wall boundary condition (where losses depend on dielectric loss and finite metal conductivity, but there is no radiation), and with radiation condition (where also radiation leakage is considered). The electric field amplitude of the four modes is practically unchanged in the two cases, and it is plotted in Fig. 30. In TABLE II, the resonance frequencies and the quality factors of the modes are reported, for the two cases (no radiation and with radiation). The resonance frequencies of the four modes exhibit a very limited variation between the two cases, and practically coincide with the four poles of the frequency response of the filter (Fig. 29(c)).

Conversely, the quality factors are significantly affected by radiation: in particular, the first mode reduces its quality factor from 187 to 61. The physical explanation of this effect can be found in the field distribution along the open boundary of the half-mode SIW: in the first mode, the electric field exhibits a uniform phase, thus leading to a non-negligible radiation leakage. This reduction in the quality factor is more significant for the first and second mode, and it is marginal for the other two modes. For instance, in the fourth mode, the alternate phase of the electric field along the open boundary leads to very limited radiation. The variation of the modal quality factors determines the slope of the insertion loss of the filter.

6 PERFORATED FOLDED HALF-MODE SIW FILTER

An ulterior filter topology, starting from the half-mode structure, has been studied. As explained in the introduction, a folded filter configuration can be adopted reduce the radiation losses of the half-mode SIW filter (Fig. 31(*a*)). The face-to-face location of the open boundary limits the radiation losses in particular for the first cavity mode, because of the uniform phase along the entire open boundary. A different advantage of this topology is the ability to obtain a direct input-output coupling that determines a transmission zero in the frequency response.

A three-pole half-mode SIW filter in folded configuration was designed by using HFSS. The design is aimed to locate the transmission zero close to the pass band. The geometry of the filter and the final dimensions are shown in Fig. 31(*a*). Also for this prototype the same fabrication process has been used as previously mentioned (Fig. 31(*b*)). The comparison of simulated and measured scattering parameters is reported in Fig. 31(*c*), in the frequency band from 2.0 GHz to 7.0 GHz. The filter bandwidth, defined at 10 dB input matching, is 735 MHz in the simulation and 800 MHz in the measurement. The frequency of the transmission zero is 4.65 GHz in the simulation and 4.59 GHz in the measurement. The insertion loss at the central frequency f_0 = 3.65 GHz is 1.25 dB in the simulation and 1.20 dB in the measurement. The different contributions of losses, can be attributed to: 0.45 dB to the SIW filter loss (0.28 dB as dielectric loss and 0.17 dB as conductor loss) and 0.40 dB to transition losses (each of them). The contribution to the radiation loss is negligible (0 dB) and that results in a flat insertion loss, as shown in Fig. 11(*c*). The size of the circuit is practically identical to the half-mode SIW filter in Fig. 29, being the footprint area $(l+d_3+d_4)\times(2w+g)=693$ mm^2.

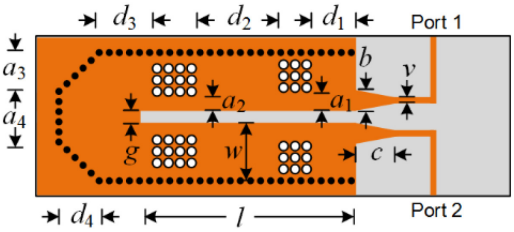

(*a*)

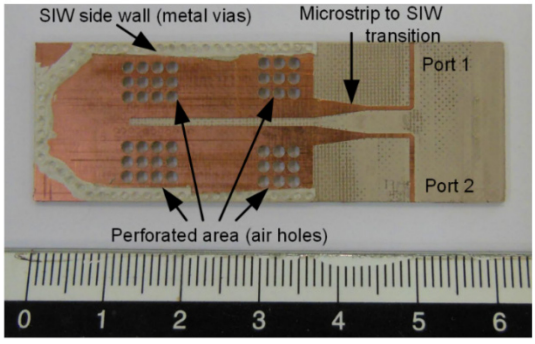

(*b*)

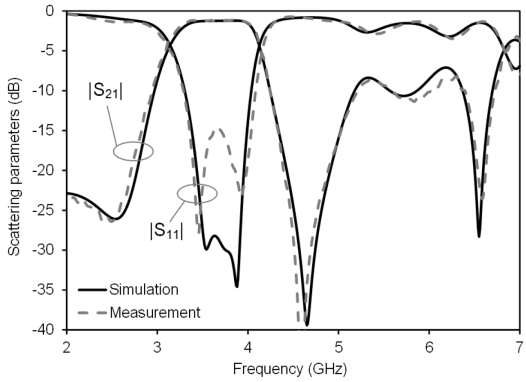

(*c*)

Fig. 31. Prototype of the first three-pole folded filter based on perforated half-mode SIW structure: (*a*) geometry of the filter (dimensions in mm: v=0.6, b=2.6, d_1=1.65, d_2=10.56, d_3=3.9, d_4=6.7, a_1=2.45, a_2=1.95, a_3=5, a_4=9.45, w=9.2, c=7, g=1, l=25.1); (*b*) photograph of the prototype; (*c*) scattering parameters of the three-pole filter (HFSS simulation compared with measured data). [3]

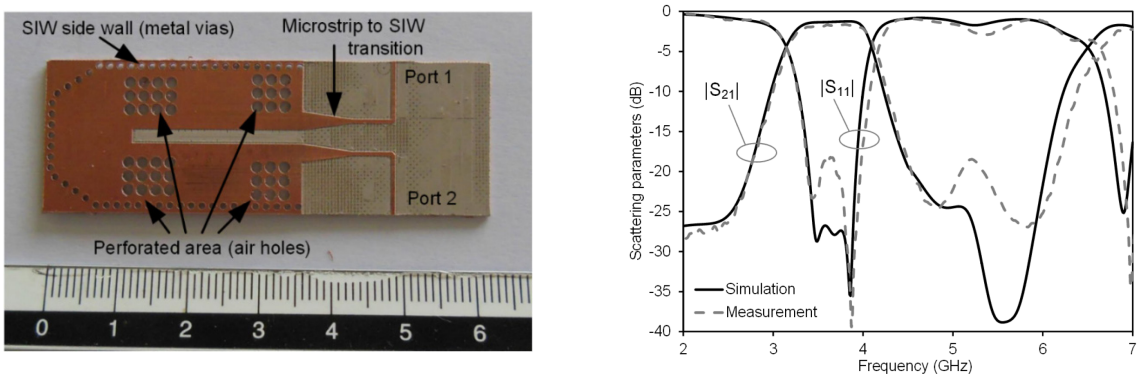

(*a*) (*b*)

Fig. 32. Prototype of the second three-pole folded filter based on perforated half-mode SIW structure (dimensions in mm: v=0.6, b=2.6, d_1=1.65, d_2=10.56, d_3=3.9, d_4=6.7, a_1=2.45, a_2=1.95, a_3=5, a_4=9.45, w=9.2, c=7, g=2, l=25.1): (*a*) photograph of the prototype; (*b*) scattering parameters of the three-pole filter (HFSS simulation compared with measured data). [3]

The ability change the position of the transmission zero is a fundamental request to show the full control on the filter design. For this reason different three-pole half-mode SIW filters in folded configuration were designed. The transmission zero frequency location is controlled with the geometrical parameter g (Fig. 31(*a*)). In a first design the transmission zero is placed close to pass-band of the filter. In a second design, the transmission zero was located at a higher frequency, with the aim to broaden the out-of-band rejection. The geometry of the filter is shown in Fig. 31(*a*), and the final dimensions are given in the caption of Fig. 32. A prototype has been fabricated by milling machining, and a picture of the filter is shown in Fig. 32(*a*). The comparison of simulated and measured scattering parameters is reported in Fig. 32(*b*), in the frequency band from 2.0 GHz to 7.0 GHz. The filter bandwidth, defined at 10 dB input matching, is 718 MHz in the simulation and 795 MHz in the measurement. A broad out-of-band rejection is found in the frequency response, with the transmission below -20 dB from 4.54 GHz to 6.02 GHz in the simulation, and from 4.54 GHz to 6.13 GHz in the measurement. The insertion loss at the central frequency f_0 = 3.65 GHz is 1.33 dB in the simulation and 1.68 dB in the measurement. Also in this case, the different contribution of losses have been investigated through simulations. Each transition contributes with a loss of 0.40 dB, whereas the SIW filter loss is 0.53 dB, which is attributed to dielectric loss (0.30 dB), conductor loss (0.19 dB), and very small radiation loss (0.04 dB). The size of the circuit is slightly larger than the one of the filter in Fig. 11, being the footprint area $(l+d_3+d_4)\times(2w+g)$=728 mm^2.

7 CONCLUSIONS

In this chapter a new class of SIW filter has been studied. These structures can be helpful in case of low-cost, mass-production filters. This new technique relies on the periodic perforation of the dielectric substrate to achieve an inductive iris filtering function. The periodic perforations, that realizes the immittance inverters, helps to realize low-cost filters, with a punching technique because of the tolerance strength to the fabrication tolerances. Starting from the full-mode SIW filter theory, a comparison with the inductive iris filter to highlight the advantages is presented. Other topologies have been studied to overcome the limitation related to the dimensions. For this reason, a half-mode SIW filter is studied, that reduces the overall footprint dimensions, with the disadvantage of the radiation losses through the open boundary. An ulterior evolution of this topology leads to the folded SIW filter that helps reducing the radiation losses of the Half-mode structure while maintaining the same overall footprint. Moreover the out-of-band rejection is improved with the introduction of source-to-load coupling that generates a transmission zero. This new class of SIW filter can be helpful in case of low-cost, mass-production filters.

REFERENCES

[1] L. Silvestri, E. Massoni, C. Tomassoni, A. Coves, M. Bozzi, and L. Perregrini, "Modeling and Implementation of Perforated SIW Filters," *IEEE MTT-S International Conference on Numerical Electromagnetic and Multiphysics Modeling and Optimization (NEMO2016)*, Beijing, China, July 27-29, 2016.

[2] L. Silvestri, E. Massoni, C. Tomassoni, A. Coves, M. Bozzi, and L. Perregrini, "A New Class of SIW Filters Based on Periodically Perforated Dielectric Substrate," *46th European Microwave Conf. (EuMC2016)*, London, UK, Oct. 3–7, 2016.

[3] L. Silvestri, E. Massoni, C. Tomassoni, A. Coves, M. Bozzi and L. Perregrini, "Substrate Integrated Waveguide Filters Based on a Dielectric Layer With Periodic Perforations," *IEEE Transactions on Microwave Theory and Techniques,* vol. 65, no. 8, pp. 2687-2697, Aug. 2017.

[4] A. Coves, E. Bronchalo, G. Torregrosa-Penalva, A.A. San-Blas, M.A. Sanchez-Soriano, A. Martellosio, and M. Bozzi, "A Novel Bandpass Filter Based on a Periodically Drilled SIW Structure," *Radio Science*, Vol. 51, No. 4, pp. 328–336, April 2016.

[5] M. Pasian, M. Bozzi, and L. Perregrini, "Low-cost Dichroic Mirrors Manufactured by Punching Technique," *Intern. Journal of Microwave and Wireless Technologies*, Vol. 3, No. 6, pp. 595–600, Dec. 2011.

[6] Y. Cassivi, L. Perregrini, P. Arcioni, M. Bressan, K. Wu, and G. Conciauro, "Dispersion Characteristics of Substrate Integrated Rectangular Waveguide," *IEEE Microw. Compon. Lett.*, Vol. 12, No. 9, pp. 333-335, Sept. 2002.

[7] M. Bozzi, A. Georgiadis, K. Wu, "Review of Substrate Integrated Waveguide (SIW) Circuits and Antennas," *IET Microwaves Antennas Propag.,* Vol. 5, No. 8, pp. 909-920, June 2011.

[8] A. Patrovsky and Ke Wu, "Substrate integrated image guide (SIIG) - a low-loss waveguide for millimetre-wave applications," *2005 European Microwave Conference*, Paris, 2005, pp. 4 pp.-900.

[9] A. Patrovsky and Ke Wu, "Substrate integrated image guide (SIIG)-a planar dielectric waveguide technology for millimeter-wave applications," *IEEE Transactions on Microwave Theory and Techniques*, vol. 54, no. 6, pp. 2872-2879, June 2006.

[10] Tlaxcalteco-Matus, M. A. and Torres-Torres, R., "Modeling a SIW filter with IRIS windows using equivalent circuits," *Microw. Opt. Technol. Lett*., 2012 54: 2865-2868.

[11] S. Moscato, N. Delmonte, L. Silvestri, M. Bozzi and L. Perregrini, "Half-mode versus folded SIW filters: Modeling and design," *2015 IEEE MTT-S International Conference on Numerical Electromagnetic and Multiphysics Modeling and Optimization (NEMO)*, Ottawa, ON, 2015, pp. 1-3.

[12] G. Macchiarella, C. Tomassoni, E. Massoni, M. Bozzi and L. Perregrini, "A novel class of half-mode SIW filters with extracted poles," *2017 47th European Microwave Conference (EuMC)*, Nuremberg, 2017, pp. 807-810.

[13] M. Salehi, J. Bornemann and E. Mehrshahi, "Compact folded substrate integrated waveguide filter with non-resonating nodes for high-selectivity bandpass applications," *2013 European Microwave Conference*, Nuremberg, 2013, pp. 155-158.

Chapter 3

NOVEL CLASS OF BANDPASS FILTERS BASED ON A DUAL-MODE AIR-FILLED SIW CAVITY

[1][2][3]

In this Chapter a novel class of filters based on a dual-mode air-filled SIW cavity is presented.

In filter design, when size-reduction is a necessity, the use of dual-mode cavities appears as a very promising solution. As shown in Chapter 1, different topologies can be used to reduce the overall footprint such as Folded SIW [6], Half-mode [7] or Quarter-mode cavities [8]. The drawbacks are primarily related to a more complex fabrication or to the higher radiation losses due to the open boundaries, respectively. In Chapter 2, the design of a new class of low-cost SIW filters was introduced (based on the periodic perforation of the dielectric substrate), along with the topologies able to reduce the size (maintaining a simple structure) whilst still achieving relatively high performances. However, the out-of-band rejection performances are still limited. Differently, the use of dual-mode cavities helps to reduce the overall dimensions of the filter - still maintaining a simple structure - and introduces transmission zeros through non-resonating modes to improve the out-of-band performances ([9], [10], [11], [12] and [13]). In addition, the air-filled structure is able to reduce the losses and increase the power handling capability ([14], [15]). In this design, the two features are combined. The air parts, obtained by partially removing the dielectric material inside the SIW cavity (Fig. 33), allow the resonance frequency of the first cavity modes to be controlled, creating a doublet. This structure was initially proposed in [1] with a SIW feeding line and further extended in [2] in which the cavity is fed by a microstrip line. In [3], a modal analysis of the air-filled cavity resonator and a detailed study of the dual-mode air-filled SIW cavity demonstrate how to control the filtering characteristics. The basic doublet has been used as a building block for the design of higher order filter (five-pole filter). The dual-mode air-filled SIW cavity realizes compact filters with the advantage of a low cost structure. In addition, the out-of-band rejection is improved by adding and controlling the position of transmission zeros. All these results, are in [1], [2] and [3].

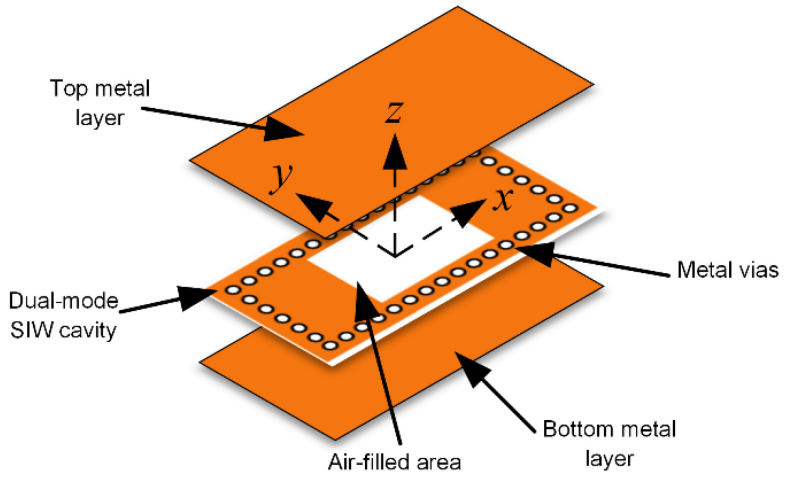

Fig. 33. Geometry of the dual-mode air-filled SIW cavity.

1 THEORY OF DUAL-MODE AIR-FILLED CAVITY

This Section introduces an equivalent model for the analysis of a dual-mode air-filled cavity. More specifically, various analyses, based on the theoretical model introduced, have been carried out, relating the filter characteristics to the geometrical parameters. Generally speaking, the resonance frequencies of the cavity modes can be obtained with time-consuming eigenmode simulations. At first this approach has been used as reported in [1] and [2]. The ability to define an efficient transmission line theoretical model to derive a characteristic equation of the air-filled cavity, simplifies the approach.

The partially air-filled cavity is divided in three homogeneous portions (a central air-filled part and two external dielectric filled parts), and each portion is described as a transmission line. The equivalent waveguide approximation [4] is adopted, and therefore a solid-wall rectangular cavity is considered. Finally, a transverse resonance technique is used to achieve the resonance modes of the overall (piecewise homogeneous) cavity. Namely, the solution of the characteristic equation provides a relation between the TE_{mn} cavity mode resonant frequencies and the cavity dimensions.

Fig. 34(*a*) represents an air-filled cavity of transversal length A and longitudinal length B. The height of the cavity is small compared to A and B, because a SIW structure is considered. The dielectric is removed from the central part of the cavity (air-filled region) of relative permittivity $\varepsilon_{r0}=1$ and length a. The lateral portions of the cavity are still dielectric filled with relative permittivity ε_{r1} (Fig. 34 (*a*)). Fig. 34 (*b*) shows the equivalent transmission line model of the cavity. The short-circuited dielectric loaded regions are represented by a homogeneous transmission line of length $l_1=(A-a)/2$ with TE_{mn} mode guide impedance Z_{1mn}, propagation constant β_{1mn} and dielectric permittivity $\varepsilon_{r1}>1$.

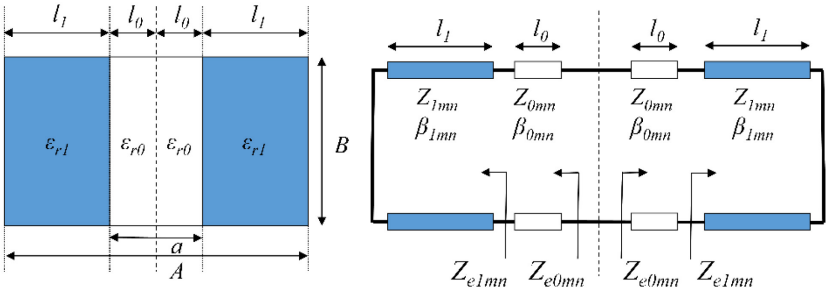

(*a*) (*b*)

Fig. 34. Simplified model of the air-filled cavity: (*a*) air-filled cavity with its sections; (*b*) equivalent transmission-line model. [3]

Instead, the central air-filled region is modelled as two sections of length $l_0=a/2$ with TE_{mn} mode guide impedance Z_{0mn}, propagation constant β_{0mn} and dielectric permittivity $\varepsilon_{r0}=1$. The guide impedance and propagation constant of both types of equivalent transmission lines are given by:

$$\beta_{mn}=\sqrt{\left(2\pi f\sqrt{\mu_0\varepsilon_0\varepsilon_{r0,1}}\right)^2-\left(\frac{n\pi}{B}\right)^2} \tag{18}$$

and

$$Z_{mn} = \sqrt{\frac{\mu_0}{\varepsilon_0 \varepsilon_{r0,1} - \left(\frac{n}{2Bf\sqrt{\mu_0}}\right)^2}} \tag{19}$$

where f is the frequency, μ_0 is the vacuum permeability and ε_0 is the vacuum permittivity.

From transmission line theory, the Z_{e1mn} equivalent impedance shown in Fig. 34(*b*) is determined by:

$$Z_{e1mn} = jZ_{1mn}\tan(\beta_{1mn} l_1) \tag{20}$$

Then, the equivalent impedance Z_{e0mn} at the cavity symmetry plane looking toward one side is given by:

$$Z_{e0mn} = Z_{0mn} \frac{Z_{e1mn} + jZ_{0mn}\tan(\beta_{0mn} l_0)}{Z_{0mn} + jZ_{e1mn}\tan(\beta_{0mn} l_0)} \tag{21}$$

For odd modes (odd values of m), at the cavity resonance, the imaginary part of (21) is:

$$\mathrm{Im}(Z_{e0mn}) = \infty \tag{22}$$

whereas, for even modes (even values of m), at the cavity resonance, the imaginary part of (21) is:

$$\mathrm{Im}(Z_{e0mn}) = 0 \tag{23}$$

To solve (22) and (23), the Newton–Raphson method can be used to determine the cavity resonance frequencies [5].

For illustration purposes, the total cavity length considered is $A = 50$ mm and a dielectric permittivity $\varepsilon_{r1} = 10.5$. Fig. 35(*a*) and Fig. 35(*b*), reports the first four cavity mode resonance frequencies obtained solving (22) and (23) of air-filled cavities of width $B = 19$ mm and 22.5 mm, respectively, versus the air-filled area length a. It should be noted that the cavity mode resonance frequencies are related to both the geometrical parameters a and B.

The first two cavity modes (namely, TM_{110} and TM_{210}, where TM is defined respect with the z axis of Fig. 33) have a small resonant frequency separation when the value a is comprises between 10 mm and 35 mm. This result can be explained considering the TM_{110} and TM_{210} modal fields: when the cavity is dielectric-filled, the former is maximum at the center of the cavity, whilst the latter is null that of the mode is null (Fig. 36(*a*)). Therefore, it follows that, when removing the dielectric in the central portion of the cavity, the TM_{110} mode is more affected than the TM_{210} mode, as shown in Fig. 36(*b*). The consequence is that the frequency separation between the two modes can be controlled, playing on the geometrical parameter a.

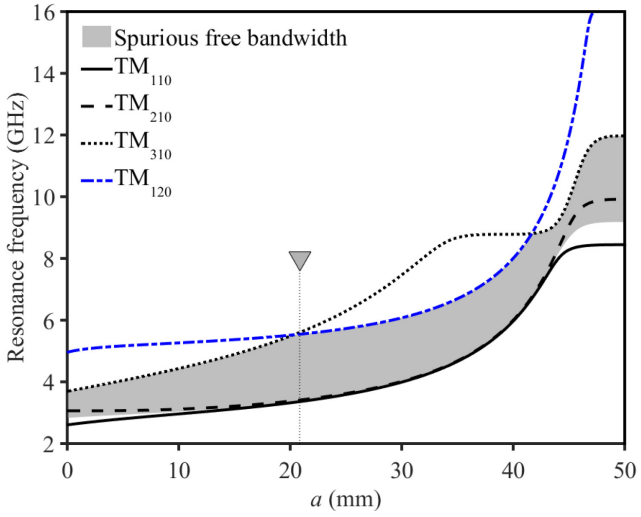

(*a*)

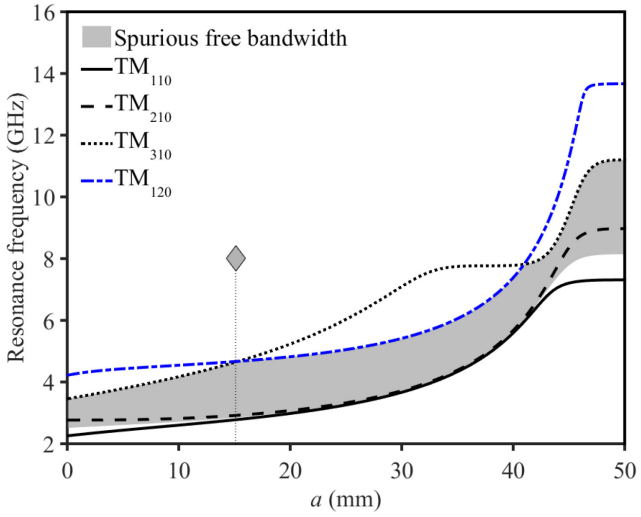

(*b*)

Fig. 35. Calculated first four cavity modes resonance frequencies and spurious free bandwidth versus parameter a (with A = 50 mm and ε_{r1} = 10.5): (*a*) B = 19 mm (▼ marker at optimum spurious free bandwidth); (*b*) B = 22.5 mm (♦ marker at optimum spurious free bandwidth). [3]

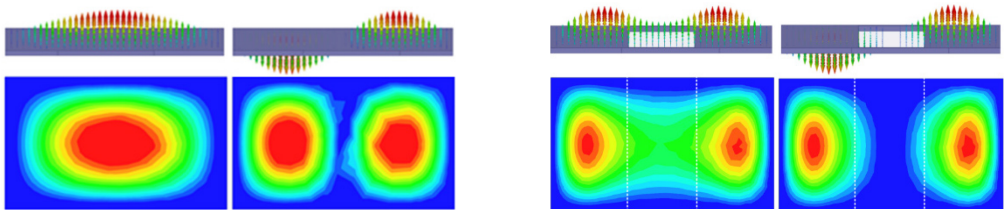

(*a*) (*b*)

Fig. 36. Electric modal field of the TM_{110} and TM_{210} (and related signs): (*a*) in dielectric-filled cavity; (*b*) in air-filled cavity. [3], [2] and [1]

The relative frequency separation Δf between the TM_{110} and TM_{210} modes, given by:

$$\Delta f = \frac{2\,(f_{TM110} - f_{TM210})}{f_{TM110} + f_{TM210}} \tag{24}$$

can be obtained by varying the geometrical parameter a whilst retaining a specific value of B (Fig. 37). If a lower relative frequency separation is needed, a smaller value of B should be used maintaining a fixed. The frequency separation can be easily decreased until a=35 mm (Fig. 37). With a>35mm, the cavity becomes similar to a hollow cavity, increasing dramatically the relative frequency separation

The spurious free bandwidth of the dual-mode air filled cavity is limited by the first superior order mode. It is defined as the difference between the third mode resonance frequency and the central frequency f_c (25).

$$f_c = \frac{f_{TM110} + f_{TM210}}{2} \tag{25}$$

$$BW = \frac{\min(f_{TM310}, f_{TM120}) - f_c}{f_c} \tag{26}$$

In particular, in Fig. 35, the third and fourth mode resonance frequencies are plotted. It can be noted that either the TM_{310} or the TM_{120} modes can be the first superior mode, depending on the dimension a. The spurious-free bandwidth BW is shown in Fig. 37 versus a. Optimum values are obtained for a = 15.1 mm and B = 19 mm (▼ marker) and a = 20.85 mm and B = 22.5 mm (♦ marker), respectively. These optimum values correspond to the smallest value a in Fig. 35, at which the TM_{120} mode become the third resonating mode.

Particular cases can be found with a=0 mm (empty cavity) and a=50 mm (dielectric filled cavity). These represent the homogeneous cavities where, as shown in Fig. 37, the resonance frequency separation is maximum. In addition, the frequency separation also depends on B and therefore can be controlled by the ratio A/B.

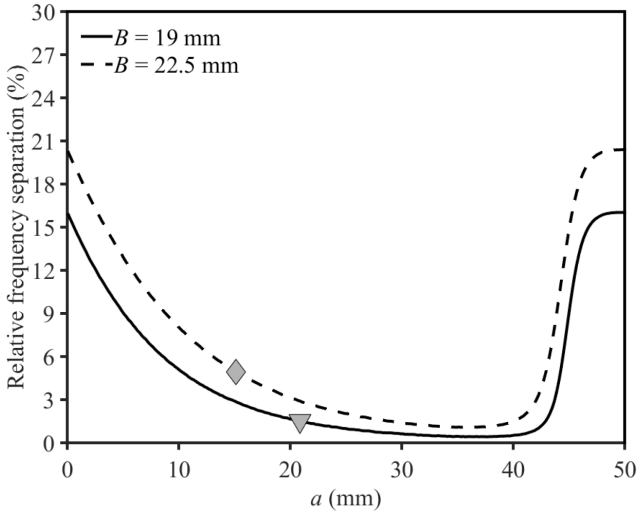

Fig. 37. Relative resonance frequency separation versus a for B = 19 mm and 22.5 mm (with A = 50 mm and ε_{r1} = 10.5). [3]

In order to define a guideline for the filter design, Fig. 38 summarizes: central frequency f_c (two-dimensional plot); relative resonance frequency separation (isocurves - black straight lines) and relative spurious free bandwidth (isocurves - white straight lines). The geometrical parameters a and B are varied to create each set. For a specific set of f_c and frequency separation, two sets of values a and B can be chosen but only one leads to a larger spurious-free bandwidth. A relative spurious-free bandwidth (represented by a white dotted line) exceeding 60% separation can be obtained using a selection of a and B. In addition, the resonance frequency separation can be adjusted within the range exceeding 60% spurious free bandwidth.

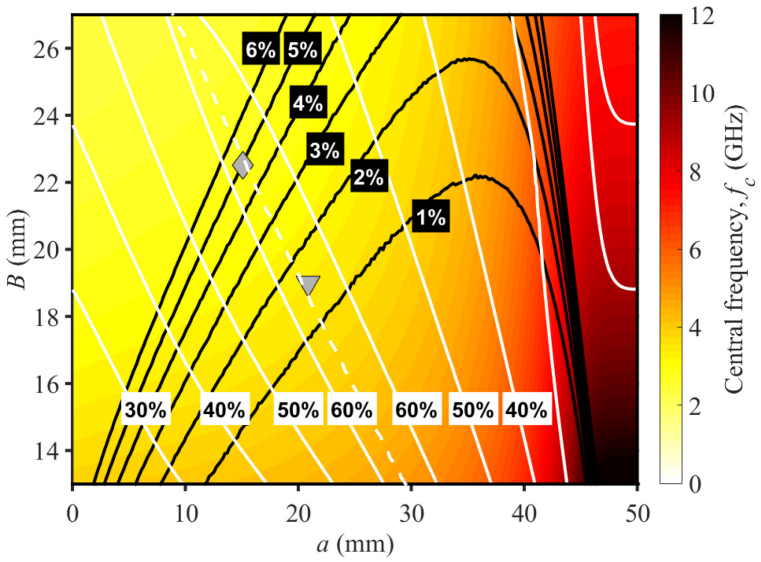

Fig. 38. Theoretical central frequency f_c with isocurves of the relative resonance frequency separation (black straight lines), relative spurious free bandwidth (white straight lines) and optimal relative spurious free bandwidth (white dotted line) versus dimensions a and B (A = 50 mm, ε_{r1} = 10.5, ▼ marker for B=19mm, ♦ marker for B=22.5mm). [3]

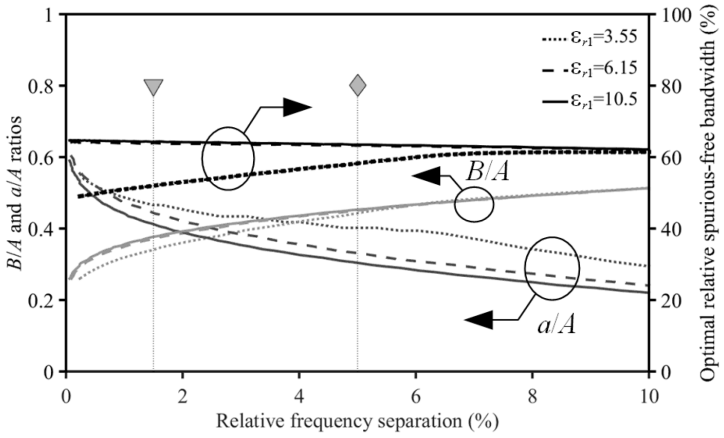

Fig. 39. Optimal spurious free bandwidth (black lines) and corresponding B/A ratio (dark gray lines) and a/A ratio (light gray lines) versus relative resonance frequency separation (ε_{r1} = 3.55, 6.15 and 10.5) [3]

In Fig. 39, three different values of ε_{r1} (10.5, 6.15 and 3.55) have been considered. This graph provides an optimal spurious-free bandwidth with corresponding ratios B/A and a/A for high, medium and low ε_{r1}, respectively, with a desired relative resonance frequency separation. In order to create uniformity, all considered parameters are normalized with respect to A. The relative spurious free bandwidth ranges from 62% to 65% for all three substrates. The procedure to design an optimal spurious-free bandwidth dual-mode cavity consists of selecting, in Fig. 39, the dimensional ratios for a desired relative resonance frequency

separation. Then the overall cavity length A is adjusted, whilst keeping constant ratios to obtain the desired central frequency f_c.

2 DETAILED INVESTIGATION OF THE DOUBLET

The doublet, capable of two poles and two transmission zeros, based on the air-filled dual-mode SIW cavity, is here analyzed and studied. The air-filled dual-mode SIW cavity implements the topology of Fig. 40. The pass-band of the filter is related to the resonance frequencies separation between the first two cavity modes (f_1 and f_2). In order to implement the topology of Fig. 40, three coupling values with the same sign and the fourth with an opposite sign are necessary. It is shown that, for this reason, the input/output feedings are positioned anti-symmetrically respect to the center of SIW cavity.

Two different external excitations of the resonator (playing the role of source S and load L in the topology of Fig. 40) have been studied; SIW waveguide excitation [1] and microstrip excitation [2].

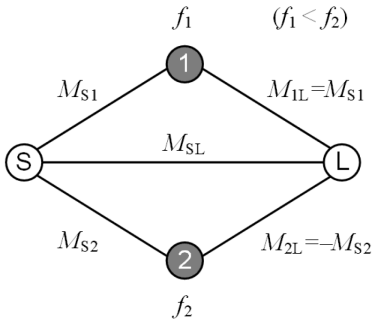

Fig. 40. Transversal topology of the doublet, impleented by using the air-filled dual-mode SIW cavity. [3], [2]

Starting with the SIW waveguide input/output, illustrated in Fig. 43(*a*), the coupling with the first two resonant modes can be controlled by the inductive iris of width w. The larger the width w, the higher the couplings (M_{S1} and M_{S2}). The asymmetric position, s, of the input-output (with respect of the center of the cavity) is used to separately control M_{S1} and M_{S2} and realizes the coupling with the opposite sign of Fig. 40. The control of the couplings and, therefore, on the location of the transmission zeros, is shown in case of microstrip line feeding (Fig. 45) but it is valid also in this specific case.

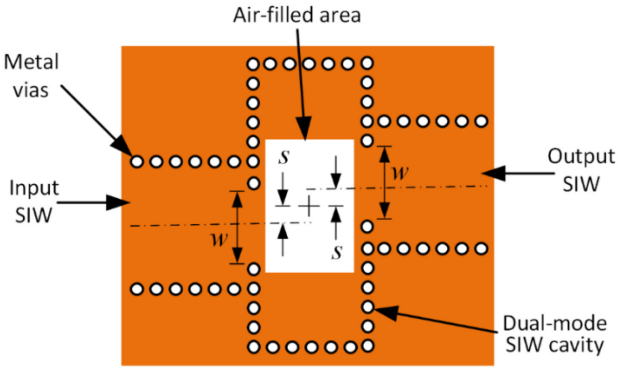

Fig. 41. Geometry of the doublet fed by SIW waveguides. [1], [3]

A first frequency response of the filter has been plotted, comparing the coupling matrix and the full-wave simulation (Fig. 42).

	S	1	2	L
S	0	1.4959	0.4668	0.1854
1	1.4959	1.0975	0	1.4959
2	0.4668	0	-1.0975	-0.4668
L	0.1854	1.4959	-0.4668	0

(*a*)

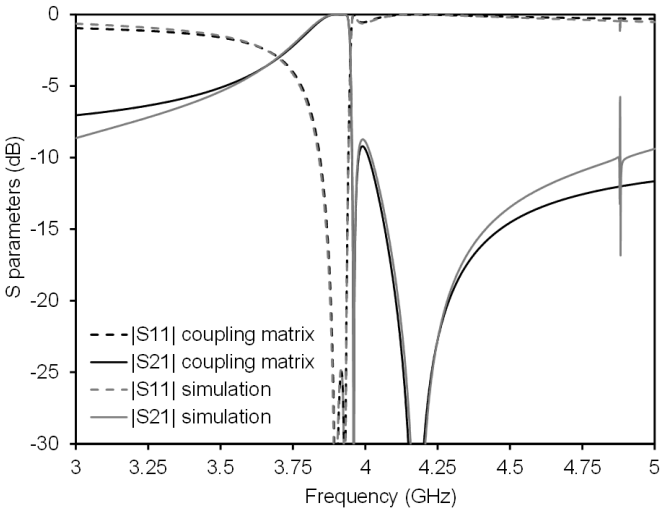

(*b*)

Fig. 42. Frequency response of the filter: (*a*) coupling matrix; (*b*) comparison with full-wave simulation. [1]

Considering the different feeding method, microstrip lines can be adopted to reduce the overall size. Feeding lines excite the resonator through apertures obtained by removing several side-wall posts (Fig. 43). The coupling is predominantly controlled by the microstrip taper (*c* and *h*) and by the aperture of width *e* that resembles the effect of the value *w* of the previous case. According to Fig. 43 and considering the symmetric electric field distribution of the fundamental mode (Fig. 36(*b*), left), M_{S1} and M_{1L} couplings have an identical sign. Conversely, the asymmetric distribution of the second mode electric field (Fig. 36(*b*), right) leads to coupling values M_{S2} and M_{2L} with the opposite sign. The first transmission zero is controlled, as aforementioned, with the offset *s* shown in Fig. 43. Also in this case, the second transmission zero is obtained for the direct source-to-load coupling and it is affected, indirectly, by the changing of the parameter *s*. Fig. 44 shows the comparison between the full-wave simulation of a second order filter with the relevant coupling matrix.

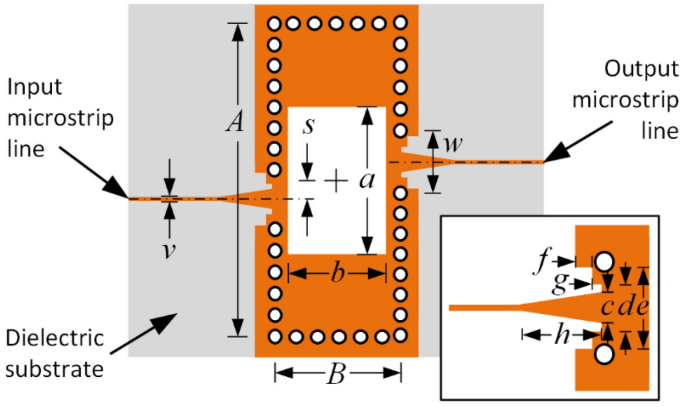

Fig. 43. Geometry of the doublet and geometrical dimensions. [2]

	S	1	2	L
S	0	1.0413	0.7456	0.0233
1	1.0413	1.8353	0	1.0413
2	0.7456	0	-1.4141	-0.7456
L	0.0233	1.0413	-0.7456	0

(*a*)

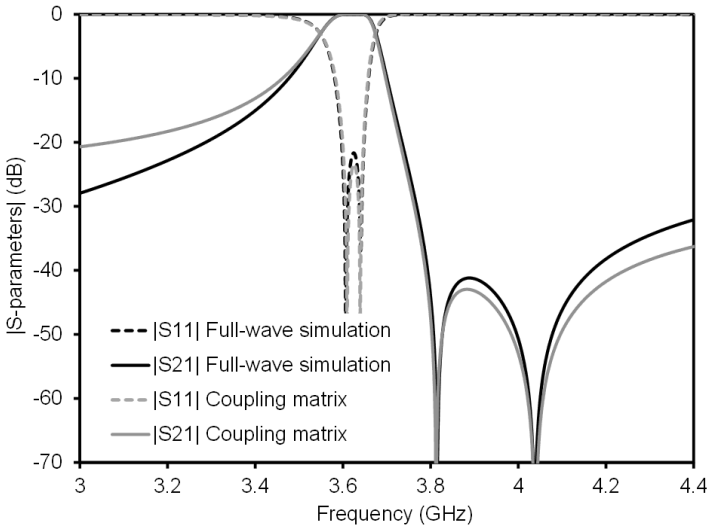

(*b*)

Fig. 44. Frequency response of the filter with a microstrip feeding line: (*a*) coupling matrix; (*b*) comparison with simulation. [2]

The control of the transmission zeros is shown in Fig. 45. Considering the position of the feeding lines centered (s=0), only one mode of the cavity is excited by the microstrip line (Fig. 36(*b*)). This results in a frequency response of the structure with one single pole (Fig. 45(*a*)). The single transmission zero is a result of the source-to-load coupling, and it is due to proximity between input/output. Increasing the offset s of a small amount two poles appear (corresponding to the first two cavity modes) and two transmission zero, one of them very close to pass-band (Fig. 45(*b*)). Of course, modifying the offset s allows the ratio between the couplings of the two modes as well as the direct source-to-load coupling to be controlled. When s increases, the ratio M_{S1}/M_{S2} decreases, due to the modal field pattern (Fig. 36(*b*)), and the M_{SL} coupling also decreases, due to larger separation of the input and output ports. For this reason, the positions of both transmission zeros

are shifted in the same direction. Two more examples are shown in Fig. 45(*c*) and Fig. 45(*d*), where the value of *s* is larger and the transmission zeros are shifted far from the pass-band.

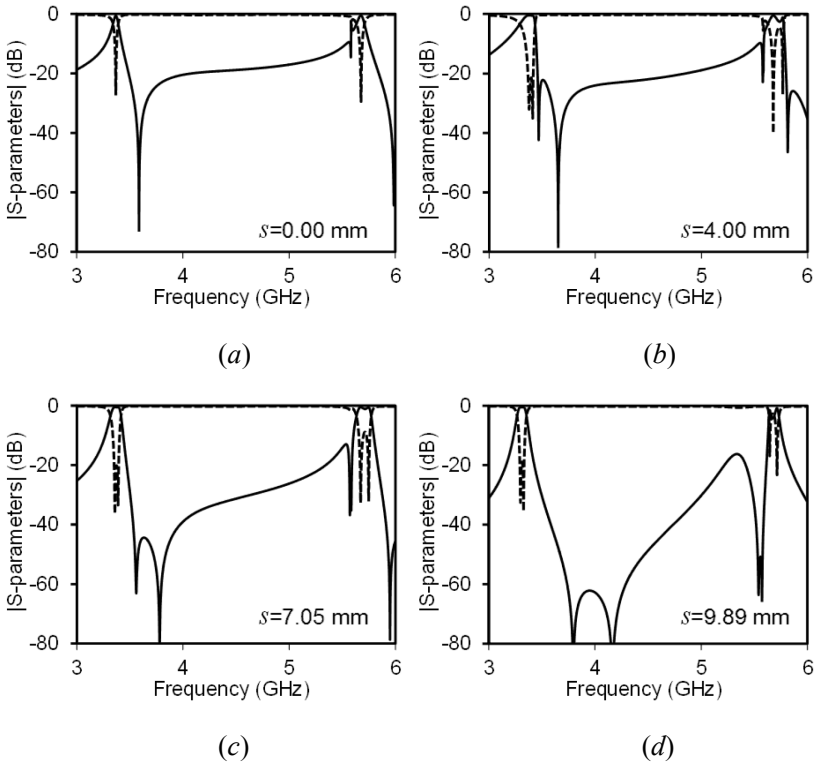

Fig. 45. Investigation of the control of the first transmission zero in the two-pole filter with 1.5% relative fractional bandwidth and 20-dB input matching: (*a*) symmetric structure; (*b*) very close transmission zero; (*c*) relatively close transmission zero; (*d*) far transmission zero [3]

2.1 Design of doublets

In order to demonstrate the ability to fully control the filter characteristics starting from the geometrical parameters, two doublets have been designed, with 1.5% and 5% relative frequency separation. In addition different pass-band input matchings (10 dB, 20 dB, and 30 dB) have been simulated. Considering a small external coupling (10dB pass-band input matching), the almost identical frequency positions of the poles and the resonance frequencies of the cavity modes can be demonstrated.

The control of the location of the transmission zeros is shown in the specific case of 1.5% relative frequency separation. The same procedure can be applied to the other cases.

2.1.1 1.5% relative frequency separation

The first doublet is based on the cavity with 1.5% relative frequency separation. The geometrical dimensions of the cavity in TABLE III have been used (except the transformation from effective dimensions to actual dimensions, according to the equivalent waveguide concept [4]). The simulation results (from Ansys HFSS) are shown in Fig. 46. It is possible to modify the input matching by altering the external coupling. With a 10 dB input matching, corresponding to a small external coupling, the position of the two poles of the frequency response are located at 3.355 GHz and 3.401 GHz, respectively.

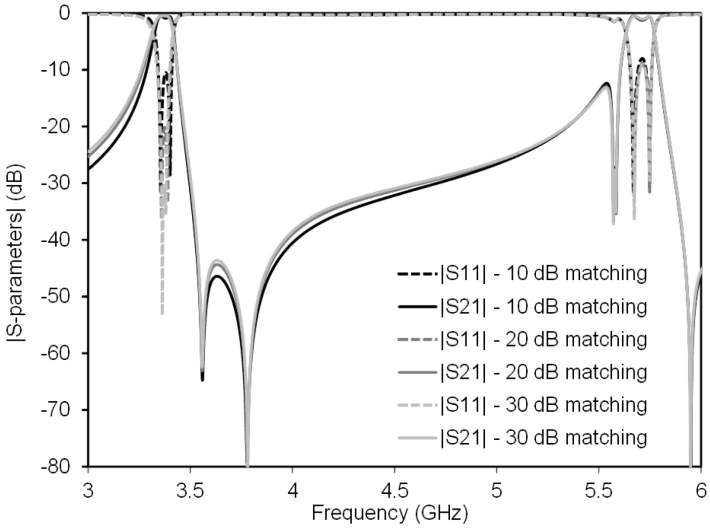

(*a*)

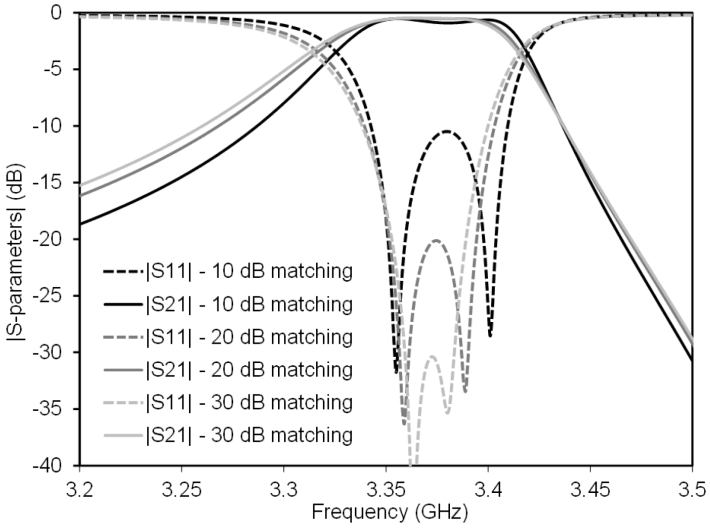

(*b*)

Fig. 46. Design of a two-pole filter with 1.5% fractional bandwidth: (*a*) pass-band simulation of three cases, with 10 dB, 20 dB, and 30 dB input matching; (*b*) detail of the pass-band. [3]

TABLE III
PARAMETERS ANALYTICALLY CALCULATED FOR
1.5% AND 5% RELATIVE FREQUENCY SEPARATION

Two-resonance cavity	▼	♦
A (mm)	50	50
B (mm) | *B*/*A*	19 | 0.38	22.5 | 0.45
a (mm) | *a*/*A*	20.85 | 0.417	15.1 | 0.302
TM_{110} resonance frequency (GHz)	3.359	2.778
TM_{210} resonance frequency (GHz)	3.410	2.919
Relative frequency separation (%)	1.5	5
Central frequency, f_c (GHz)	3.385	2.849
First higher order mode resonance (GHz)	5.543	4.647
Relative spurious free bandwidth (%)	63.70	63.16

These values are almost equivalent with the resonance frequencies of the cavity modes, reported in TABLE III (3.359 GHz and 3.410 GHz). The resulting fractional bandwidth is 1.36%. The first spurious pass-band appears at 5.574 GHz, with a weak coupling of the mode supposed to resonate at 5.543 GHz in TABLE III. Increasing the external coupling leads to a better input matching, whilst maintaining the spurious-free bandwidth and without affecting the position of the transmission zeros (Fig. 46). The relative frequency separation, as shown in Fig. 46, decreases.

2.1.2 5% relative frequency separation

The same approach has been followed for the design of a second doublet, based on the cavity with 5.0 % relative frequency separation, whose dimensions are shown in TABLE III. Also, in this case, the dimensions are unchanged (with the exception of the transformation from equivalent waveguide to actual dimension). The transitions have been optimized to achieve a filtering function with 10 dB, 20 dB, and 30 dB input matching in the pass-band (Fig. 47).

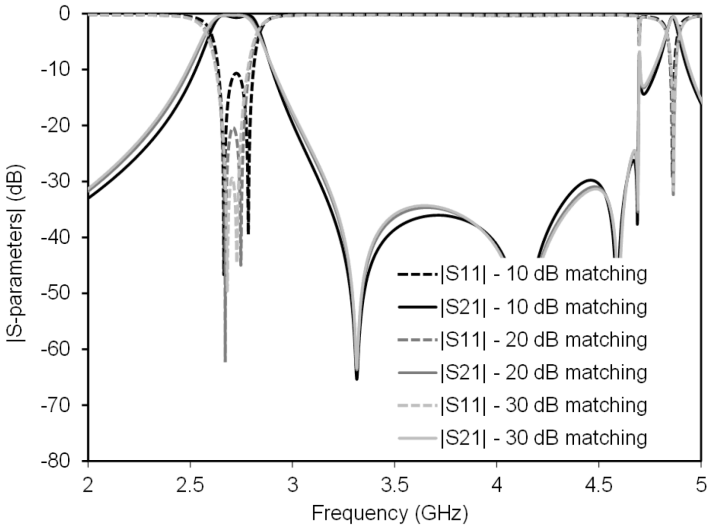

(*a*)

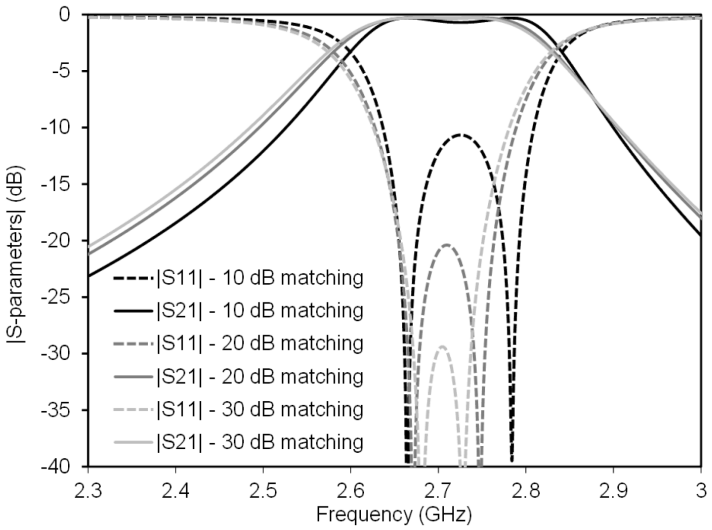

(*b*)

Fig. 47. Design of a two-pole filter with 5.0% relative fractional bandwidth: (*a*) wideband simulation of three cases, with 10 dB, 20 dB, and 30 dB input matching; (*b*) detail of the pass-band. [3]

In the case of 10-dB matching (corresponding to weak external coupling), the poles of the frequency response appear at 2.664 GHz and 2.784 GHz, corresponding to a fractional bandwidth of 4.41%. If the filter is optimized to achieve a better input matching, the frequency separation decreases as in the previous example.

2.2 Fabrication and measurements

Different filters have been realized and measured to confirm the theoretical study. Considering the previous designs, the filters with 1.5% and 5% fractional pass-bandwidths (dimensions in TABLE IV and TABLE V) and 20 dB input matching in the pass-band have been fabricated. In addition, the filter with 1.5% fractional pass-bandwidth and transmission zero far from the pass-band (dimensions in TABLE VI) is fabricated. The dielectric laminate is the Taconic CER-10 (with relative dielectric permittivity ε_{rl}=10.5, loss tangent tanδ=0.0035, and thickness 1.27 mm). The structures have been realized with the milling machine LPKF E33 and the metal vias have been metallized with the LPKF ProConduct paste. The photographs (Fig. 48(*a*), Fig. 49(*a*), Fig. 50(*a*)) show the prototypes before the metallization of the metal vias and the closing of the top/bottom air-filled area by copper sheets. The copper sheets at the top and bottom of the air-filled area have been applied and soldered as close as possible to the perforated region. Measurements have been performed using an Anritsu Universal Test Fixtures (UTF) 3680 and an Anritsu 37347C vector network analyzer (VNA). No de-embedding was applied to the measured results, to remove the effects of connectors and transitions. The comparison between simulations and measurements is shown in Fig. 48(*b*) and Fig. 49(*b*). The measured insertion losses in the pass-band are slightly larger in the measured results than in the simulated. The overall agreement between simulation and results is very good, even in the out-of-bands.

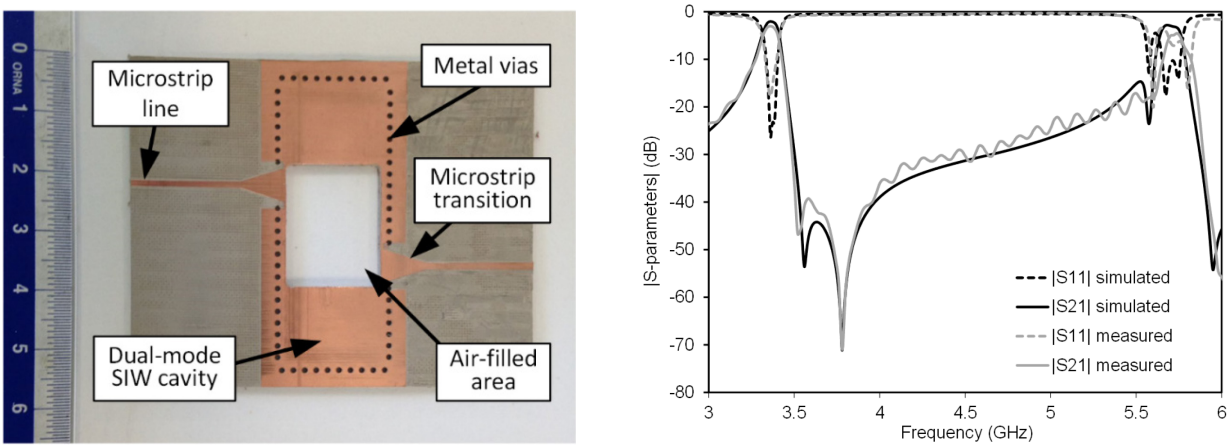

(*a*) (*b*)

Fig. 48. Realized and measured two-pole filter with 1.5% relative fractional bandwidth and 20-dB input matching: (*a*) photograph of the prototype (before vias metallization and air-filled area covering); (*b*) comparison between simulation and measurement. [3]

TABLE IV
DIMENSIONS OF THE FILTER IN FIG. 48 (IN MM)

A=50.54	*B*=19.54	*a*=21.39	*b*=16.54
c=5.85	*d*=7.85	*e*=8	*f*=3
g=1	*h*=7.85	*s*=7.05	*w*=8

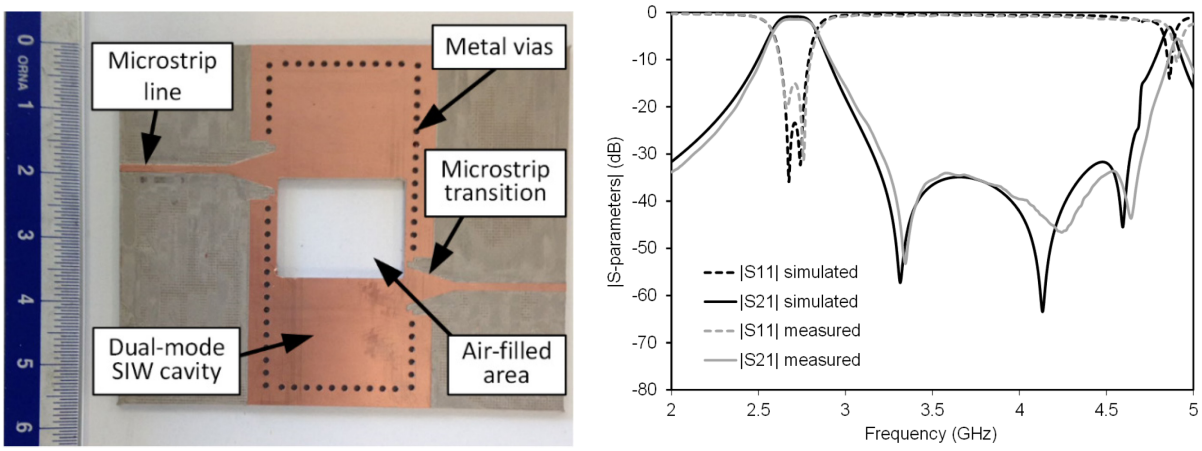

(*a*) (*b*)

Fig. 49. Realized and measured two-pole filter with 5.0% relative fractional bandwidth: (a) photograph of the prototype; (b) comparison between simulation and measurement. [3]

TABLE V
DIMENSIONS OF THE FILTER IN FIG. 49 (IN MM)

A=50.54	*B*=23.04	*a*=15.64	*b*=20.04
c=5.85	*d*=7.85	*e*=9	*f*=3
g=1	*h*=7.5	*s*=9.05	*w*=9

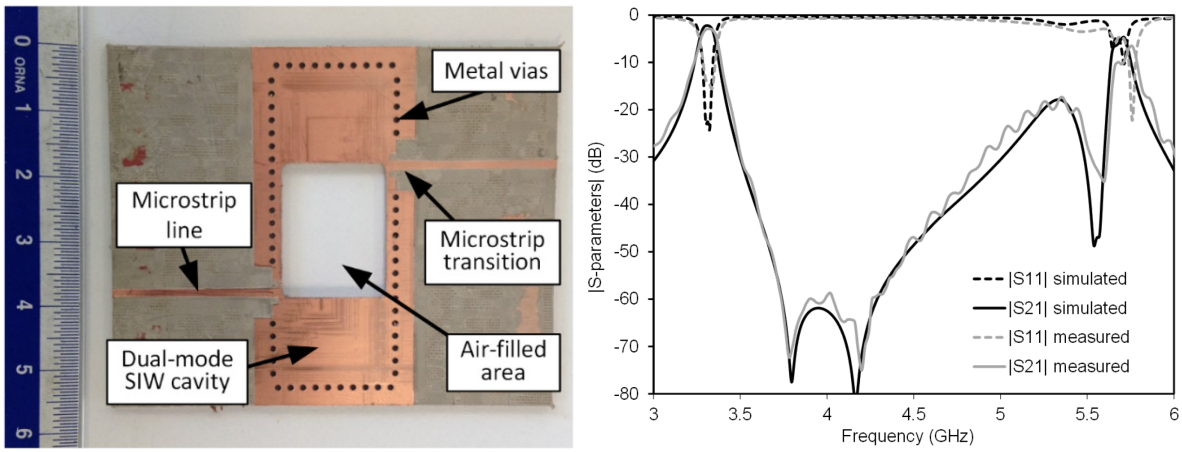

(*a*) (*b*)

Fig. 50. Realized and measured two-pole filter with 1.5% relative fractional bandwidth and far transmission zero: (*a*) photograph of the prototype; (*b*) comparison between simulation and measurement. [3]

TABLE VI
DIMENSIONS OF THE FILTER IN FIG. 50 (IN MM)

A=50.54	*B*=19.54	*a*=21.39	*b*=16.54
c=1.5	*d*=3.5	*e*=8	*f*=3
g=1	*h*=7.5	*s*=9.89	*w*=8

3 DESIGN OF HIGHER ORDER FILTER

From the doublet structure defined and studied previously, higher order filters can be obtained cascading doublets through non-resonating nodes. Adopting this procedure doublets are first designed separately and then cascaded. The transmission zeros of each doublet are still present in the cascaded structure, and their position is preserved. Non-resonating nodes can be obtained with different methods: a quarter-wave transmission line sections, as in [11] and [13], can implement non-resonating nodes. After the design, if necessary, it is possible to reduce the quarter-wave section by re-optimizing the whole filter to obtain a more compact structure.

A different method implies the use of half-wave sections [11] with a procedure similar to the one based on quarter-wave sections. The advantage is the ability to introduce, if necessary, an additional filter pole due to the resonance of the half-wave section, with a larger structure (respect to the quarter-wave method).

In order to confirm the ability to design higher order filters with this methods, one of them is here shown. A five-pole filter consisting of two doublets cascaded through a half-wave transmission line Section has been designed. The filter is centered at 2.875 GHz and its fractional bandwidth is 7.5%. The coupling matrix is shown in Fig. 51 and the relevant topology in Fig. 52. According to Fig. 53(*a*), for the implementation of this topology, doublets with microstrip feeding on one side and SIW feeding on the other side have been selected. This allows the five-pole filter to be fed by microstrip lines, whereas the central resonator, consisting of half-wave transmission lines, is a SIW cavity, thus obtaining better performance in terms of losses.

The manufactured technique is the same used in the fabrication of the previous filters. The realized prototype is shown in Fig. 53(*b*) with dimensions in TABLE VII. Comparison between results and the full-wave simulation are presented in Fig. 53(*c*). A double transmission zero in the upper stop-band, consistent in two identically located in frequency zeros (each doublet generates a transmission zero in the same position), is present because of the symmetry of the structure. This double zero is very close to the filter band and guarantees a very high selectivity.

	S	1	2	3	4	5	L
S	0	0.949	0.509	0	0	0	0
1	0.949	0.506	0	0.799	0	0	0
2	0.509	0	-1.132	-0.056	0	0	0
3	0	0.799	-0.056	0.295	-0.056	0.799	0
4	0	0	0	-0.056	-1.132	0	0.509
5	0	0	0	0.799	0	0.506	0.949
L	0	0	0	0	0.509	0.949	0

Fig. 51. Coupling matrix of the five-pole filter, with FBW = 7.5% and f_c at 2.875 GHz.

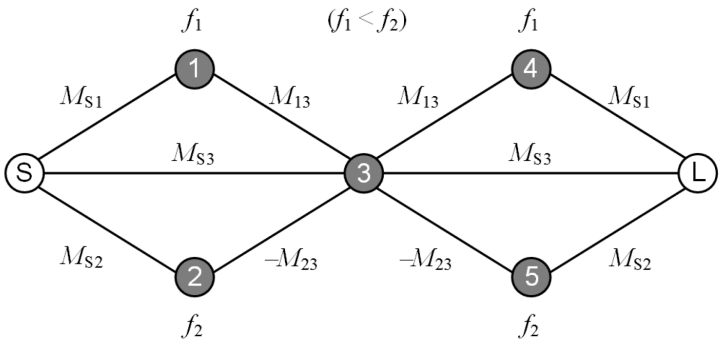

Fig. 52. Topology of the five-pole filter, based on two air-filled dual-mode SIW cavities and a standard SIW cavity.

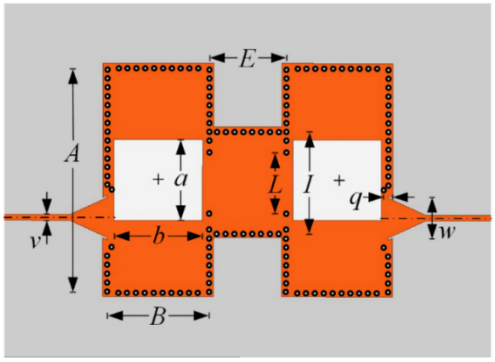

(*a*)

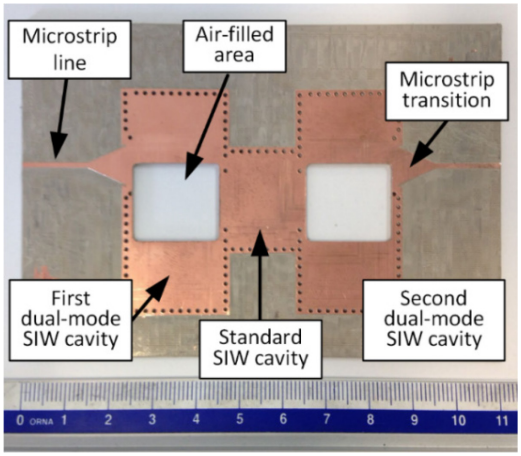

(*b*)

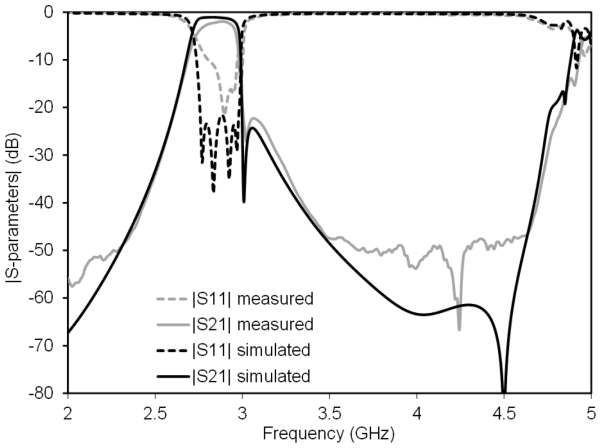

(*c*)

Fig. 53. Geometry, realized and measured five-pole filter response: (*a*) geometry of the filter; (*b*) photograph of the prototype(dimensions in TABLE VII; (*c*) comparison between simulation and measurement. [3]

TABLE VII
DIMENSIONS OF THE FIVE-POLE FILTER (IN MM)

A=50.54	B=23.04	a=18.2	b=20.04
c=9	d=10	e=10	f=1
g=1	h=8.5	s=8	w=10
E=17.4	L=13.8	I=22.95	q=2

4 CONCLUSIONS

In this Chapter, the theoretical analysis of the air-filled dual-mode SIW cavity and the application of this structure in filter design has been explained. Starting from an air filled SIW cavity and adopting a doublet able to provide two poles and two transmission zeros, different cases have been proposed – varying the fractional bandwidth and transmission zeros position to highlight the complete control of the structure. Moreover, with a design chart, all the geometrical parameters that play a role in the filter design, have been described. The doublet can be used as a building block to design higher order filters cascading the basic structure with the advantage that each generates two transmission zeros. The designed filters have been fabricated to confirm the theoretical analysis. This structure combines the advantages of a dual-mode structure (compact size) and air-filled (low losses). In addition, the simple topology realizes low cost filters with high performance in the upper stop-band for the introduction of transmission zeros.

REFERENCES

[1] C. Tomassoni, L. Silvestri, A. Ghiotto, M. Bozzi, and L. Perregrini, "A Novel Filter Based on a Dual-Mode Air-Filled Substrate Integrated Waveguide Cavity Resonator," *2017 IEEE MTT-S International Conference on Numerical Electromagnetic and Multiphysics Modeling and Optimization for RF, Microwave, and Terahertz Applications* (NEMO2017), Sevilla, Spain, 17-19 May 2017.

[2] C. Tomassoni, L. Silvestri, M. Bozzi, L. Perregrini, and A. Ghiotto, "A dual-mode quasi-elliptic filter in air-filled substrate integrated waveguide technology," 47th European Microwave Conference (EuMC), Nuremberg, Germany, 10-12 Oct. 2017.

[3] C. Tomassoni, L. Silvestri, A. Ghiotto, M. Bozzi and L. Perregrini, "Substrate-Integrated Waveguide Filters Based on Dual-Mode Air-Filled Resonant Cavities," in *IEEE Transactions on Microwave Theory and Techniques*, vol. 66, no. 2, pp. 726-736, Feb. 2018.

[4] M. Bozzi, A. Georgiadis, and K. Wu, "Review of Substrate Integrated Waveguide (SIW) Circuits and Antennas," *IET Microwaves, Antennas and Propagation*, vol. 5, no. 8, pp. 909–920, June 2011.

[5] S. Adhikari, A. Ghiotto, and K. Wu, "Simultaneous electric and magnetic two-dimensionally tuned parameter-agile SIW devices," *IEEE Trans. Microw. Theory Techn.,* vol. 61, no. 1, pp. 423-435, Jan. 2013.

[6] R. Moro, S. Moscato, M. Bozzi and L. Perregrini, "Substrate Integrated Folded Waveguide Filter with Out-of-Band Rejection Controlled by Resonant-Mode Suppression," *in IEEE Microwave and Wireless Components Letters*, vol. 25, no. 4, pp. 214-216, April 2015.

[7] N. Delmonte, L. Silvestri, M. Bozzi, and L. Perregrini, "Compact Half-Mode SIW Cavity Filters Designed by Exploiting Resonant Mode Control," *International Journal of RF and Microwave Computer-Aided Engineering,* vol. 26, no. 1, pp. 72–79, Jan. 2016.

[8] S. Moscato, C. Tomassoni, M. Bozzi, and L. Perregrini, "Quarter-Mode Cavity Filters in Substrate Integrated Waveguide Technology," *IEEE Trans. Microw. Theory Techn.*, vol. 64, no. 8, pp. 2538-2547, Aug. 2016.

[9] C. Tomassoni, L. Silvestri, M. Bozzi, and L. Perregrini, "Substrate Integrated Waveguide Filters Based on Mushroom-Shaped Resonators," International Journal of Microwave and Wireless Technologies, vol. 8, no. 4-5, pp. 741-749, June 2016.

[10] S. Bastioli, C. Tomassoni, and R. Sorrentino, "TM Dual-Mode Pseudoelliptic Filters using Nonresonating Modes," *IEEE MTT-S 2010 International Microwave Symposium*, Anaheim, CA, 23-28 May 2010.

[11] C. Tomassoni, S. Bastioli, and R.V. Snyder, "Propagating Waveguide Filters Using Dielectric Resonators," *IEEE Trans. Microw. Theory Techn.*, vol. 63, no. 12, pp. 4366-4375, Dec. 2015.

[12] S. Bastioli and R. V. Snyder, "Waveguide evanescent mode filters using high-Q bypassed cavities for extreme close-in rejection," *44th European Microwave Conference,* pp. 175–178, Rome, Italy, Oct. 6–9, 2014.

[13] C. Tomassoni, S. Bastioli, and R.V. Snyder, "Compact Mixed-Mode Filter Based on TE101 Cavity Mode and TE01δ Dielectric Mode," *IEEE Trans. Microw. Theory Techn.*, vol. 64, no. 12, pp. 4434-4443, Dec. 2016.

[14] F. Parment, A. Ghiotto, T. P. Vuong, J. M. Duchamp, and K. Wu, "Air-Filled Substrate Integrated Waveguide for Low-Loss and High Power-Handling Millimeter-Wave Substrate Integrated Circuits," *IEEE Trans. Microw. Theory Techn.*, vol. 63, no. 4, pp. 1228-1238, April 2015.

[15] F. Parment, A. Ghiotto, T. P. Vuong, J. M. Duchamp, and K. Wu, "Double Dielectric Slab-Loaded Air-Filled SIW Phase Shifters for High-Performance Millimeter-Wave Integration," *IEEE Trans. Microw. Theory Techn.,* vol. 64, no. 9, pp. 2833-2842, Sept. 2016.

Chapter 4

NOVEL CLASS OF BANDPASS FILTERS BASED ON A DUAL-MODE AIR-FILLED SIW CAVITY (A FURTHER STUDY) [1]

In this Chapter a structure, complementary to the filter proposed in Chapter 3 is presented. In particular, this new dual-mode air filled cavity is realized by removing part of the dielectric substrate from the two lateral portions of the SIW cavity (Fig. 54), unlike what has been studied in Chapter 3. As a consequence, the considered modes - used to create the passband of the filter - are the second and third cavity mode (namely, quasi TM_{120} and TM_{210} modes, where TM is defined with respect to z axis of Fig. 54). The choice of these modes is explained in the following pages. This structure is capable of introducing two transmission zeros: a first transmission zero is introduced by the asymmetric coupling with the modes, while the other is due to the direct source-to-load coupling. This structure maintains the advantages of the previous dual-mode air-filled cavity ([6], [7], [8] and [9]), namely size reduction and increased performances but, whereas the structure proposed in Chapter 3 is able to locate two transmission zeros only above the passband, this dual-mode air-filled cavity allows us to freely locate the two transmission zeros; either both below or both above the filter passband, or one below and one above.

The doublet has been deeply investigated from the theoretical point of view to the final realized prototypes. Two different coaxial probe positions have been studied, showing the control on the location of the transmission zeros related to the source-to-load coupling. In addition, it is shown, with a comparison, that this structure is able to guarantee an incremental 40% spurious free bandwidth respect with a homogeneous filter (able to realize an almost identical in-band response). The analyzed doublet can be used as a building block for higher order filter design. In order to demonstrate the feasibility of the design, two four-poles have been designed. One of them has been realized and measured. The results of this work have been submitted in [1].

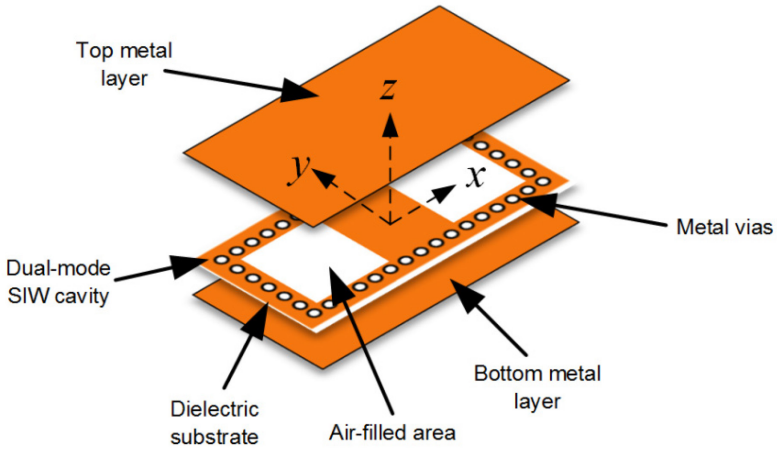

Fig. 54. Geometry of the dual-mode cavity (doublet) in air-filled SIW technology.

1 THEORY OF DUAL-MODE AIR-FILLED CAVITY

The modal analysis of the dual-mode partially air-filled cavity is here presented along the lines of the analysis introduced in Chapter 3 [3]. In order to derive a characteristic equation of this dual-mode air-filled cavity (Fig. 55(*a*)), a transmission-line model is used as shown in Fig. 55(*b*). The cavity is represented by the geometrical dimensions A (length) and B (width). The lateral portions of the cavity have been perforated ($\varepsilon_{r0}=1$), while the central portion remains untouched with permittivity ε_{r1} and length a. The central dielectric-filled region is modelled as a section of length $l_1 = a$, while Z_{1mn} and β_{1mn} represent the modal impedance and the propagation constant, respectively, of the TE_{mn} mode of the SIW structure filled with dielectric material with permittivity ε_{r1}. Instead, the lateral air-filled regions are represented by transmission lines of length $l_0 = (A\text{-}a)/2$, short-circuited at the end, with modal impedance Z_{0mn} and propagation constant β_{0mn}, referred to the TE_{mn} mode of the air-filled SIW structure. At this point, by calculating the modal impedances Z_A, Z_B, and Z_C, an eigenvalue problem is obtained by imposing $Z_A=0$. The solution can be retrieved by the Newton–Raphson method [10], and allows us to determine the resonance frequencies of the cavity modes [3]. The procedure can be repeated for any TE_{mn} mode of the SIW, to calculate the complete set of cavity modes.

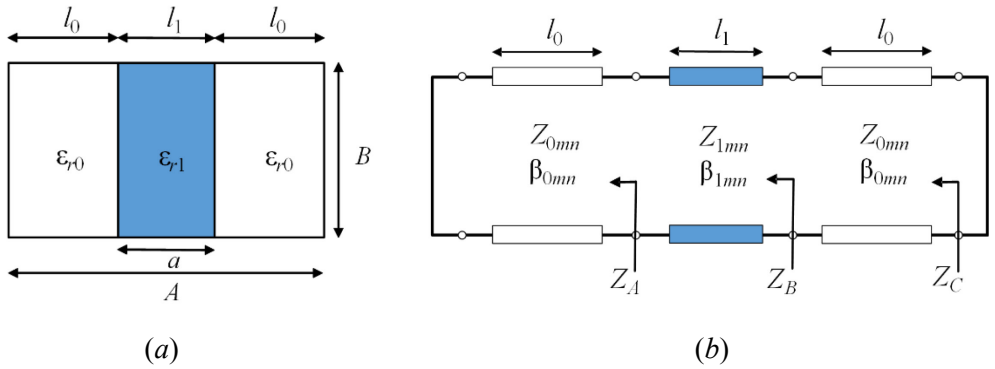

Fig. 55. Partially air-filled SIW cavity model: (*a*) top view; (*b*) equivalent transmission-line model. [1]

Different analyses can be performed by using this method to exploit the impact of the variation of the geometrical parameters on the resonance frequencies of the cavity modes.

A first analysis has been performed by calculating the resonance frequencies of the first six cavity mode versus dimension a (Fig. 56 , A = 50 mm, B=21 mm and dielectric permittivity $\varepsilon_{r1}=10.2$). It can be noted in Fig. 56 that the variation of this geometrical parameter has a huge impact on the shift of the resonance frequencies of the cavity modes. The mode at lower resonance frequency between the quasi - TM_{120} and quasi - TM_{210} changes by varying a. More specifically, for values $a<12$ mm, the TM_{120} mode has lower resonance frequency than the TM_{210} mode while, for $a=12$ mm, the two resonance frequencies cross (Fig. 56). By specifically choosing a (a=12 mm, marker ♦ in Fig. 56) - close to the crossing point - the frequency separation between these two modes (used to define the passband of the filter) can be controlled, obtaining a narrow-band filter. On the other hand, by increasing the distance from the crossing point, larger bandwidth can be created. Conversely, the fundamental quasi TM_{110} mode is exploited to obtain one transmission zero.

In order to visualize the first three resonant modes the amplitude of the modal electric fields are plotted in Fig. 57 with the use of the commercial electromagnetic solver Ansys HFSS (with A = 50 mm, B = 21 mm, a = 12 mm, ε_{r1} = 10.2). In addition, the signs are reported in the figure because they are useful in the following analyses. It can be noted that the field distribution of the modes is mostly concentrated in the dielectric central portion (Fig. 57), hence a variation of the parameter a affects significantly the resonance frequencies of the cavity modes.

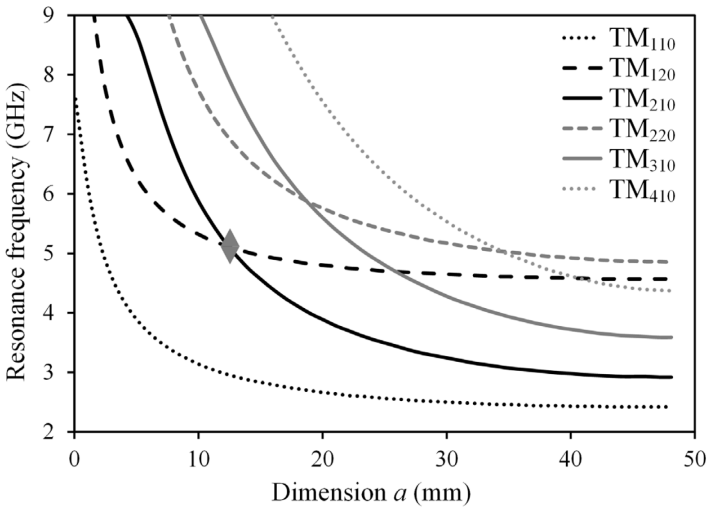

Fig. 56. Theoretical first six resonance frequencies versus dimension a (A = 50 mm, B = 21 mm, ε_{r1} = 10.2). Marker ♦ defines the point of intersection of the TM_{120} and TM_{210} modes. [1]

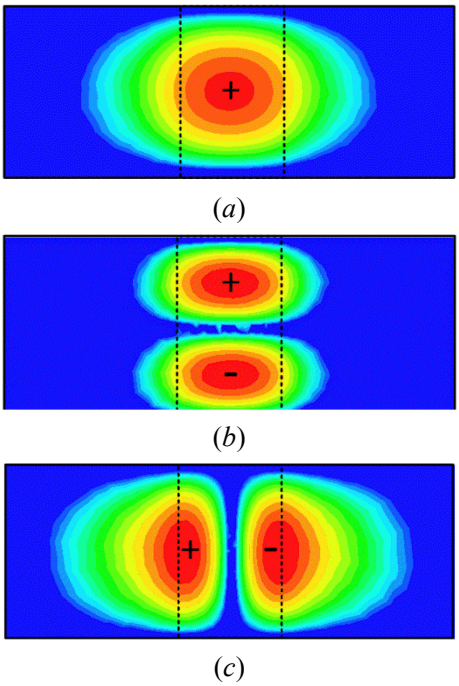

Fig. 57. Amplitude of the electric modal fields of the first three cavity modes: (*a*) TM_{110}; (*b*) TM_{120}; (*c*) TM_{210}. [1]

In order to completely understand the effects of the other geometrical parameters on the frequency separation of the modes and on their control, a parametric investigation of the other relevant geometrical dimensions has been performed. At first, the variation of dimension A (with B = 21 mm, ε_{r1} = 10.2), for four fixed different values of dimension a, has been carried out as shown in Fig. 58. Marker ♦ in Fig. 58(*a*) represents the point for A = 50 mm, B = 21 mm, ε_{r1} = 10.2 and a=12mm that is the same shown in Fig. 56. It can be noted that the total cavity dimension, A, does not play an important role when A>30 mm because of the field distribution of the modes, mostly concentrated in the dielectric-filled portion of the cavity, as shown in Fig. 57. From this value, the condition of maximum spurious free-bandwidth is satisfied.

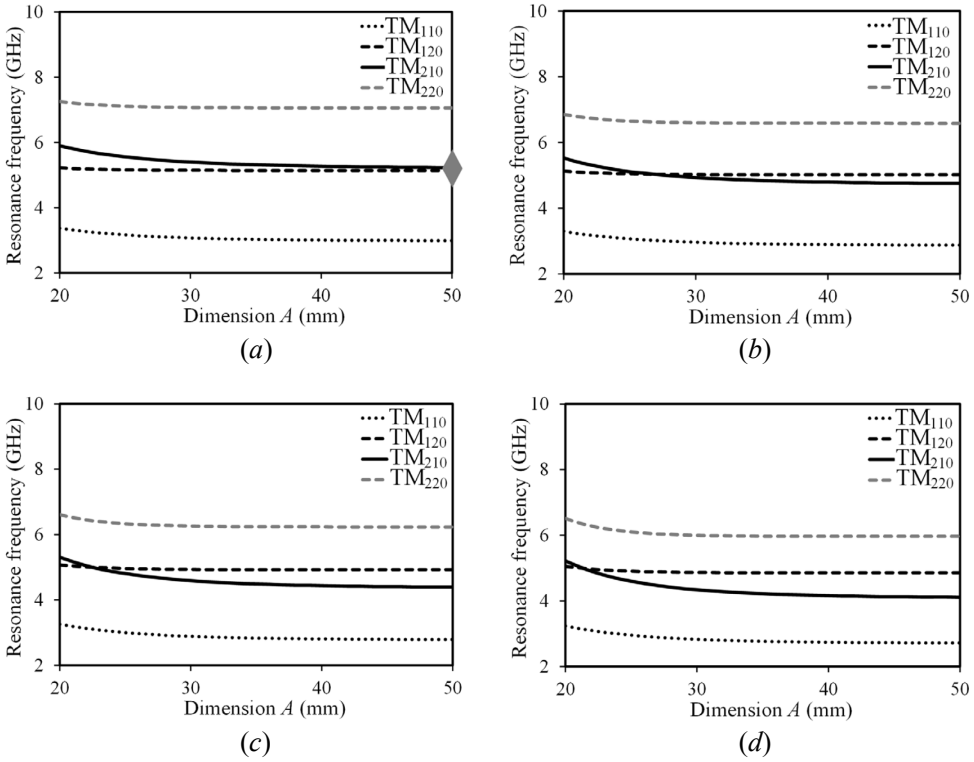

Fig. 58. Resonance frequencies of the first four cavity modes versus A (with $B = 21$ mm): (*a*) $a = 12$ mm; (*b*) $a = 14$ mm; (*c*) $a = 16$ mm; (*d*) $a = 18$ mm. [1]

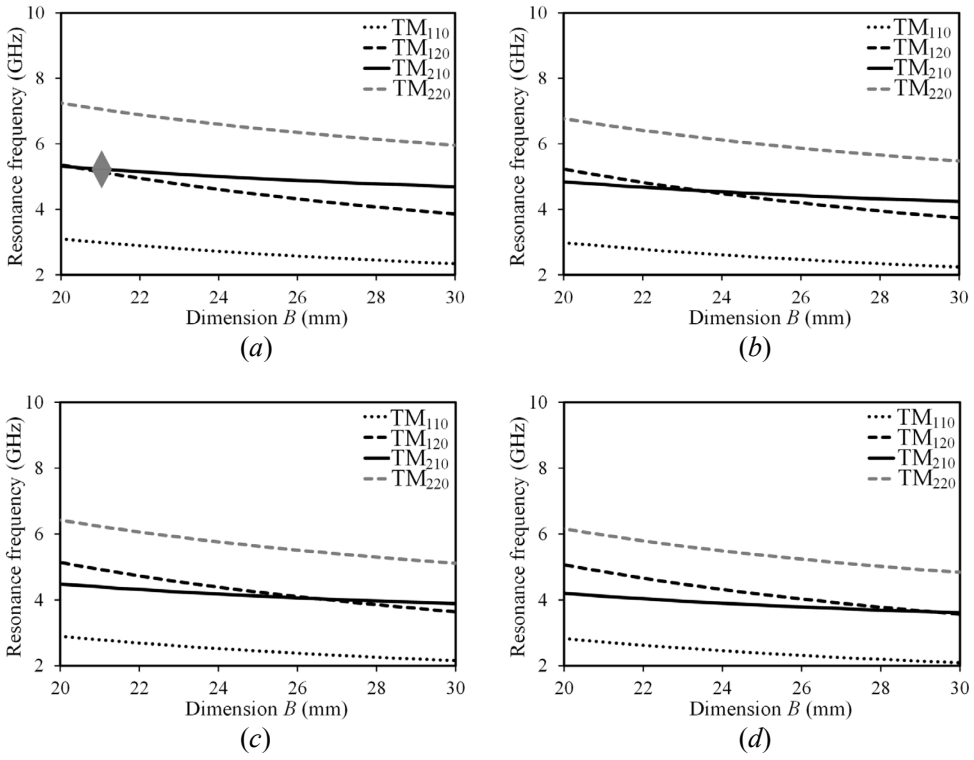

Fig. 59. Resonance frequencies of the first four cavity modes versus B (with A = 50 mm): (*a*) $a = 12$ mm; (*b*) $a = 14$ mm; (c) $a = 16$ mm; (d) $a = 18$ mm. [1]

Conversely, Fig. 59 illustrates that the variation of dimension B more notably affects the frequency separation of the second and third modes. The analysis has been performed with four different values of a, the same used

in Fig. 58. Also in this case, the marker ♦ in Fig. 59(*a*) represents the point for A=50 mm, B=21 mm, ε_{r1}=10.2 and a=12mm. In particular, the TM_{120} is predominately affected (Fig. 59) due to its field distribution along the y axis (Fig. 57).

Fig. 60 provides in a graph a preliminary design guideline. This figure has been derived from the aforementioned transmission-line model and it shows: relative frequency separation Δf (in colors), that is related to the filter passband, central operation frequency f_c (black straight line), and relative spurious-free bandwidth BW (black dashed lines) versus the geometrical dimensions a and B (A = 50 mm and ε_{r1} = 10.2). As previously shown, dimension A plays a minor to null role in the behavior of the cavity (Fig. 58), and for this reason A is fixed in this analysis. The definitions of these parameters have been introduced in Chapter 3: the only difference is the fact that the modes here considered are different. In particular, for this structure, the modes used to define the relative frequency separation and central operation frequency are the TM_{120} and TM_{210}. Particular attention should be given when considering the spurious-free bandwidth because the first superior mode can be either the TM_{220} or TM_{310}. Once the central frequency, f_c, has been chosen, different pairs of a and B can be used. Moreover, only a specific pair results in a desired frequency separation Δf or spurious-free bandwidth BW. BW and Δf are not independent and once one is fixed the other follows. In Fig. 59 can be noticed that 35% of spurious free bandwidth can be obtained with 1.5% fractional. The maximum of spurious-free bandwidth is obtained at the minimum of the relative frequency separation, which results in the crossing point of the modes. Considering this extreme case the filter cannot be implemented.

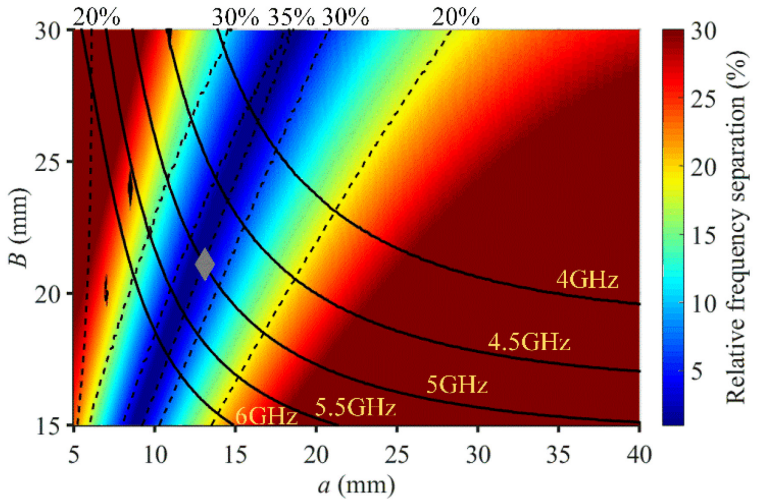

Fig. 60. Relative frequency separation Δf (colors), central frequency f_c (black straight lines), and relative spurious free bandwidth BW (black dashed lines) versus dimensions a and B (with A=50mm and ε_{r1}=10.2). [1]

2 IMPLEMENTATION OF THE DOUBLET

In the previous Section, all the geometrical parameters of the dual-mode air-filled SIW cavity have been related to the control of specific filter characteristics. This Section describes the analysis and the design strategy of the doublet based on the cavity previously analyzed. These doublets are able to provide two poles and two transmission zeros. The dimensions, previously calculated, refer to the equivalent waveguide [4], and need to be transformed into the real SIW dimensions: usually, a small tuning is sufficient. In particular, the 3D model of the SIW doublet with its layers is shown in Fig. 61.

In this structure, coaxial probes are used - differently from the design of Chapter 3. The degree of freedom, related to the positioning of the coaxial probes both along the axes x or y, helps to change the location (above or below the passband) of the transmission zero related to the source-to-load coupling. The other transmission

zero location is related to the asymmetric coupling with the modes and can be controlled with the parameter *a*. In the following sub-sections the position of the coaxial probes as well as the variation of the parameter *a* is deeply investigated.

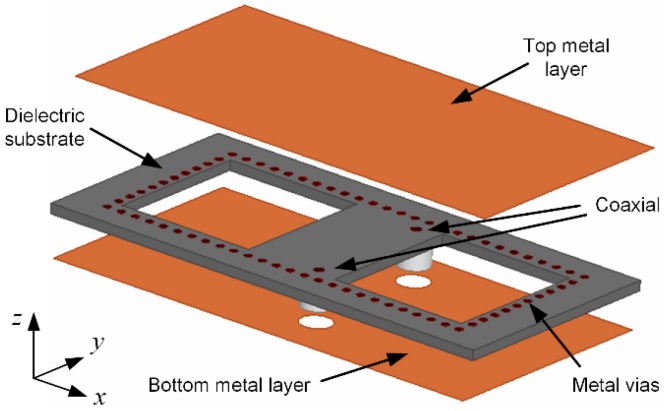

Fig. 61. 3-D model of the dual-mode air-filled SIW cavity decomposed in its different layers. [1]

2.1.1 Doublet with Coaxial probes aligned along the y axis

As briefly previously discussed, the role of the coaxial probes in this cavity is particularly important as their position determines the location of the source-to-load transmission zero. Particular attention should be paid to the possible small shift of the cavity resonance frequencies, due to the presence of the coaxial probes. In this Section, the analyses have been carried out locating the coaxial ports as in Fig. 62, aligned along the *y* axis (of Fig. 61). The geometrical model of the doublet is shown in Fig. 62.

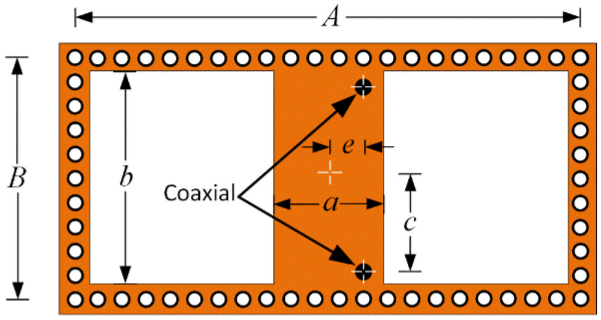

Fig. 62. Geometrical model of the dual-mode air-filled SIW cavity. Coaxial probes along the longitudinal dimension of the cavity. [1]

Considering that the variation of the parameter *a* can vary the resonant frequencies and, therefore, the order of the cavity modes, the topologies of Fig. 63 have been introduced. In particular, it can be noted that the mode at lower resonant frequency (f_1) changes from the TM_{120} of Fig. 63(*a*), for $a<12$mm, to the TM_{210} of Fig. 63(*b*) for $a>12$mm. Due to the field distribution of the TM_{120} and TM_{210} modes, shown in Fig. 57(*b*) and Fig. 57(*c*), respectively, this topology exhibits three couplings with the same sign and a fourth with the opposite sign, thus determining a transmission zero outside the passband. In particular, in Fig. 63(*a*), due to the value *a* and to the position of the coaxial ports, $M_{1L}=-M_{S1}$ and $M_{2L}=M_{S2}$. In Fig. 63(*b*) the mode responsible for the changing of the sign is, again, the TM_{120} but now is at f_2, resulting in $M_{2L}=-M_{S2}$

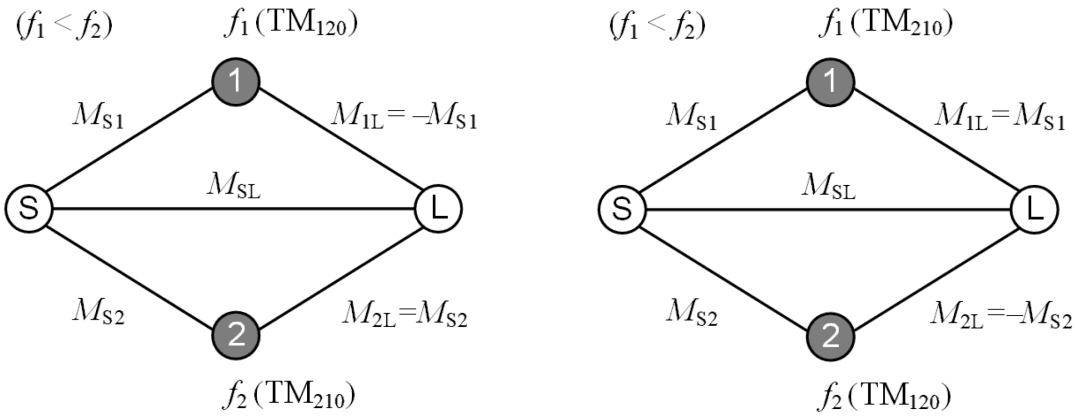

(*a*) (*b*)

Fig. 63. Topology of the doublet, implemented by using the partially air-filled dual-mode SIW cavity: (*a*) a<12mm; (*b*) a>12mm. The changing of the sign is related to the TM_{120} [1]

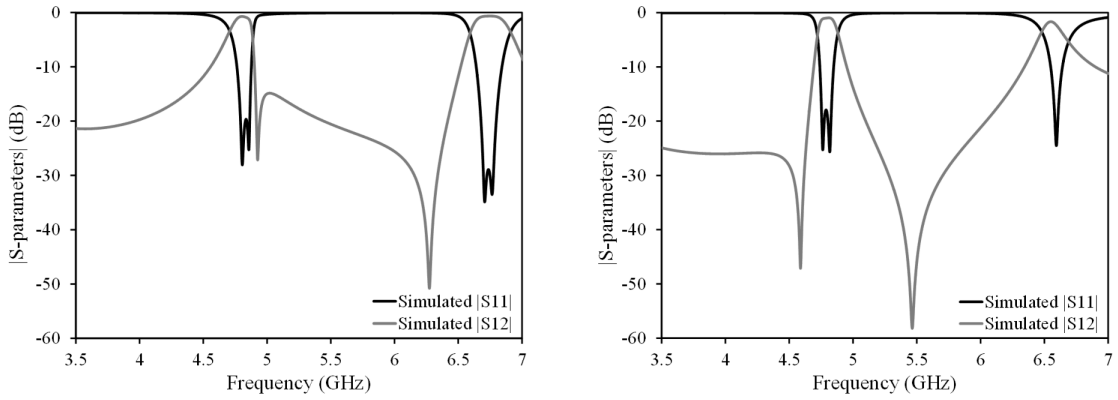

(*a*) (*b*)

Fig. 64. Frequency response considering the topologies of Fig. 63: (*a*) topology of Fig. 63(*a*); (*b*) topology of Fig. 63(*b*). [1]

TABLE VIII
DIMENSIONS OF THE FILTERS (IN MM)

	Fig. 64(*a*)	Fig. 64(*b*)
A	50	50
B	21.7	21.7
a	11.7	13.1
b	18.7	18.7
c	8.4	8.4
e	3.1	4.8

In this way, one transmission zero, related to the asymmetric coupling, can be placed either above or below the passband of the filter as in Fig. 64 (dimensions in TABLE VIII). In Fig. 64(*a*) the coupling is stronger with the TM_{120} (at f_1) - also responsible for the changing of the sign. In Fig. 64(*b*), the coupling is, once again, stronger with the TM_{120}, but now is at f_2. The other transmission zero is related to the source-load coupling and is not easily controllable. The parameters e and c control the coupling M_{S1} and M_{S2}. Considering the extreme case e=0 only the TM_{120} is coupled, presenting only one pole.

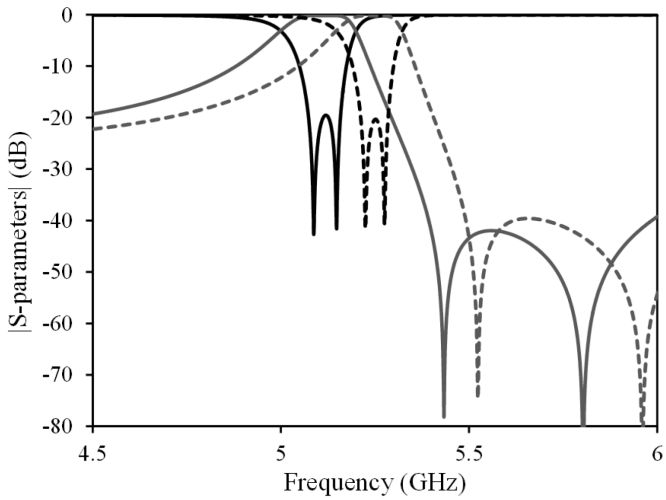

Fig. 65. Frequency responses with different central operational frequency, f_c

In order to show the ability to use the design guideline of Fig. 60, two frequency responses with 1% fractional bandwidth have been designed (Fig. 65) with different central operational frequencies; specifically, f_{c1} = 5.1GHz and f_{c2} = 5.3GHz.

2.1.2 *Doublet with coaxial probes aligned along the x axis*

In this Subsection the position of the coaxial probes have been moved along the *x* axis in order to change the coupling with the modes. Therefore, this new configuration moves the transmission zero, related to the source-to-load coupling, below the passband of the filter. This is interesting because, together with the previous configuration (showing in Sec.2.1.1), the transmission zeros can be located either both below or both above or one above-one below, the passband. The mode responsible for the changing of the sign is the TM_{210} mode instead of the TM_{120}.

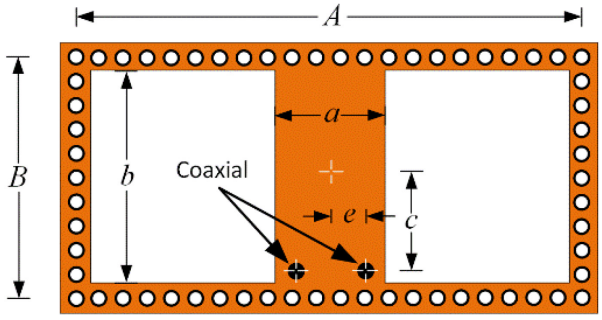

Fig. 66. Geometrical model of the dual-mode air-filled SIW cavity. Coaxial probes along the transversal dimension of the cavity. [1]

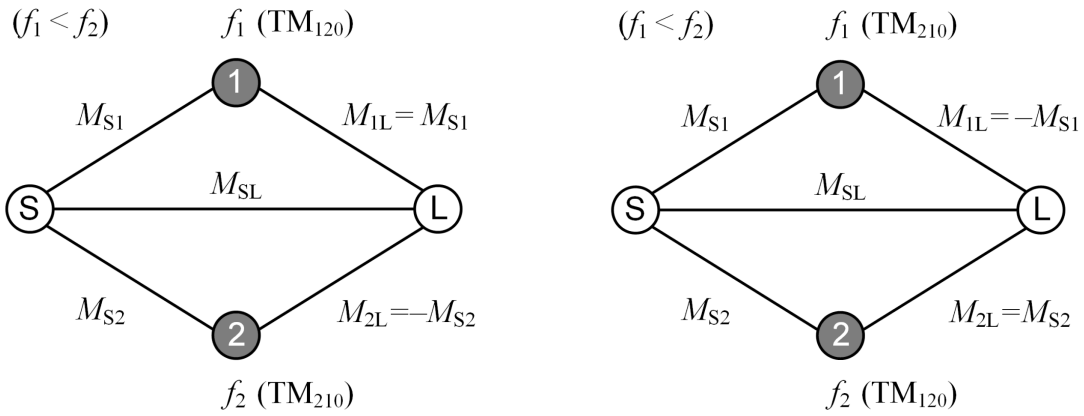

(*a*) (*b*)

Fig. 67. Topology of the doublet, implemented by using the partially air-filled dual-mode SIW cavity: (*a*) a<12mm; (*b*) a>12mm. The changing of the sign is related to the TM$_{210}$ [1], [3]

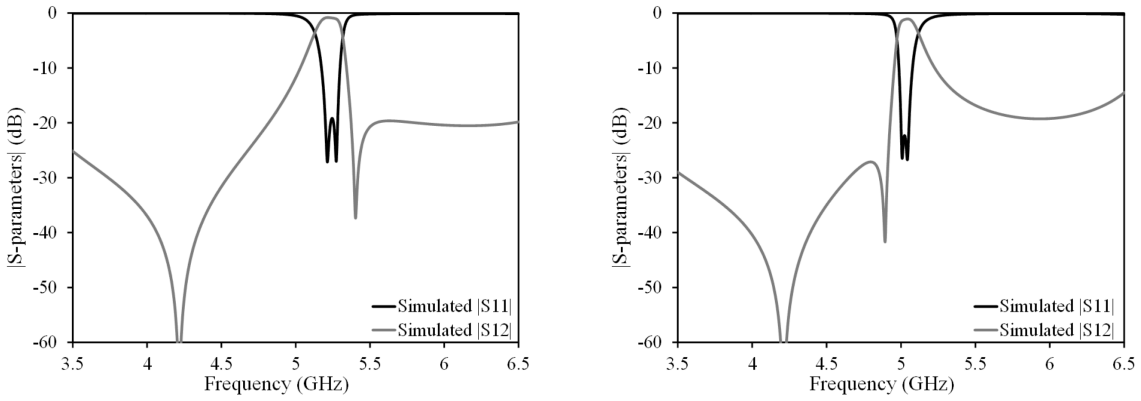

(*a*) (*b*)

Fig. 68. Frequency response considering the topologies of Fig. 67: (*a*) topology of Fig. 67(*a*); (*b*) topology of Fig. 67(*b*). [1]

TABLE IX
DIMENSIONS OF THE FILTERS (IN MM)

	Fig. 68(*a*)	Fig. 68(*b*)
A	50	50
B	21.7	21.7
a	11.7	12.9
b	18.7	18.7
c	8.4	8.6
e	4.1	4.3

Continuing in the same direction as in Sec.2.1.1, the frequency response of Fig. 68(*a*) and Fig. 68(*b*) (dimensions in TABLE IX) have been obtained with the position of the transmission zero related to the source-load coupling below the passband. By varying parameter *a*, the other transmission zero, related to the asymmetric coupling, can be placed above or below the filter passband.

3 COMPARISON BETWEEN THE PROPOSED FILTER AND THE HOMOGENEOUS CAVITY FILTER

In order to demonstrate the advantages of this filter respect to the homogeneous cavity filter a comparison is proposed. In fact, a filtering response almost identical (with respect to the air-filled cavity) inband can be obtained by adopting a homogeneous, dielectric filled, SIW almost-square cavity (Fig. 69).

By using the modal analysis introduced in Sec. 1, the homogeneous cavity has been analyzed (A=22.65mm, dielectric permittivity ε_{r1}=10.2). The first six resonance frequencies, versus A-B, have been plotted in Fig. 71. When the difference approaches 0 the cavity is square and the TM_{120} and TM_{210} modes are degenerate modes. By adjusting the difference between A and B the desired relative frequency separation can be obtained. It can be noted (Fig. 71) that the spurious free bandwidth, defined as the separation between the central passband frequency and the first upper mode, is approximately 26%. In the structure proposed in this Chapter the value reaches 36% (Par.1).

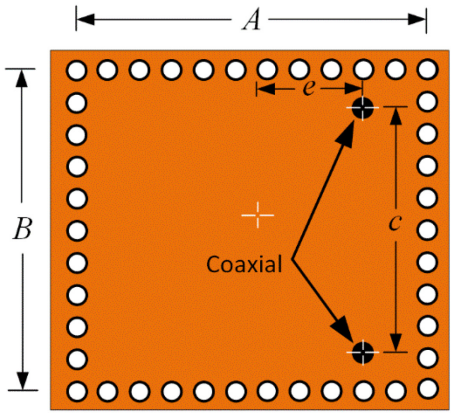

Fig. 69. Geometrical model of the homogeneous, dielectric filled filter (dimensions in mm: A=22.65, B=23.7, c=17.65, e=4.45. Dielectric permittivity ε_{r1}=10.2). [1]

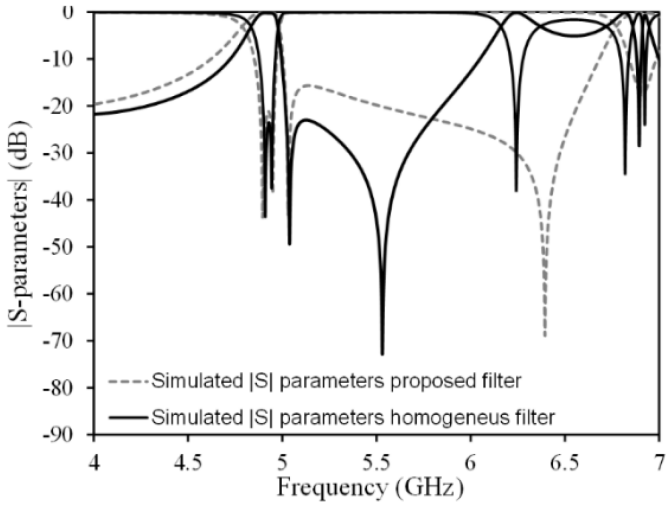

Fig. 70. Comparison between the proposed filter and the homogeneous dielectric filled filter. No losses have been considered for the comparison [1]

The homogeneous cavity filter (Fig. 69) has been designed to achieve a frequency response similar to the one in Fig. 64(c), with the help of the modal analysis. Fig. 70 shows that the passbands of the two filters are

practically identical, but the air-filled SIW filter presents a wider spurious free bandwidth that confirms the values previously obtained. The use of a substrate with different dielectric permittivity leads to identical results in the case of the homogeneous cavity filter. Conversely, the spurious free bandwidth of the partially air-filled SIW filter slightly degrades when using substrates with lower dielectric permittivity. For instance, in the case of $\varepsilon_{r1} = 2$, the spurious free bandwidth is reduced to 32%, but is still larger than in the case of the homogeneous cavity.

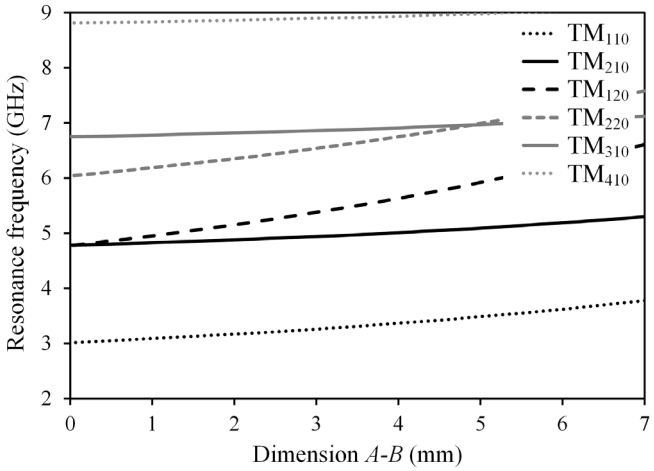

Fig. 71. Theoretical first six resonance frequencies of the homogeneous SIW cavity versus dimension *A-B* (*A*=22.65 mm, ε_{r1}=10.2). [1]

4 FABRICATION AND MEASUREMENTS

Two different prototypes have been fabricated and measured, as explained in this Section.

The filters have been realized on Rogers 3010 substrate with ε_r = 10.2, tgδ = 0.0022 and thickness 1.27mm and machined with the milling machine LPKF ProtoMat S103. The filters are composed by three different layers: top cover, dielectric substrate (dual-mode partially air-filled SIW cavity) and bottom cover. Top and bottom covers have been machined on the dielectric substrate Rogers 3003 (thickness 0.25mm) in order to realize all the layers in a single fabrication step. Because of a good electrical contact between coaxial connectors, the dual-mode air-filled SIW cavity and the top/bottom covers' metal is necessary, holes have been drilled in both top/bottom cover. These should be big enough for easy soldering. The metal lateral vias of the SIW cavity have been metallized with a LPKF ProConduct paste. The final filter is mounted as shown in the axonometric projection of Fig. 72(*a*) and all layers are aligned with alignment pins. Finally the coaxial probes have been soldered. All the prototypes have been measured with a Keysight VNA N5242A.

The first filter, with frequency response already shown in Fig. 64(*a*) (with dimensions in TABLE VIII), has been realized and measured. The first prototype (Fig. 73(*b*)) shows a simulated insertion loss of 0.8dB while the measured one is slightly superior, being 1.4dB (1% *FBW*).

For completeness, here, also the filter response with transmission zeros symmetrically placed respect with the passband, is presented (dimensions in TABLE X). In Fig. 73(*a*) the comparison between simulated and measured results, for the second prototype, are shown. In this case, the measured insertion loss is 1.2dB while the simulated one is 1.1dB (1.5% *FBW* at f_c=4.8GHz). No de-embedding has been applied. In both cases simulations and measurements show a good agreement both in the entire passband and in the out-of-band confirming the theoretical studies and the fabrication process.

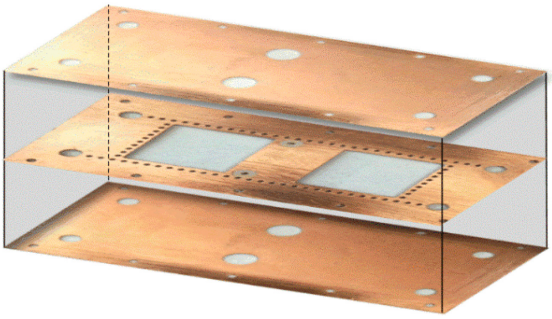

(*a*)

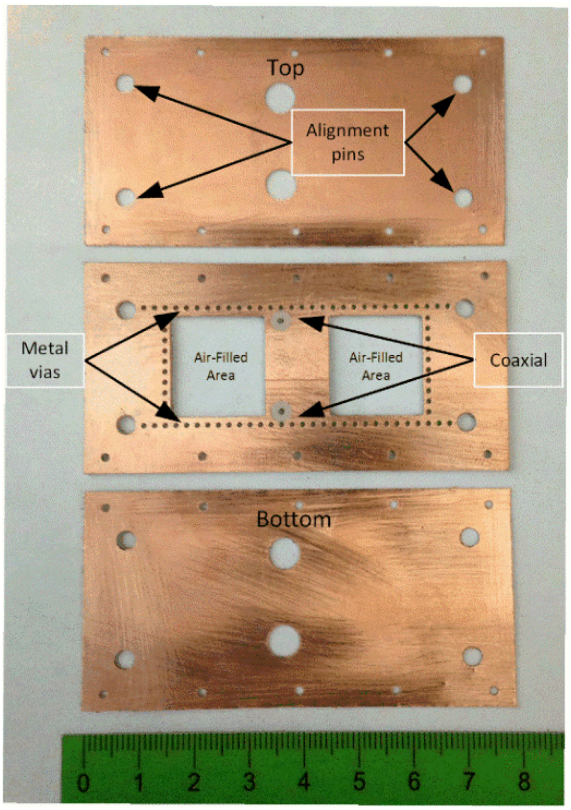

(*b*)

Fig. 72. Realized prototype: (*a*) axonometric projection of the realized filter; (*b*) disassembled filter. [1]

TABLE X
DIMENSIONS OF THE FILTER FIG. 73(*a*) (IN MM)

A=50	*B*=21.7
a=13.7	*b*=18.7
c=6.9	*e*=5.5

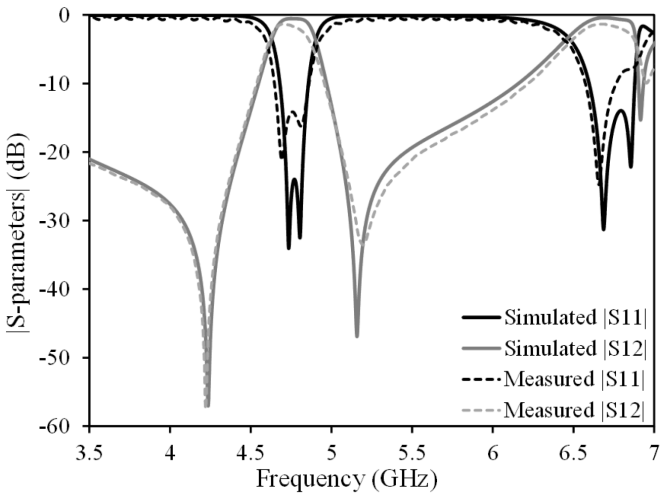

(*a*)

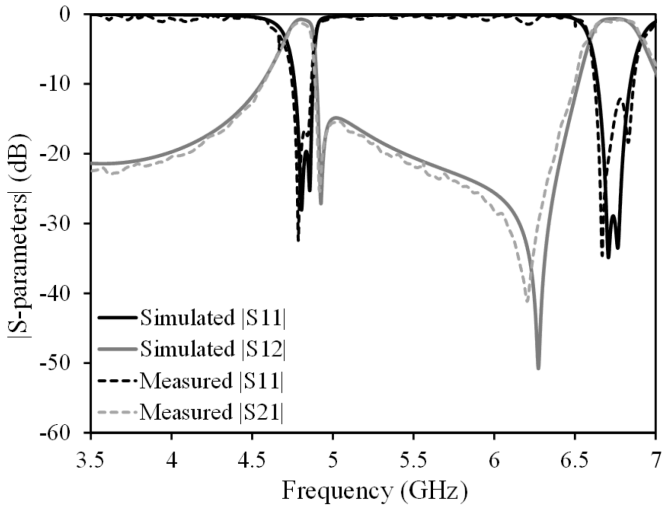

(*b*)

Fig. 73. Measurements and simulations of the frequency response of the filter: (*a*) simulated and measured results of the filter with dimensions in TABLE X; (*b*) simulated and measured results of the filter with dimensions in TABLE IX). [1]

5 HIGHER ORDER FILTER DESIGN

In order to extend the study to the design of higher order filters, two four pole filters have been designed, fabricated and measured. They can be obtained cascading different doublets through non resonating nodes, as done in the Chapter 3 [3], [6] and [7]. In this specific case, a coupling window has been used to reduce the dimensions of the filter. As previously demonstrated, the doublets can realize transmission zeros close to the passband, either below or above, in order to improve the out-of-band rejection. As well as for the doublets, also in this case, the two frequency responses show that the transmission zeros can be placed in the same way. The coupling between the doublets is controlled by modifying the geometrical parameters *f* and *d*: *f*, defines the asymmetry of the window respect to the center of the structure [3], controlling the coupling with the modes, while parameter *d* is related to the width of the aperture and controls the value of coupling. The two central posts are used for the fine tuning of the coupling. Two filters have been designed as shown in Fig. 75 with a

double transmission zero close to the passband either below and above the pass-band (dimensions in TABLE XI and TABLE XII).

The filter with a transmission zero below the passband of the filter has been realized with dimensions in TABLE XI. Fabrication and measurement processes, as well as the dielectric substrates, are identical to what described in Sec.4. Simulations and measurements have been compared showing good agreement as in Fig. 75(*b*). It can be noticed in Fig. 75(*b*), that, even though the calibration of the VNA is not excellent, it does not have a detrimental effect on the measurements. The fractional bandwidth of the filter is 2% with 1.6dB insertion loss at 4.45GHz.

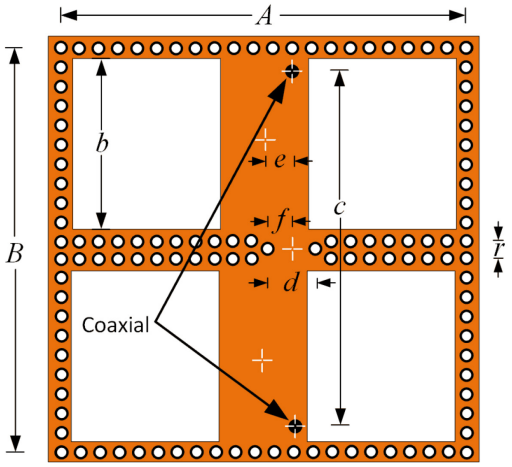

Fig. 74. Geometry of the four poles filter, obtained cascading two doublets. [1]

TABLE XI
DIMENSIONS OF THE FOUR POLES FILTER IN FIG. 75(*b*) (IN MM)

A=50	*B*=45.1	*d*=6.5
a=14.3	*b*=18.7	*e*=5.1
c=38.25	*r*=2.7	*f*=0.7

TABLE XII
DIMENSIONS OF THE FOUR POLES FILTER IN FIG. 75(*c*) (IN MM)

A=50	*B*=47.7	*d*=5.5
a=13.6	*b*=19.4	*e*=2
c=22.6	*r*=2.4	*f*=4

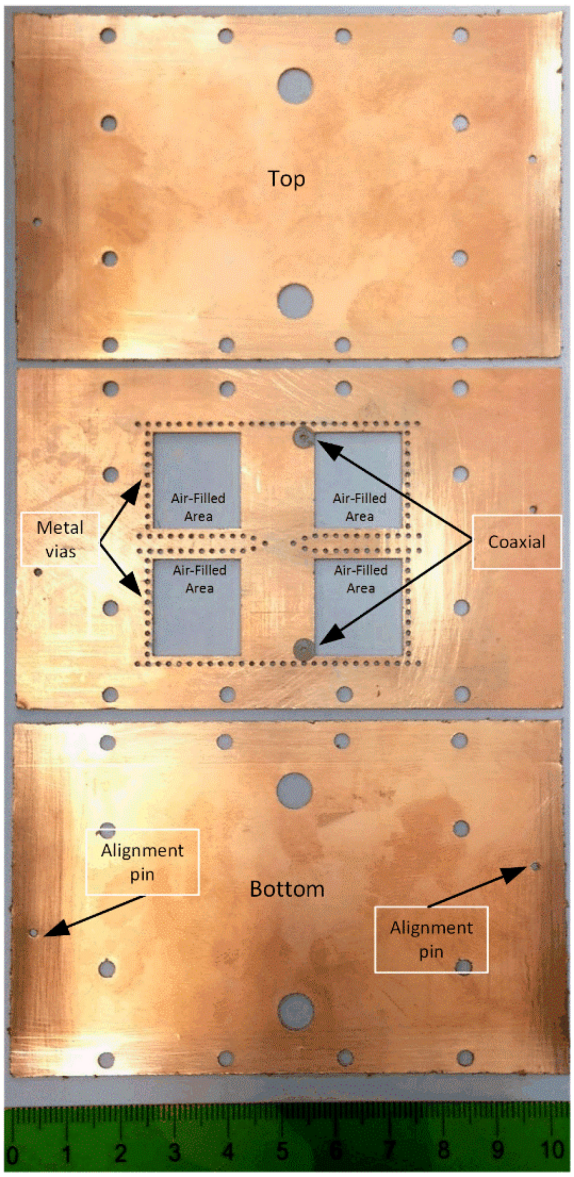
Top
Air-Filled Area
Air-Filled Area
Air-Filled Area
Air-Filled Area
Metal vias
Coaxial
Alignment pin
Bottom
Alignment pin
0 1 2 3 4 5 6 7 8 9 10

(*a*)

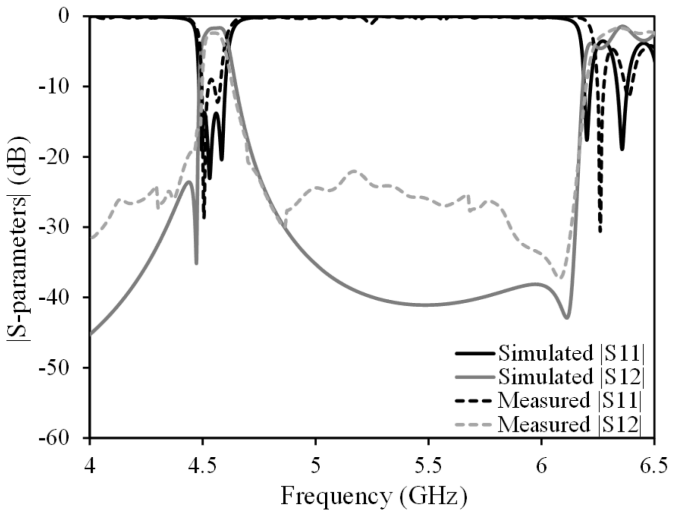
0
-10
-20
-30
-40
-50
-60
|S-parameters| (dB)
4
4.5
5
5.5
6
6.5
Frequency (GHz)
Simulated |S11|
Simulated |S12|
Measured |S11|
Measured |S12|

(*b*)

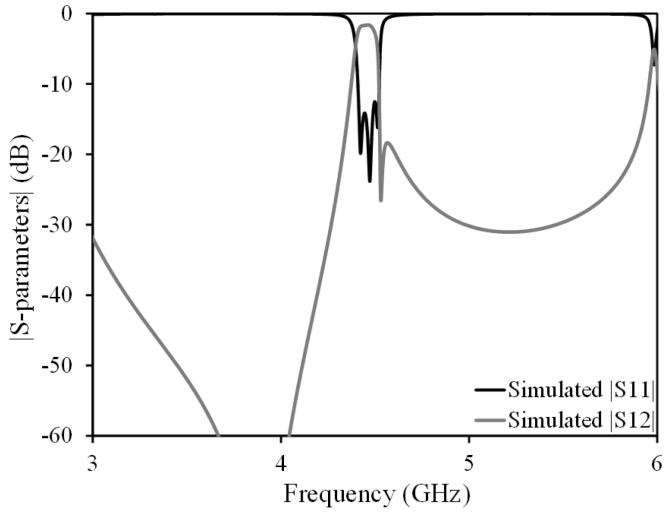

(*c*)

Fig. 75. Validation of the four-pole filter design: (*a*) Photograph of the prototype; (*b*) Simulation and measurement of the frequency response of the filter with one tx zero close and below the passband; (*c*) Simulation of the frequency response of the filter with one tx zero close and above the passband. [1]

6 CONCLUSIONS

This paper presents a novel class of dual-mode air-filled SIW filters. In particular, this cavity is complementary respect to the structure proposed in Chapter 3, because it is excavated in its lateral portions. Expanding on what has previously studied, the theoretical study with the design guideline has been presented, relating the filter characteristics to the geometrical parameters of the doublet. This structure has the advantage of positioning both the transmission zeros either below or above the filter passband or one above and one below, affirming valuable design flexibility. In addition, an almost 40% improvement of spurious free bandwidth (compared to the homogeneous - dielectric filled - filter) has been demonstrated. Several prototypes have been realized and measured to show the validity of the proposed structure, including a four-pole filter. In this case, the extension to higher order filter design is presented.

REFERENCES

[1] L. Silvestri, A. Ghiotto, C. Tomassoni, M. Bozzi, and L. Perregrini, "Novel partially air-filled substrate integrated waveguide filters", *Submitted to IEEE Transactions on Microwave Theory and Techniques*

[2] C. Tomassoni, L. Silvestri, M. Bozzi, L. Perregrini, and A. Ghiotto, "A dual-mode quasi-elliptic filter in air-filled substrate integrated waveguide technology," 47th European Microwave Conference (EuMC), Nuremberg, Germany, 10-12 Oct. 2017.

[3] C. Tomassoni, L. Silvestri, A. Ghiotto, M. Bozzi and L. Perregrini, "Substrate-Integrated Waveguide Filters Based on Dual-Mode Air-Filled Resonant Cavities," in *IEEE Transactions on Microwave Theory and Techniques*, vol. 66, no. 2, pp. 726-736, Feb. 2018.

[4] C. Tomassoni, L. Silvestri, A. Ghiotto, M. Bozzi, and L. Perregrini, "A Novel Filter Based on a Dual-Mode Air-Filled Substrate Integrated Waveguide Cavity Resonator," *2017 IEEE MTT-S International Conference on Numerical Electromagnetic and Multiphysics Modeling and Optimization for RF, Microwave, and Terahertz Applications* (NEMO2017), Sevilla, Spain, 17-19 May 2017.

[5] M. Bozzi, A. Georgiadis, and K. Wu, "Review of Substrate Integrated Waveguide (SIW) Circuits and Antennas," in *IET Microwaves, Antennas and Propagation*, vol. 5, no. 8, pp. 909–920, June 2011.

[6] W. Shen, X. Sun, W. Yin, J. Mao and Q. Wei, "A Novel Single-Cavity Dual Mode Substrate Integrated Waveguide Filter With Non-Resonating Node," in *IEEE Microwave and Wireless Components Letters*, vol. 19, no. 6, pp. 368-370, June 2009.

[7] M. Salehi, J. Bornemann and E. Mehrshahi, "Compact folded substrate integrated waveguide filter with non-resonating nodes for high-selectivity bandpass applications," *2013 European Microwave Conference*, Nuremberg, 2013, pp. 155-158.

[8] C. Tomassoni, S. Bastioli, and R.V. Snyder, "Compact Mixed-Mode Filter Based on TE101 Cavity Mode and TE01δ Dielectric Mode," *IEEE Transactions on Microwave Theory and Techniques.,* vol. 64, no. 12, pp. 4434-4443, Dec. 2016.

[9] S. Bastioli, C. Tomassoni and R. Sorrentino, "TM dual-mode pseudoelliptic filters using nonresonating modes," *2010 IEEE MTT-S International Microwave Symposium*, Anaheim, CA, 2010, pp. 880-883.

[10] S. Adhikari, A. Ghiotto, and K. Wu, "Simultaneous electric and magnetic two-dimensionally tuned parameter-agile SIW devices," *IEEE Transactions on Microwave Theory and Techniques.,* vol. 61, no. 1, pp. 423-435, Jan. 2013.

Chapter 5

NOVEL CLASS OF BANDPASS FILTERS BASED ON MUSHROOM-SHAPED RESONATORS

[1], [2], [3] and [4]

In this chapter, a novel class of pseudo-elliptic in-line bandpass SIW filter based on mushroom-shaped resonators is presented. This structure uses non-resonating modes to obtain coupling between non-adjacent nodes. The non-resonating modes resonate far away from the filter band, allowing some power to bypass the resonator: this generates a source-to-load coupling able to insert transmission zeros in the filter response. Non-resonating modes have been used in different configurations. In particular, they have been used in combination with TM cavities [5], with resonant post in rectangular waveguide [6] or with high permittivity dielectric pucks [7], [8].

As described in Chapter 1, inductive posts, behaving as inductive obstacles, have been widely adopted in in-line filter design. In literature, partial-height posts have been presented as band-reject elements. Finally, in [9], a pair of partial-height posts is used to generate a couple of resonances. The lower resonance is used as non-resonating mode to create a transmission zero. These filters, compared to the classical in-line filters with inductive obstacles, are shorter and exhibit a number of transmission zeros up to the number of poles [7].

The structure proposed in this chapter yields to a response with the maximum number of transmission zeros, i.e. equal to the number of resonators, with considerable advantages in terms of selectivity. The basic idea is to use the odd mode of the singlet (composed by two strongly coupled mushrooms) to obtain the filter pole. At the same time, the even mode, resonating far away from the filter pass-band, is used as a non-resonating mode to bypass the resonator itself, creating a transmission zero. Starting from the analysis of the singlet, some examples have been proposed to determine the geometrical parameters that play an important role (for the couplings) in the resonance frequency separation of the modes (even and odd) and the related quality factor, Q. Higher order filters have been designed, realized and tested starting from singlets and doublets. The results of this work, explained in this Chapter, have been published and can be found in [1], [2], [3]. [4] has been submitted.

1 SINGLET

Singlets can be considered as a building block to obtain higher order filters and, for this reason, they have been studied and analyzed as the first and most important basic structure. They consist of a dual mushroom-shaped resonator (Fig. 76) composed of circular patches suspended in the dielectric substrate of the SIW and short-circuited to the waveguide upper wall by metallized holes. The first two resonant modes of the singlet (Fig. 76) present an even and odd field distribution, respectively. The even and odd combination of their own resonant modes is due to the strong coupling between the two resonators (each 'mushroom' is a resonator itself).

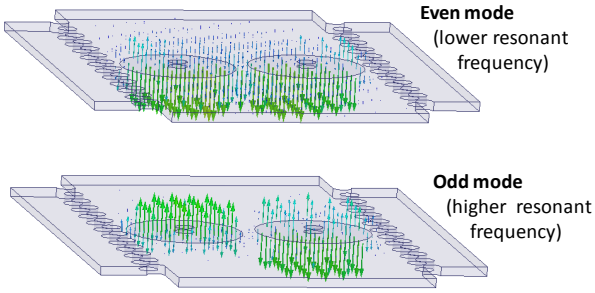

Fig. 76. Singlet composed by a dual-mushroom resonator in a SIW: electric field distribution of the first two resonating modes. [1], [2]

The idea is to use the odd mode to obtain a filter pole whilst the even mode, resonating far away from the filter pass-band, is used as 'non-resonating' mode to bypass the resonator itself. With this approach, a transmission zero is then created with the direct source-to-load coupling. For this reason, the odd-mode and even mode are also called resonating-mode and non-resonating mode, respectively. In order to avoid spurious frequencies in the lower stop-band, generated by the non-resonating modes, it is convenient to use a SIW width with a cut-off frequency higher than the resonance frequency of non the non-resonating mode (as shown in Par. 3). The resonance frequencies of both modes have been plotted in Fig. 77 versus the mushroom cap radius *r*: the odd mode has a resonance frequency always superior respect to the even mode. The height of the mushroom's stem is limited by the height of the commercial substrates.

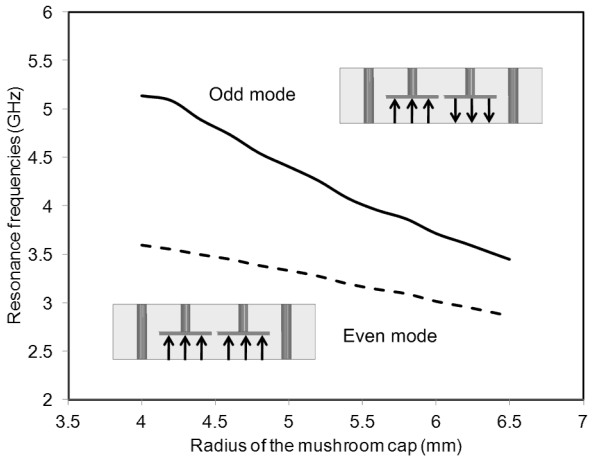

Fig. 77. Resonance frequencies of the odd and even modes of the double-mushroom resonator in relation to the variation of the resonator's cap radius. [2]

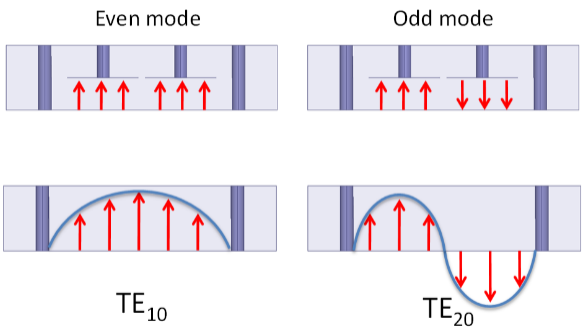

Fig. 78. Dual-mushroom resonator modes (above) and SIW modes (bottom). [3]

In Fig. 78, a comparison between the modes of a resonator composed by two identical 'mushrooms' (symmetrically placed along the transverse cross-section of the SIW) and the first two SIW modes is shown. For symmetry reason, the even mode of the resonator couples to the quasi-TE_{10} mode of the SIW and is uncoupled to the quasi-TE_{20}. Analogously, the odd mode couples to the second mode and is uncoupled with the fundamental mode of the SIW (Fig. 79(*a*) and Fig. 79(*b*)). For this reason, the symmetric structure does not produce any filtering function. At the same time, it should be noted that a small amount of the incident power bypasses the resonator (Fig. 79(*d*)). This is because the fundamental mode (source) excites the non-resonating mode of the dual-mushroom resonator and, in turn, the non-resonating mode excites the load.

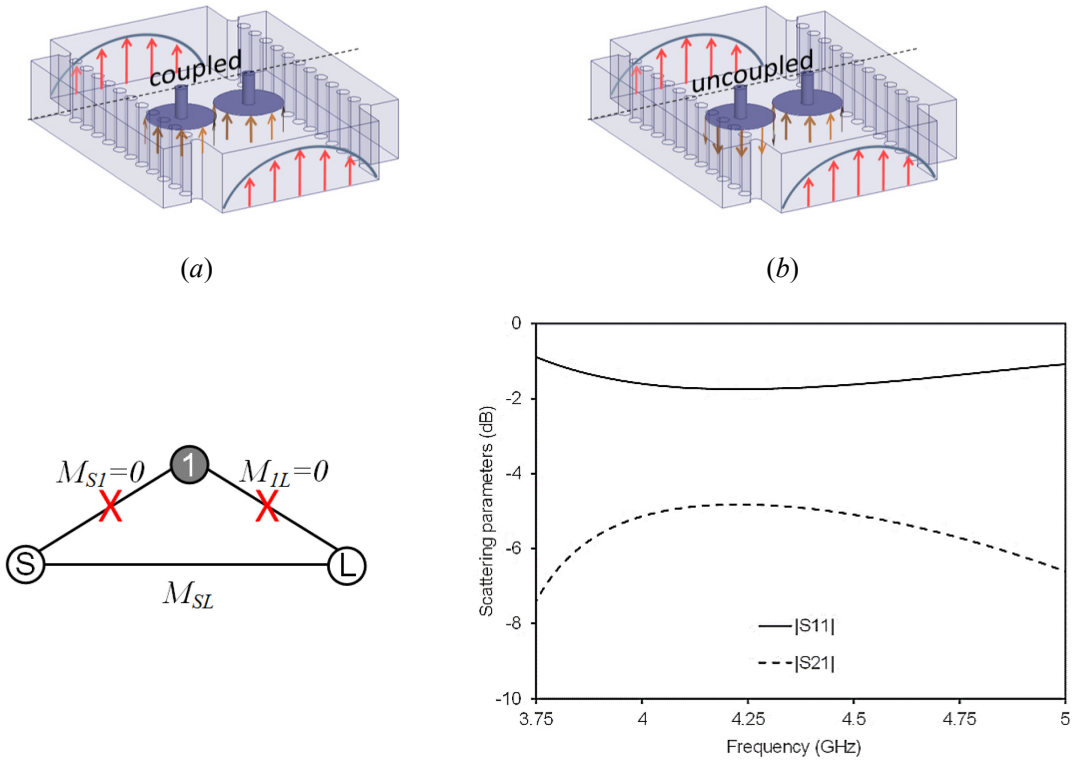

(*a*) (*b*)

(*c*) (*d*)

Fig. 79. Coupling between the SIW and the resonator modes: (*a*) 3-D structure with the coupled TE_{10}; (*b*) 3-D structure with the uncoupled TE_{20}; (*c*) relevant topology; (*d*) response of a doublet having symmetric dual-mushroom resonators. [3]

1.1 Analysis of the dual-mushroom symmetric singlet

In order to comprehend the impact on the resonant frequency separation of the modes and the quality factor of the resonator, various analyses have been carried out by changing several geometrical parameters (Fig. 80). In particular, Fig. 80 displays two mushrooms with same cap diameter symmetrically placed with respect to the longitudinal axis of the SIW waveguide.

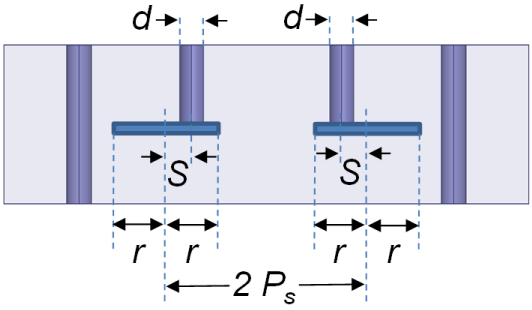

Fig. 80. Dual-mushroom symmetric singlet with geometrical parameters. [3]

The geometrical parameters included in the analysis, are: distance P_s between the center of the waveguide and the circular patch (mushroom cap); the distance S between the center of the post (mushroom stem) and the center of the circular patch, and finally the post diameter d (Fig. 80).

The first parameter analyzed was the distance between the center of the waveguide and the circular patch, P_s. It can be noted (Fig. 81(*a*)) that this parameter plays a small role in the frequency separation between the resonating and non-resonating mode, leaving the Q factor practically unaffected (Fig. 82(*a*)). However, when the stems are not centered with the mushroom cap, the Q factor of the resonator is strongly affected. Considering the stem shift, S, it can be noted (Fig. 82(*b*)) that the Q factor is maximum for S=0, and it decreases when the stem is shifted toward the SIW center (S>0) or toward the SIW walls (S<0). On the other hand, the mode separation increases when the two stems become closer (Fig. 81(*b*)). Finally, when diameter d is varied, the Q factor is modified and better results are obtained for larger diameters (Fig. 82(*c*)). Incrementing the diameter, a higher resonant frequency separation can be obtained resulting in a better behavior in the lower stop-band (Fig. 81(*c*)).

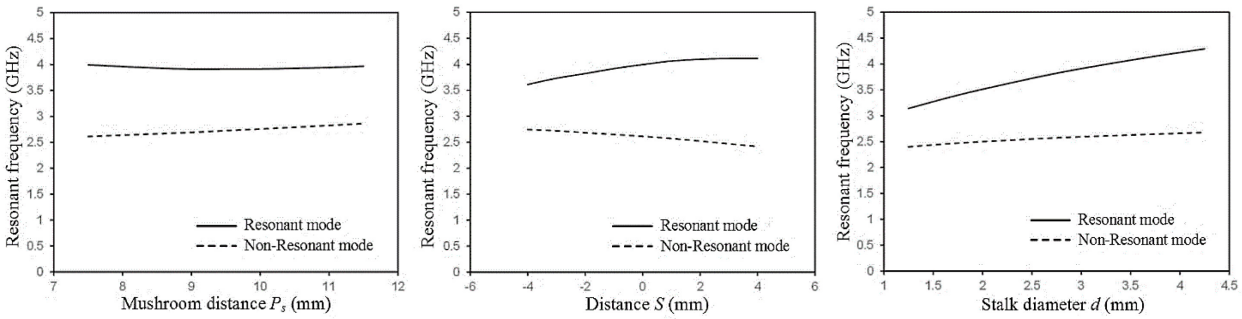

(*a*) (*b*) (*c*)

Fig. 81. Resonant frequency separation between resonant and non-resonant modes, varying different geometrical parameters (SIW width=40mm, vias diameter=2 mm, longitudinal spacing between vias=3.5 mm, ε_r=2.2 and thickness=1mm): (*a*) mushroom distance, P_s; (*b*) distance S between the center of the post (mushroom stem) and the center of the circular patch; (*c*) post diameter d [3]

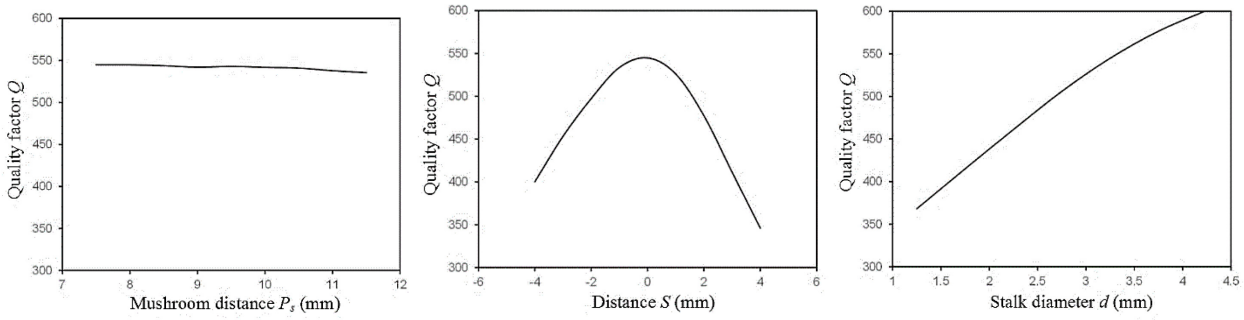

(*a*) (*b*) (*c*)

Fig. 82. Quality factor, *Q*,of the resonator obtained by varying different geometrical parameters (SIW width = 40mm, vias diameter = 2 mm, longitudinal spacing between vias = 3.5 mm, $\varepsilon_r = 2.2$ and thickness = 1mm): (*a*) mushroom distance, P_s; (*b*) distance *S* between the center of the post (mushroom stem) and the center of the circular patch; (*c*) post diameter *d* [3]

1.2 Analysis of the dual mushroom asymmetric singlet

In order to obtain a filtering response, the odd mode needs to be excited and this can be achieved, a-symmetrizing the structure. In this paragraph, two different methods are explained. The first method is related to the use of different dimensions of the mushroom cap, whereas, the second refers to the use of a rotated mushroom. Different analyses have been performed to show the ability to control the coupling of the resonant mode to source (M_{S1}) and load (M_{1L}).

1.2.1 Varying the mushroom cap radius

In the first method, according to Fig. 83, mushroom cap with different radii are used. In this structure, the field pattern of the resonating modes is slightly different from the symmetric singlet field with identical mushrooms. In particular, the field distribution is no longer symmetric thus allowing the fundamental SIW mode to couple to both resonating and non resonating mode.

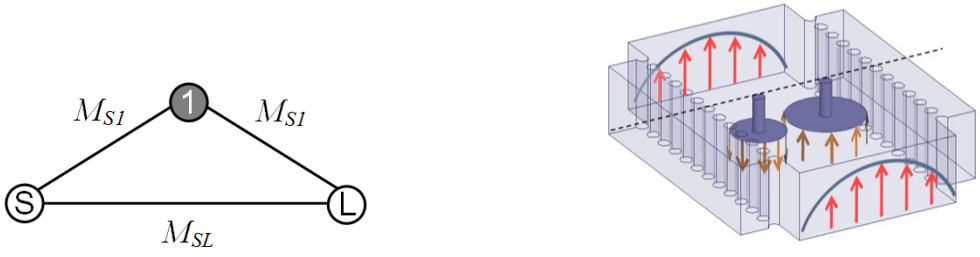

(*a*) (*b*)

Fig. 83. Different mushroom cap dimensions: (*a*) relevant topology; (*b*) 3-D structure of the asymmetric singlet [2]

The coupling of the resonant mode to source (M_{S1}) and load (M_{1L}) is controlled with *dr* and it can be noted that a significant value *dr* results in a wide filtering band. This has been shown in Fig. 84 by varying *dr* from 0.2 mm to 1 mm (SIW width = 33 mm, vias diameter = 2 mm, longitudinal spacing between vias = 3.5 mm, *r* = 6.5mm, $\varepsilon_r = 2.2$ and thickness = 1mm). The direct source-to-load coupling M_{SL} produces a transmission zero.

The transmission zero is present in the lower stop band because M_{S1} and M_{1L} have the same amplitude and sign ($M_{S1}=M_{1L}$). Fig. 85 displays the non-normalized couplings versus the variation *dr*.

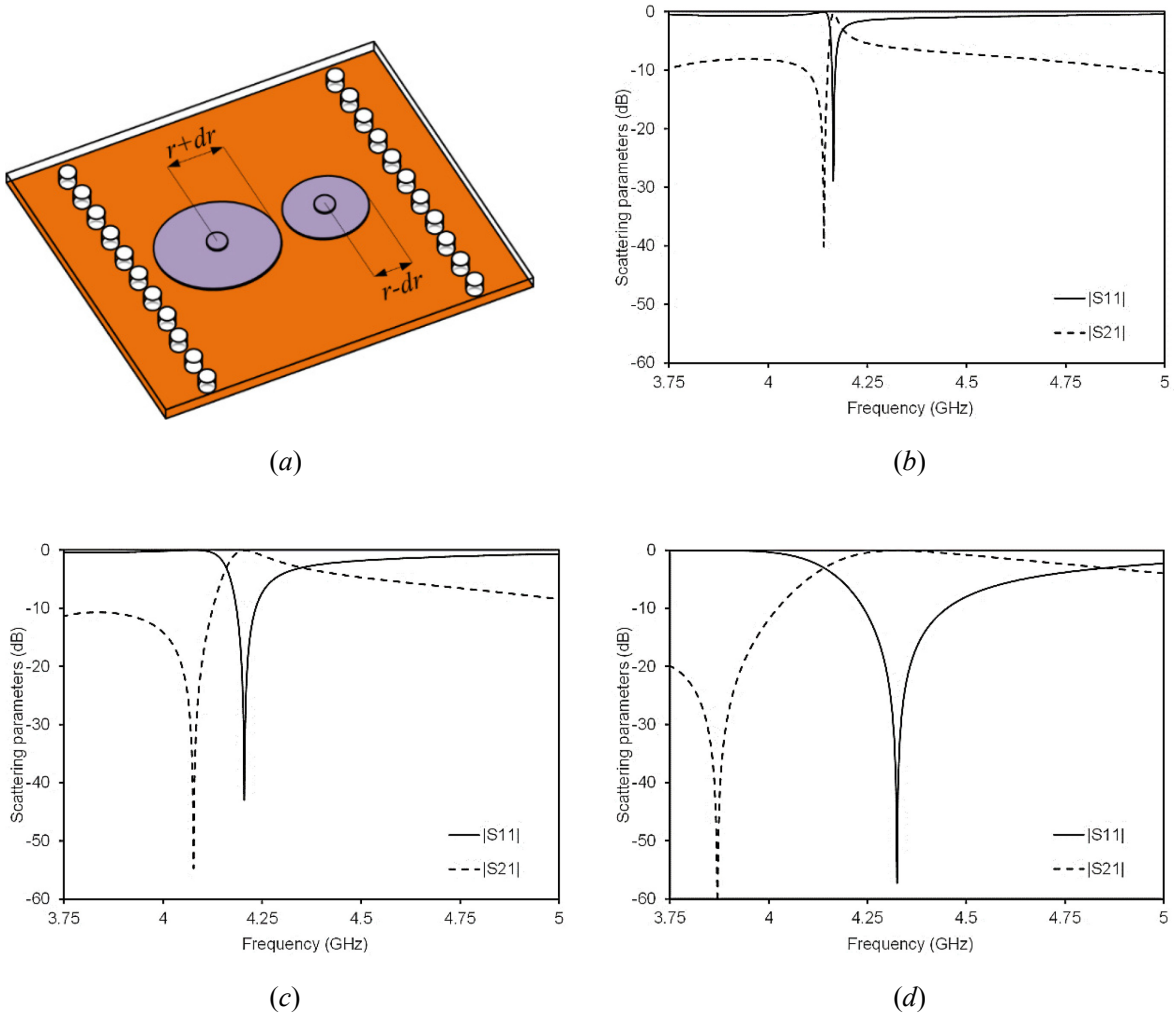

Fig. 84. Analysis of the singlet with the resonators with different mushroom cap size: (*a*) geometry of the singlet; (*b*) frequency response for *dr* = 0.2 mm; (*c*) frequency response for *dr* = 0.5 mm; (*d*) frequency response for *dr* =1 mm.[2], [3]

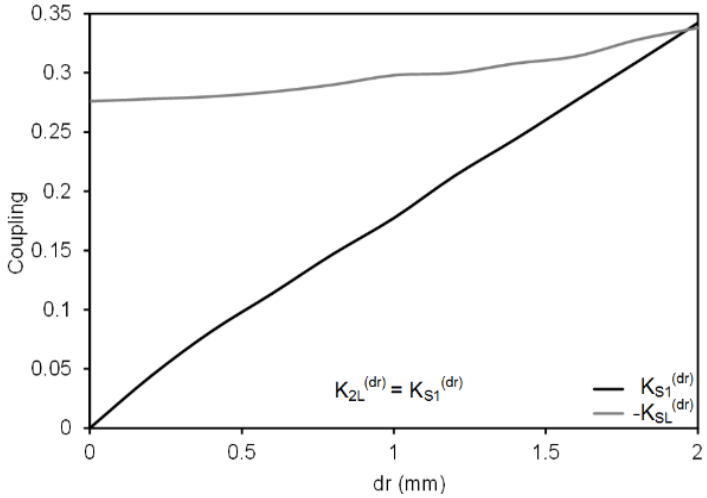

Fig. 85. Variation of non-normalized coupling coefficients versus the different mushroom cap dimensions. [4]

1.2.2 Rotation of the mushrooms

The odd mode can also be excited by rotating the resonator around its axis as shown in Fig. 86(*b*). Simple considerations about the new E-field distribution symmetry suggests that the couplings of the resonant mode to source and load have the same amplitude but different signs (M_{S1}=-M_{1L}). Accordingly, the filtering response presents a pole and a transmission zero in the upper stop-band.

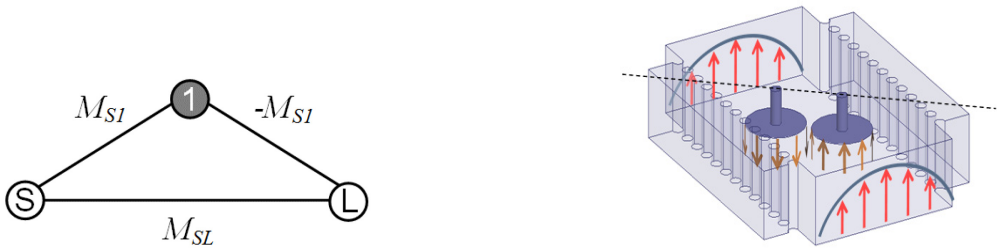

(*a*) (*b*)

Fig. 86. Rotation of the mushrooms: (*a*) relevant topology; (*b*) 3-D structure of the asymmetric singlet [4]

This is shown in Fig. 87 (SIW width = 33 mm, vias diameter = 2 mm, longitudinal spacing between vias = 3.5 mm, r=6.5mm, ε_r=2.2 and thickness = 1mm), where different responses for different rotation angles are shown. It is evident from the figure that the rotation angle φ allows for easy control of M_{S1} (and M_{1L}) amplitude in a wide range. More precisely, there is a correlation between φ and M_{S1} (or M_{1L}). Fig. 88 displays the non-normalized couplings versus the rotation angle, φ.

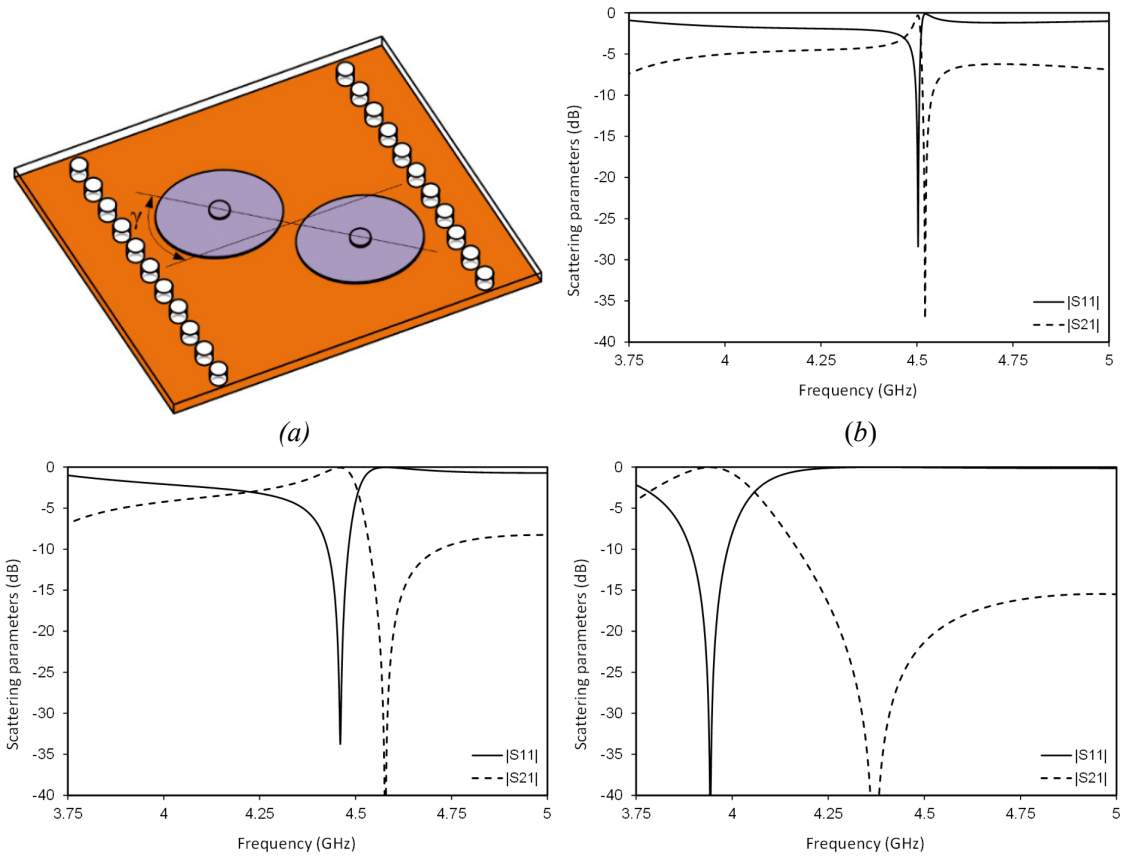

(*a*) (*b*)

(*b*) (*d*)

Fig. 87. Analysis of the singlet with the rotation of the mushroom: (*a*) geometry of the singlet; (*b*) frequency response for γ = 8°; (*c*) frequency response for γ = 20°; (*d*) frequency response for γ = 40°. [4]

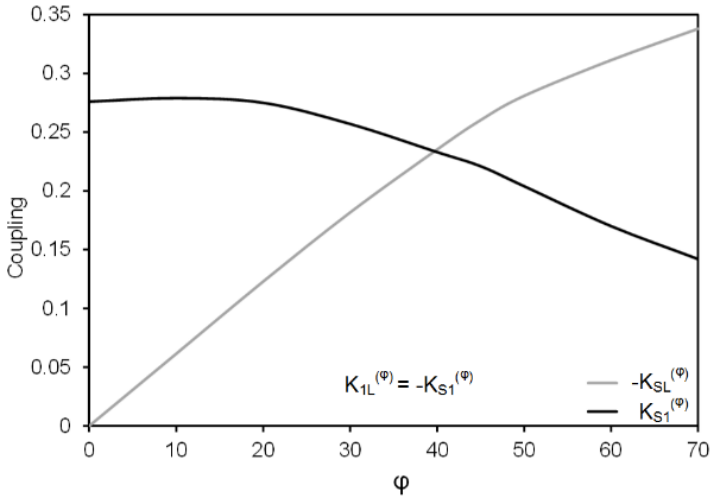

Fig. 88. Variation of non-normalized coupling coefficients versus the mushroom rotation. [4]

1.3 Singlets design with non-normalized coupling coefficients

In order to easily design a singlet, the non-normalized coupling coefficients *K*, introduced in Fig. 85 and Fig. 88, can be used. This section demonstrates how to easily combine the features obtained with the rotation and the different mushroom radii into the design of a singlet. These combined properties give an independent control of the input and output couplings ($|K_{S1}| \neq |K_{1L}|$).

The coupling coefficients are related to the normalized coupling matrix elements *M* in the following way:

$$\begin{aligned} K &= M \cdot FBW && resonator - resonator \\ K &= M \cdot \sqrt{FBW} && source\ (or\ load) - resonator \\ K &= M && source - load \end{aligned}$$

where FBW represents the Fractional Bandwidth. In the case of the coupling between two synchronous resonators:

$$|K| = \frac{\left|f_2^2 - f_1^2\right|}{f_2^2 + f_1^2} \tag{27}$$

where f_1 and f_2 are the resonant frequencies of the coupled resonators. Singlets having $|K_{S1}| \neq |K_{2L}|$ are required in the multi-pole filter design, and they can be obtained using rotated dual-mushroom resonators with different disk radii. A very simple way to design a singlet is by using both the diagrams of Fig. 85 and Fig. 88 with the following equations:

$$\begin{aligned} K_{S1}^{(dr,\varphi)} &= K_{S1}^{(dr)} + K_{S1}^{(\varphi)} \\ K_{1L}^{(dr,\varphi)} &= K_{S1}^{(dr)} - K_{S1}^{(\varphi)} \end{aligned} \tag{28}$$

where $K_{S1}^{(dr,\varphi)}$ and $K_{1L}^{(dr,\varphi)}$ are the non-normalized coupling coefficients of a singlet rotated by an angle of φ and having disks with different radii (*dr*). In (29), a superposition property has been considered. Inverting (29) we can obtain the formulation, creating a singlet.

$$K_{S1}^{(dr)} = \frac{1}{2}\left(K_{S1}^{(dr+\varphi)} + K_{1L}^{(dr,\varphi)}\right)$$
$$K_{S1}^{(\varphi)} = \frac{1}{2}\left(K_{S1}^{(dr+\varphi)} - K_{1L}^{(dr,\varphi)}\right) \quad (29)$$

The legitimacy of the use of the superposition property is confirmed with the design of doublets in Sec. 2.

2 DOUBLET

Considering the cascade of two singlets, a doublet topology as in Fig. 89, can be obtained. In particular, the coupling between source and resonator 2, as well as the coupling between load and resonator 1, should be zero (resonator is coupled to the waveguide fundamental mode just on one side). In order to obtain such couplings, the singlets design of Par 1.3 results in the combination of the specific values of Fig. 83 and Fig. 86. In particular, the source-load coupling has been obtained with the fundamental mode travelling through the resonators. Resonators 1 and 2 can be coupled through the TE_{20} (below cut-off) because the fundamental mode is not able to couple them. By using the TE_{20} below cut-off, one advantage is immediate: the coupling between resonators can be controlled by the resonators distance. In addition, it should be noted that the diagrams of Fig. 85 and Fig. 88 and the formulations aforementioned can be used also for the design of doublets having the topology shown in Fig. 89.

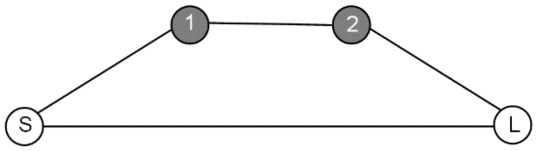

Fig. 89. Doublet topology.

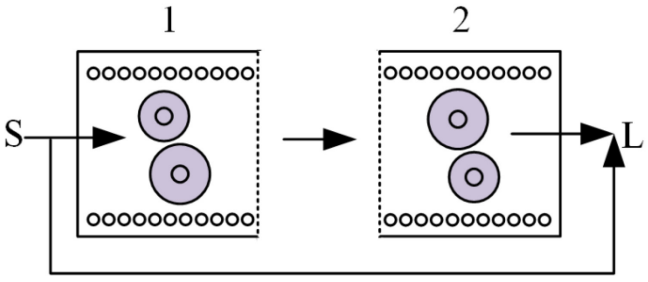

Fig. 90. Doublet obtained by cascading two singlets, together with the relevant coupling pattern.

As an example, the doublet having coupling coefficients K_{S1}=0.2, K_{12}=-0.052, K_{2L}=-0.2 has been designed. In this specific case, two identical singlets - with coupling between source and resonator equal to 0.2 and coupling between resonator and load equal to zero - have been cascaded. This structure corresponds to the doublet in Fig. 91. The distance between the singlets has been chosen in order to obtain the required K_{12}. Fig. 91 shows a good agreement between the full wave response and the equivalent circuit response. Note that in the doublet of Fig. 91, the sign of the coupling between resonator 2 and load is negative (odd symmetry in Fig.

90)). A change of this sign (by using an even symmetry of the structure instead of the odd symmetry) produces a movement of the zeros from the imaginary to real axis.

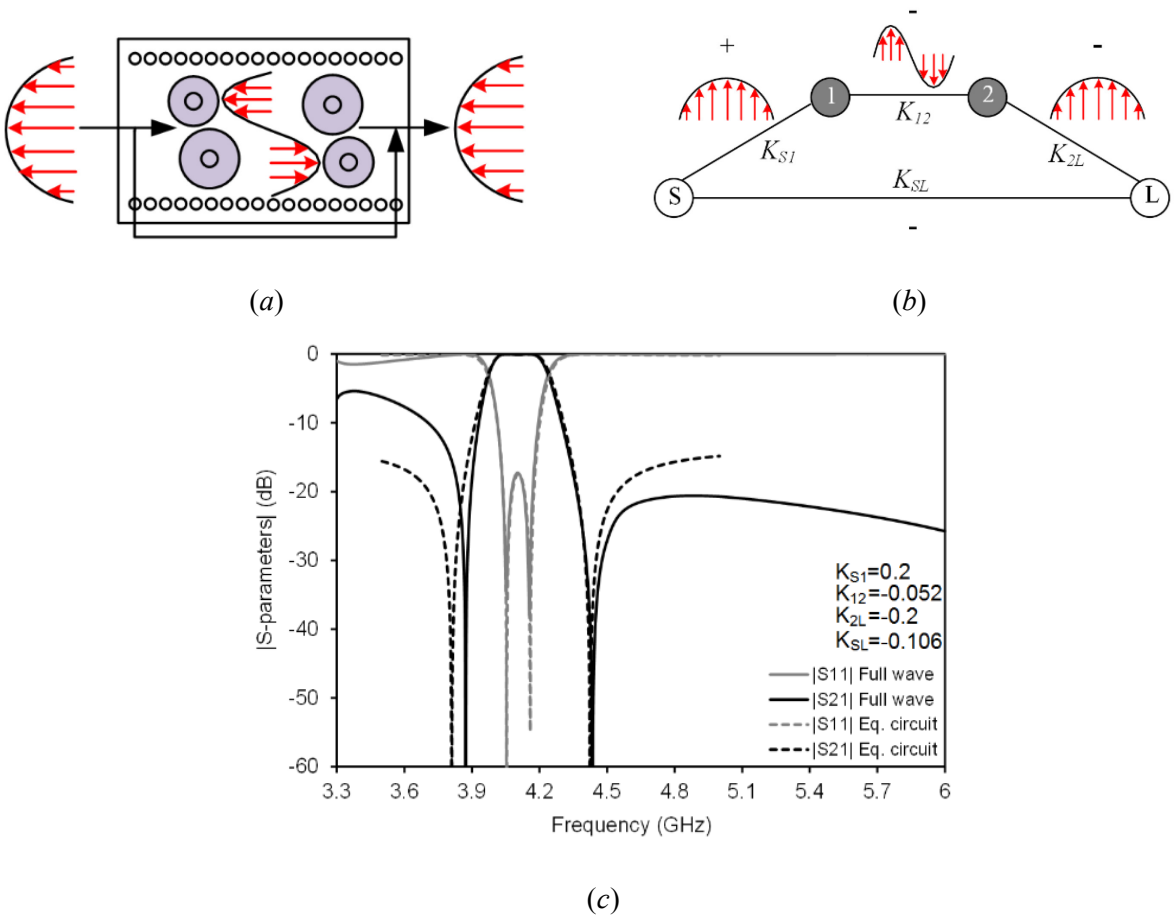

Fig. 91. Doublet obtained by cascading two singlets. Non-normalized couplings, *K*, used to obtain the filter response, are shown (*a*) geometry of the singlet; (*b*) relevant topology and couplings; (*c*) comparison between full-wave and equivalent circuit response obtained by cascading two singlets. [4]

3 HIGHER ORDER FILTERS

A simple way to design higher order filters can be obtained cascading symmetric pairs (respect to the central axis of the SIW waveguide) of identical mushrooms, with the exception of the first and last one, that control the coupling with source/load through the fundamental SIW mode (Fig. 92). The first and last resonators can be realized adopting only the asymmetry due to the different cap radii. Therefore, the couplings with source and load can be adjust selecting the value *dr* (as explained in Par.1.2.1). The coupling between resonators is controlled with the TE_{20} mode: the higher the distance between two adjacent resonators, the smaller the coupling. The fundamental mode of the SIW generates additional coupling between non-adjacent elements, namely: direct source-to-load coupling M_{SL}, coupling M_{SN} between source and last (N^{th}) resonator, coupling

M_{1L} between first resonator and load, and coupling M_{1N} between first and last resonators. Such additional couplings allow for a filtering function with transmission zeros.

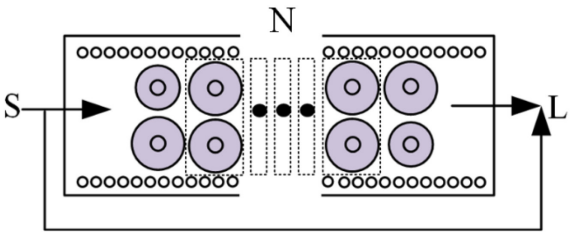

Fig. 92. Higher order (N^{th}) filter obtained cascading symmetric pairs of mushroom with first/last asymmetric resonators.

However, this filter topology does not allow the control of all transmission zeros.

A different method, consisting in cascading singlets or doublets through non resonating nodes (as in Chapter 3) can be implemented. This method maintains the number and the position of the transmission zeros after the cascade. The disadvantage, respect to the aforementioned filter, is the introduction of lambda/4 lengths, incrementing the overall dimensions. In this case, a four-pole filter has been designed starting from the following coupling matrix representing the filter of Fig. 94:

$$\begin{bmatrix} 0 & 1.0809 & 0 & 0.0849 & 0 & 0.0112 \\ 1.0809 & 0 & -1.0037 & 0 & 0 & 0 \\ 0 & -1.0037 & 0 & 0.641 & 0 & 0.0849 \\ 0.0849 & 0 & 0.641 & 0 & -1.0037 & 0 \\ 0 & 0 & 0 & -1.0037 & 0 & 1.0809 \\ 0.0112 & 0 & 0.0849 & 0 & 1.0809 & 0 \end{bmatrix}$$

It can be noted that this coupling matrix is the cascade of two identical doublets (Fig. 93) with the following coupling matrix.

$$\begin{bmatrix} 0 & 1.089 & 0 & -0.106 \\ 1.0809 & 0 & -1.0037 & 0 \\ 0 & -1.0037 & 0 & -0.8006 \\ -0.106 & 0 & -0.8006 & 0 \end{bmatrix}$$

In particular, in Fig. 93, the comparison between the full-wave analysis and the equivalent circuit is reported as well as the non-normalized couplings, *K*. The doublet has been designed using the method introduced in Par. 1.3 but, in contrast to the previous examples, here the two singlets to be cascaded are not identical, resulting in an asymmetric doublet. By adopting this method it is possible to have different positioning of the transmission zeros. It should be noted that the response (dashed line) of Fig. 94 presents two double-transmission zeros. This is due to the fact that two identical doublets have been cascaded and the position of the zero of each doublet has been maintained in the same position after the cascade. In the practical full-wave implementation however, some spurious couplings appear and each double zero is separated into two zeros, resulting in a four pole four zero filtering function (continuous lines).

The main problem of the designed filter is the spurious frequencies appearing both in the lower and higher stop-band. Fortunately, such spurious frequencies can be removed. In particular, spurious frequency in the higher stop-band a result of the resonance due to the lambda/4 line used to cascade the two doublets. Reducing the distance between the doublets, the resonance can be translated at higher frequency. This variation can be compensated by altering the geometrical parameters of resonators 2 and 3. On the other hand, the spurious frequency due to the resonance in the lower stop-band is related with the even mode of double mushroom

resonators (see Par. 1.1). In this case, the idea is to push the resonance below the waveguide cut-off. This can be done, for example, by choosing mushroom resonators with posts not centered to the disks (see Par. 1.1), and changing the width of the input-output SIW waveguide.

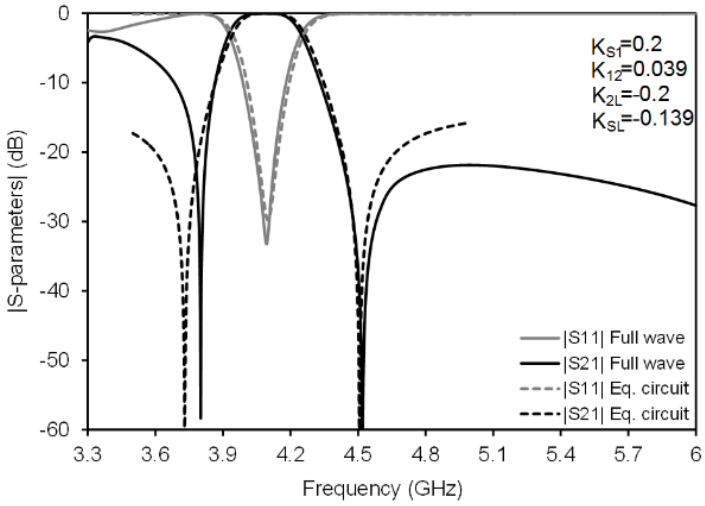

Fig. 93. Comparison between full-wave and equivalent circuit response obtained by cascading two non identical singlets. Non-normalized couplings, *K,* are shown. [4]

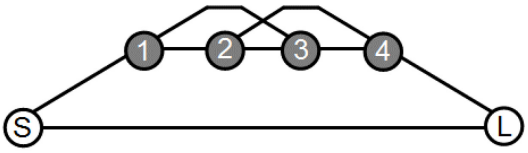

(*a*)

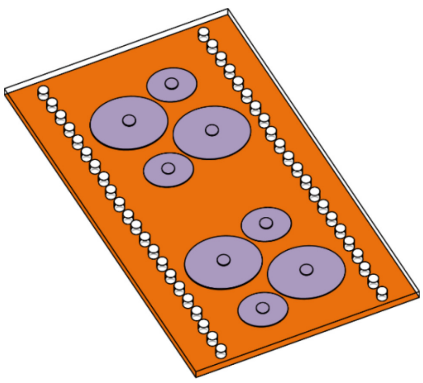

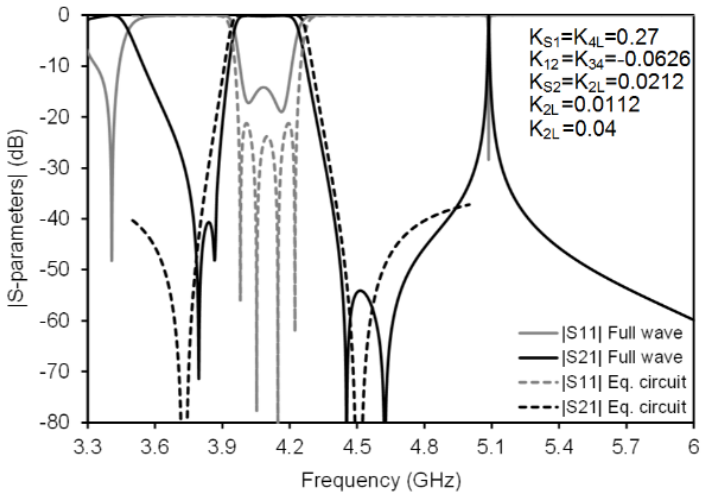

(*b*) (*c*)

Fig. 94 Four-pole filter obtained by cascading two identical doublets: (*a*) relevant topology; (*b*) geometry; (*c*) comparison between full-wave and equivalent circuit response. Non-normalized couplings, *K,* are shown. [4]

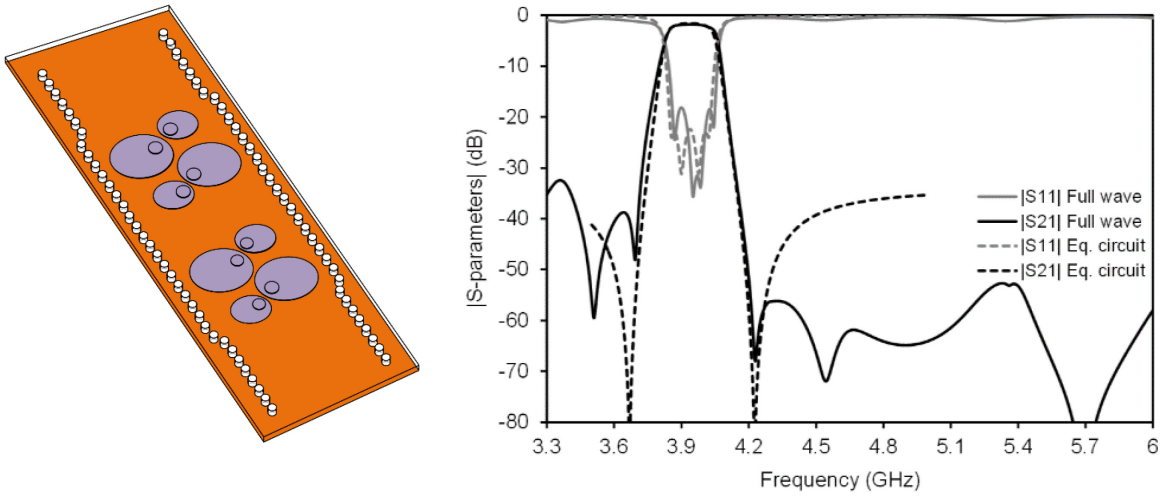

(*a*) (*b*)

Fig. 95 Four-pole filter obtained with spurious removal: (*a*) geometry; (*b*) comparison between full-wave and equivalent circuit response. [4]

4 FABRICATION AND MEASUREMENTS

Two different prototypes have been fabricated and measured by using a LPKF E33 milling machine on a commercial dielectric laminate Taconic TLY 5 (ε_r=2.2, tanδ=0.0009 and thickness 0.5mm). In order to realize the filter, consisting of suspended patches in the SIW structure (short circuited to the waveguide upper wall), two different dielectric substrates have been machined and then glued together. On the top layer of the first laminate, the tapered microstrips to SIW waveguide have been manufactured as well as the mushroom stems – consisting in holes through the substrate. On the second laminate, the mushroom patches have been realized (Fig. 97(*a*), Fig. 99(*a*)). Alignment between layers is fundamental and reference holes have been used for this purpose. The two machined layers have been glued together by using the Taconic TacBond bonding film with the exception of the mushroom caps (since electrical contact with the stems is necessary). The short-circuit between the top metal layer and the patches is realized with the LPKF ProConduct paste. The same has been used for the metallized vias of the SIW.

The first realized prototype is a doublet (geometrical parameters in Fig. 96, dimensions in TABLE XIII) with central frequency 4GHz and 5% fractional bandwidth. Simulation and measurement (Fig. 97(*b*)) show an overall good agreement: the insertion loss of the measured prototype is 2.5dB while the simulated was 1dB. The difference is due to fabrication issues, mainly related to the gluing of the two layers.

The second realized prototype (Fig. 99(*a*)) is a four-pole filter with spurious suppression (geometrical parameters in Fig. 98 and dimensions in TABLE XIV). In order to assure good electrical contact between the top and the bottom walls of the waveguide, metal sheets are realized in the middle layer (Fig. 99(*a*)). Simulations and measurements are shown in Fig. 99(*b*). The filter is centered at 3.9GHz with a 7% fractional bandwidth. The measured insertion loss is 4dB instead of the simulated 2dB. Also in this case, the problems encountered in the previous realization have been noticed. Moreover, the incremental length, results in a more complex structure to be fabricated. Different methods have been implemented, for both prototypes, to try to overcome this fabrication issue: in particular different gluing approaches, various alignment methods have

been used with no better results than the ones, here proposed. However, it should be noted that the overall filtering function is respected.

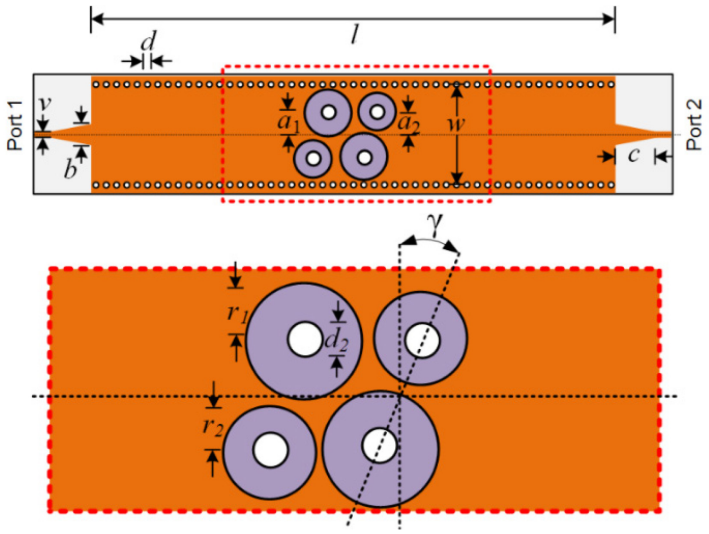

Fig. 96. Geometrical parameters of the doublet [4]

TABLE XIII
DIMENSIONS OF THE DOUBLET IN FIG. 97 (IN MM, γ IN °)

v=3.2	b=7.2	d=2	w=33
l=109	d_2=4	a_1=6.5	a_2=6.5
c=20	r_1=7	r_2=6	γ=16°

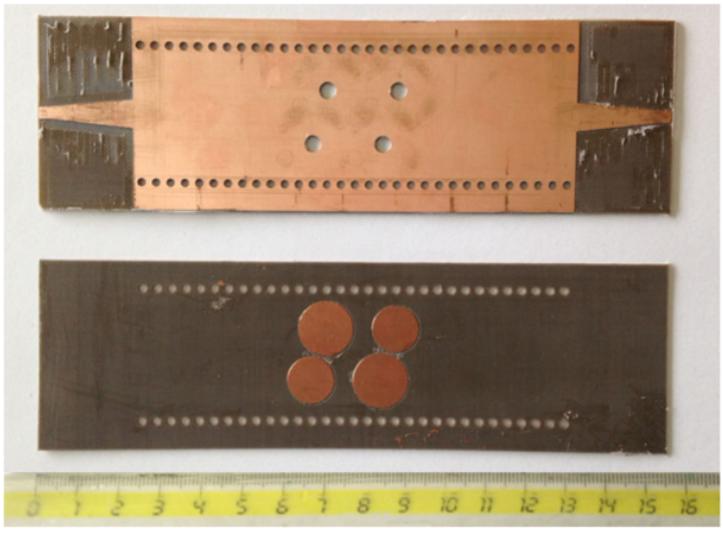

(*a*)

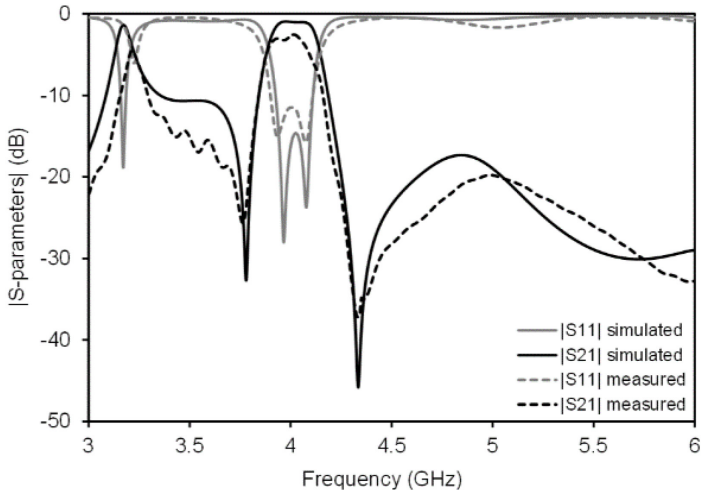

(*b*)

Fig. 97. Realized doublet filter: (*a*) disassembled prototype; (*b*) simulation and measurement of the prototype. [4]

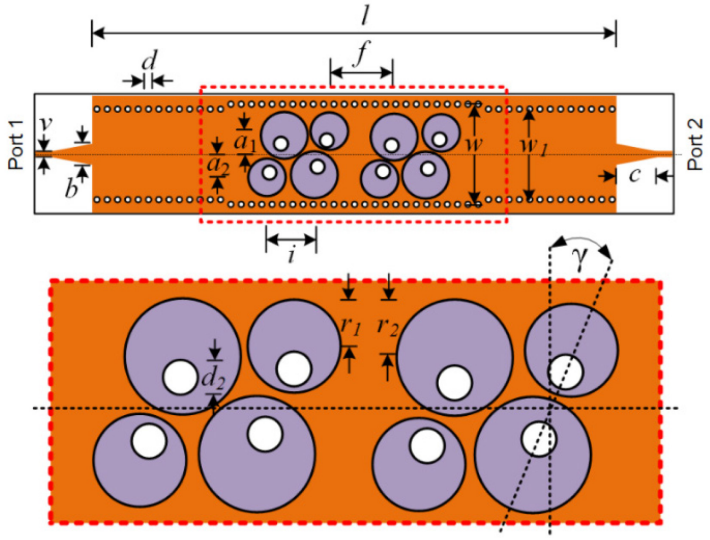

Fig. 98. Geometrical parameters of the four-pole filter [4]

TABLE XIV
DIMENSIONS OF THE FOUR-POLE FILTER IN FIG. 99 (IN MM, γ IN °)

v=3.2	b=4.4	d=2
w_1=30.6	f=24	i=17
l=172	d_2=5	a_1=8.9
c=11.6	r_1=5.1	r_2=6.8
w=35.5	a_2=6.9	γ=19°

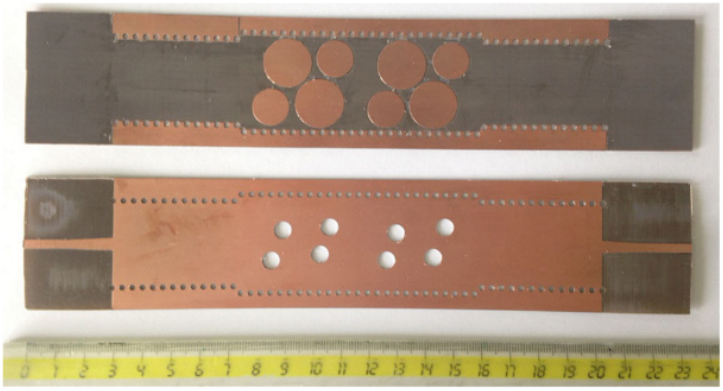

(*a*)

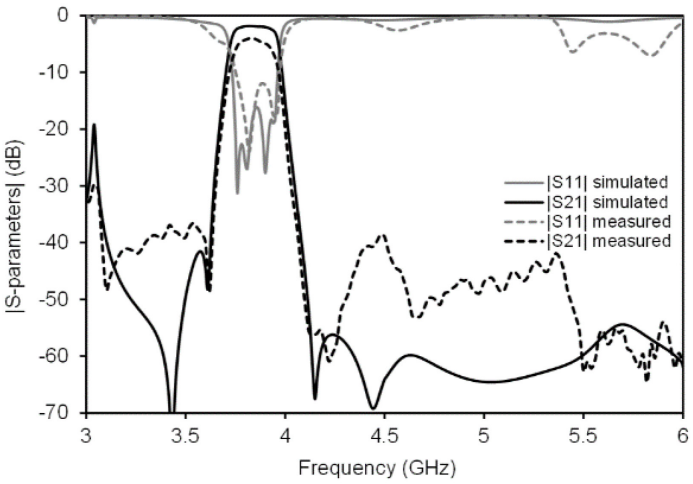

(*b*)

Fig. 99 Realized four-pole filter: (*a*) disassembled prototype; (*b*) simulation and measurement of the prototype. [4]

5 CONCLUSIONS

This paper presents a new class of pseudo-elliptic SIW filters realized with dual mushroom shaped resonators. This filter, with respect to the conventional in-line waveguide filter with inductive obstacles, shows some advantages such as the ease of optimization, shorter dimensions and a better selectivity. The basic structure is a singlet, consisting of a dual-mushroom resonator placed in the middle of a SIW waveguide and composed by a circular patch suspended in a SIW and short-circuited to the waveguide upper wall by posts. Frequency response with transmission zeros is obtained in an in-line geometry, by exploiting the non-resonating mode (even mode) to create coupling between non-adjacent resonators. The odd mode of the resonators is used to obtain poles and can be excited either by rotating the resonator or by using mushrooms with different cap radii. Singlets can be used as a building block to create higher order filters and, starting from this structure different analyses have been carried out. A design methodology has been proposed and validated with the comparison with full-wave simulations. Higher order filters have been designed cascading singlets (realizing doublets) and then doublets (realizing four-pole filters). Two different prototypes have been realized and measured to confirm the theoretical studies. The measured insertion loss, in both cases, is higher respect to the simulations and this is due to fabrication inaccuracies. In particular, this is due to the inaccurate gluing of the two layers. A different fabrication process realized with expertise can help to reduce these discrepancies. However, the theoretical design method has been demonstrated.

REFERENCES

[1] C. Tomassoni, L. Silvestri, M. Bozzi and L. Perregrini, "Quasi-elliptic SIW band-pass filter based on mushroom-shaped resonators," 2015 *European Microwave Conference (EuMC)*, Paris, 2015, pp. 749-752.

[2] C. Tomassoni, L. Silvestri, M. Bozzi and L. Perregrini, "Novel substrate integrated waveguide filter based on mushroom resonators," *2015 IEEE 15th Mediterranean Microwave Symposium (MMS)*, Lecce, 2015, pp. 1-4.

[3] C. Tomassoni, L. Silvestri, M. Bozzi and L. Perregrini, "Substrate-integrated waveguide filters based on mushroom-shaped resonators," *International Journal of Microwave and Wireless Technologies*, 2016, pp. 741-749.

[4] C. Tomassoni, L. Silvestri, M. Bozzi, L. Perregrini, "A new class of Pseudo-elliptic SIW filters based on mushroom-shaped resonators", *Submitted to IEEE Transactions on Microwave Theory and Techniques*.

[5] C. Tomassoni, S. Bastioli and R. Sorrentino, "Generalized TM Dual-Mode Cavity Filters," in *IEEE Transactions on Microwave Theory and Techniques*, vol. 59, no. 12, pp. 3338-3346, Dec. 2011.

[6] C. Tomassoni and R. Sorrentino, "A New Class of Pseudoelliptic Waveguide Filters Using Dual-Post Resonators," in *IEEE Transactions on Microwave Theory and Techniques*, vol. 61, no. 6, pp. 2332-2339, June 2013.

[7] L. Pelliccia, F. Cacciamani, C. Tomassoni and R. Sorrentino, "Ultra-compact high-performance filters based on TM dual-mode dielectric-loaded cavities," in *International Journal of Microwave and Wireless Technologies*, pp. 151-159, 2014.

[8] S. Bastioli and R. V. Snyder, "Inline Pseudoelliptic${\rm TE}_{01\delta}$-Mode Dielectric Resonator Filters Using Multiple Evanescent Modes to Selectively Bypass Orthogonal Resonators," in *IEEE Transactions on Microwave Theory and Techniques*, vol. 60, no. 12, pp. 3988-4001, Dec. 2012.

[9] M. Politi, A. Fossati, "Direct coupled waveguide filters with generalized Chebyshev response by resonating coupling structures," *European Microwave Conference*, Paris, 2010.

Conclusions

Considering the evolution of IoT, 5G and WSN markets, their technical requests and, the inevitable impact on the everyday life, the Substrate Integrated Waveguide technology (SIW) seems a perfect candidate to respond to these requests. Nowadays, in truth, it should be noted that the maturity of a technology relies, also, in the generation of a general common good, also described in terms of low environmental impact whilst, still, easy accessible. Since all these considerations and bearing in mind SIW as a promising technology in these fields, two main issues can be addressed as detrimental for the successful choice of this technology: losses (related to the performances) and size. In particular, filters are present in wireless systems and therefore, the footprint minimization and the performance improvement - at low cost - are of primarily importance. For this reason, in this Thesis, different novel classes of microwave bandpass SIW filters have been studied and implemented, in order to reduce the size and, at the same time, improve the performances.

In particular, a novel class of bandpass filters based on the periodical perforation of the dielectric substrate has been designed. Adopting this new class of filters, a punching technique can be used for a mass-produced fabrication process able to cut the final cost of the component. Another bandpass filter, widely present in literature, with a similar in-band frequency response, is the iris-type filter. A comparison shows the superior strength to the fabrication intolerances of the proposed filter respect to the iris-type filter. This characteristic is fundamental when considering a low cost fabrication process. The study has been extended to the design of two versions of this filter able to reduce the size: a half-mode and a folded half-mode. The half-mode is able to reduce the size of the filter but suffers of higher losses due to the open boundary. The folded-half mode, instead, maintains the overall area of the half mode, reducing the radiation losses and introducing a transmission zero, related to the input-output coupling, thus improving the out-of-band performances.

Two new classes of filters, based on the dual-mode air-filled SIW cavities, are presented with the combined advantages of the air-filled and dual-mode cavities, thus signifying reduced losses and size. In addition, the out-of-band performances are improved with the introduction of transmission zeros. The dual-mode air-filled SIW cavity filter is realized with the perforation of the central portion of the SIW cavity, showing an enviable design simplicity. The dual-mode air-filled cavity has been studied starting from the transmission line model that relates the geometrical dimensions of the cavity to the resonant frequencies of the cavity modes. Therefore, it is shown that the filtering characteristics are simple controllable by playing on a few geometrical parameters. Both the doublets, able to realize two poles and two transmission zeros, and the higher order filters have been deeply investigated. A further study is dedicated to a dual mode air-filled SIW complementary cavity; the dielectric substrate is excavated in the lateral portions - instead of the central part - of the dielectric substrate. The new set of cavity modes gives the advantage of controlling the position of one transmission zero that can be placed either below or above the passband of the filter. The use of the coaxial probes and their position in the cavity gives a new degree of freedom in placing the other transmission zero. A comparison with a structure able to realize a similar filtering response is shown, highlighting the wider spurious free bandwidth of the proposed dual-mode air-filled SIW filter.

Last, a new class of mushroom-resonator based inline filter is studied, able to reduce the size (respect to the inline filter with inductive obstacles) whilst introducing a number of transmission zeros equal to the number of resonators, improving the out-of-band. The use of the odd mode of the singlet (realized with two strongly coupled mushrooms shaped) to obtain the filter pole. Conversely, the even mode is used to create a transmission zero. The study starts from the analysis of the singlet with some examples in order to determine the geometrical parameters that play an important role (for the couplings) in the resonance frequency separation of the modes (even and odd) and the related quality factor, Q. The asymmetry of the mushrooms, realized with

the different heads radii or the rotation of the coupled mushroom is explained and used for the design of doublet and higher order filters.

The in-house fabrication of these prototypes confirms the simplicity in realizing these topologies, allowing for low-cost, mass produced components. In addition, these filters have been realized on commercial dielectric substrates but the use of other substrates, in relation with the use and the surrounding environment of the components, is feasible. The classes here described show a reduction in size whilst improving the performances, either in-band or in the out-of-band of the filter.

After a long wait, let me end this Thesis with a consideration, here ironic: "[…] A hundred years ago 'to be modern' meant to chase 'the final state of perfection' - now it means an infinity of improvement, with no 'final state' in sight and none desired […]". [1]

[1] Z. Bauman, "Liquid Modernity," in *Polity Press*, Foreword to the 2012 Edition: Liquid Modernity Revisited, VIII-IX, 2012.

Acknowledgements

My heartfelt thanks for this work goes to many people who were closely involved in this project - either for technical support or personal backing. In particular, I would like to thank:

- Professor Maurizio Bozzi for all he has shared, for the belief he has had in me and for driving me through my Ph.D.
- Professor Cristiano Tomassoni for the kind help and work on filter synthesis related to the topologies here introduced. Thank you for answering every question in detail, without circumstantial prejudices.
- Professor Anthony Ghiotto for the work related to Chapter 3 and 4. Furthermore, because of the period I was able to spend in his group at the IMS, Research center (Université de Bordeaux, France). The experience was culturally enriching both for the friends I met and for the technical skills I improved.
- Professor Ángela Coves for the work on the class of filters of Chapter 1.

Furthermore, I am grateful to all the friends I have met in my laboratory (Microwave lab.), for all the great (and also sometimes difficult) moments, all the good laughs and all the stimulating arguments over our different ideas.

To my family, for the energy, patience, support they have always had for me.

Last but not least, I would love to thank a person with whom I have shared all the moments during these years and since the beginning of this experience. She knows, for real, what this signifies for me. For this reason, here, we close a Chapter.

My Ph.D. Thesis is dedicated to Mary L.

List of Publications

This is the list of publications realized and awards obtained during my Ph.D., subdivided in: International Journals, International Conferences and National Conferences.

INTERNATIONAL JOURNALS

[1] N. Delmonte, L. Silvestri, M. Bozzi, and L. Perregrini, "Compact Half-Mode SIW Cavity Filters Designed by Exploiting Resonant Mode Control," *International Journal of RF and Microwave Computer-Aided Engineering*, Vol. 26, No. 1, pp. 72–79, Jan. 2016.

[2] C. Tomassoni, L. Silvestri, M. Bozzi, and L. Perregrini, "Substrate Integrated Waveguide Filters Based on Mushroom-Shaped Resonators," *International Journal of Microwave and Wireless Technologies*, Vol. 8, No. 4-5, pp. 741-749, June 2016.

[3] M. Pasian, L. Silvestri, C. Rave, M. Bozzi, L. Perregrini, A.F. Jacob, and K.K. Samanta, "Substrate Integrated Waveguide E-plane 3-dB Power Divider/Combiner Based on Resistive Layers," *IEEE Transactions on Microwave Theory and Techniques*, Vol. 65, No. 5, pp. 1498-1510, May 2017.

[4] E. Massoni, L. Silvestri, G. Alaimo, S. Marconi, M. Bozzi, L. Perregrini, and F. Auricchio, "3D-Printed Substrate Integrated Slab Waveguide for Single-Mode Bandwidth Enhancement," *IEEE Microwave and Wireless Components Letters*, Vol. 27, No. 6, pp. 536-538, June 2017.

[5] L. Silvestri, E. Massoni, C. Tomassoni, A. Coves, M. Bozzi, and L. Perregrini, "Substrate Integrated Waveguide Filters Based on a Dielectric Layer with Periodic Perforations," *IEEE Transactions on Microwave Theory and Techniques*, Vol. 65, No. 8, pp. 2687–2697, Aug. 2017.

[6] C. Tomassoni, L. Silvestri, A. Ghiotto, M. Bozzi, and L. Perregrini, "Substrate Integrated Waveguide Filters Based on Dual-Mode Air-Filled Resonant Cavities," *IEEE Transactions on Microwave Theory and Techniques*, Vol. 66, No. 2, pp. 726-736, Feb. 2018.

[7] H. Abdel Ali, E. Massoni, L. Silvestri, M. Bozzi, L. Perregrini, and A. Gharsallah, "Increasing the Bandwidth of Cavity-Backed SIW Antennas by Using Stacked Cavities," *International Journal of Microwave and Wireless Technologies*, Vol. 10, No. 8, pp. 942-947, Oct. 2018.

[8] Y. Zhou, Y. M. Huang, H. Jin, S. Ding, D. Xu, L. Silvestri, M. Bozzi, and L. Perregrini, "Slow-Wave Half-Mode Substrate Integrated Waveguide 3dB Wilkinson Power Divider/Combiner Incorporating Non-Periodic Patterning," *IEEE Microwave and Wireless Components Letters, ,* Vol. 28, No. 9, pp. 765-767, Sept. 2018.

[9] L. Silvestri, A. Ghiotto, C. Tomassoni, M. Bozzi, and L. Perregrini, "Novel partially air-filled substrate integrated waveguide filters", *Submitted to IEEE Transactions on Microwave Theory and Techniques*

[10] C. Tomassoni, L. Silvestri, M. Bozzi, L. Perregrini, "A new class of Pseudo-elliptic SIW filters based on mushroom-shaped resonators", *Submitted to IEEE Transactions on Microwave Theory and Techniques.*

INTERNATIONAL CONFERENCES

[1] S. Moscato, N. Delmonte, L. Silvestri, M. Bozzi, and L. Perregrini, "Half-Mode Versus Folded SIW Filters: Modeling and Design," *IEEE MTT-S International Conference on Numerical Electromagnetic and Multiphysics Modeling and Optimization (NEMO2015),* Ottawa, Canada, Aug. 11-14, 2015.

[2] M. Pasian, L. Silvestri, M. Bozzi, L. Perregrini, and K.K. Samanta, "E-plane 3-dB Power Divider/Combiner in Substrate Integrated Waveguide Technology," *45th European Microwave Conference (EuMC2015)*, Paris, France, Sept. 7–10, 2015.

[3] C. Tomassoni, L. Silvestri, M. Bozzi, and L. Perregrini, "Quasi-Elliptic SIW Band-Pass Filter Based on Mushroom-Shaped Resonators," *45th European Microwave Conference (EuMC2015)*, Paris, France, Sept. 7–10, 2015.

[4] S. Moscato, N. Delmonte, L. Silvestri, M. Pasian, M. Bozzi, and L. Perregrini, "Compact Substrate Integrated Waveguide (SIW) Components on Paper Substrate," *45th European Microwave Conference (EuMC2015)*, Paris, France, Sept. 7–10, 2015.

[5] M. Virili, L. Roselli, F. Alimenti, P. Mezzanotte, S. Moscato, L. Silvestri, M. Bozzi, and L. Perregrini, "GRETA Approach Towards New Green Material Technologies," *EURASIP RFID 2015 Workshop*, Rosenheim, Germany, Oct. 22-23, 2015

[6] C. Tomassoni, L. Silvestri, M. Bozzi, and L. Perregrini, "Novel Substrate Integrated Waveguide Filter Based on Mushroom Resonators," *15th Mediterranean Microwave Symposium (MMS2015)*, Lecce, Italy, Nov. 30-Dec. 2, 2015.

[7] M. Bozzi, S Moscato, L. Silvestri, N. Delmonte, M. Pasian, and L. Perregrini, "Innovative SIW Components on Paper, Textile, and 3D-Printed Substrates for the Internet of Things," *2015 Asia-Pacific Microwave Conference (APMC2015)*, Nanjing, China, Dec. 6–9, 2015 (invited paper).

[8] S. Moscato, L. Silvestri, N. Delmonte, M. Pasian, M. Bozzi, and L. Perregrini, "SIW Components for the Internet of Things: Novel Topologies, Materials, and Manufacturing Techniques," *2016 IEEE Topical Conference on Wireless Sensors and Sensor Networks (WiSNet2016)*, Austin, TX, USA, Jan. 24–27, 2016 (invited paper).

[9] S. Moscato, L. Silvestri, N. Delmonte, M. Bozzi, L. Perregrini, and C. Tomassoni, "Compact Filter Solutions in Substrate Integrated Waveguide (SIW) Technology," *2016 IEEE International Workshop on Electromagnetics: Applications (iWEM2016)*, Nanjing, China, May 16-18, 2016 (invited paper).

[10] M. Bozzi, S. Moscato, L. Silvestri, E. Massoni, N. Delmonte, G.M. Rocco, M. Pasian, L. Perregrini, and C. Tomassoni, "Novel Materials and Fabrication Technologies for SIW Components for the Internet of Things," *2016 IEEE International Workshop on Electromagnetics: Applications (iWEM2016)*, Nanjing, China, May 16-18, 2016 (invited paper).

[11] E. Massoni, L. Silvestri, M. Bozzi, L. Perregrini, G. Alaimo, S. Marconi, and F. Auricchio, "Characterization of 3D-Printed Dielectric Substrates with Different Infill for Microwave Applications," *IEEE MTT-S International Microwave Workshop Series on Advanced Materials and Processes for RF and THz Applications (IMWS-AMP 2016)*, Chengdu, China, July 20-22, 2016.

[12] L. Silvestri, E. Massoni, C. Tomassoni, A. Coves, M. Bozzi, L. Perregrini, "Modeling and Implementation of Perforated SIW Filters," *IEEE MTT-S International Conference on Numerical Electromagnetic and Multiphysics Modeling and Optimization (NEMO2016)*, Beijing, China, July 27-29, 2016.

[13] D. Montanari, L. Silvestri, M Bozzi, and D. Manstretta, "Antenna Coupling and Self-Interference Cancellation Bandwidth in SAW-less Diversity Receivers," *46th European Microwave Conference (EuMC2016)*, London, UK, Oct. 3–7, 2016.

[14] L. Silvestri, E. Massoni, C. Tomassoni, A. Coves, M. Bozzi, and L. Perregrini, "A New Class of SIW Filters Based on Periodically Perforated Dielectric Substrate," *46th European Microwave Conference (EuMC2016)*, London, UK, Oct. 3–7, 2016.

[15] C. Tomassoni, L. Silvestri, A. Ghiotto, M. Bozzi, and L. Perregrini, "A Novel Filter Based on a Dual-Mode Air-Filled Substrate Integrated Waveguide Cavity Resonator," *2017 IEEE MTT-S International Conference on Numerical Electromagnetic and Multiphysics Modeling and Optimization for RF, Microwave, and Terahertz Applications (NEMO2017)*, Sevilla, Spain, May 17-19, 2017.

[16] S. Di Meo, E. Massoni, L. Silvestri, J. Obbad, M. Pasian, D. Dondi, M. Bozzi, L. Perregrini, G. Alaimo, S. Marconi, and F. Auricchio, "Dielectric Characterization of Material for 3D-printed Breast Phantoms up to 50 GHz: Preliminary Experimental Results," *IEEE MTT-S International Microwave Workshop Series-Advanced Materials and Processes (IMWS-AMP 2017)*, Pavia, Italy, 20-22 Sept. 2017.

[17] C. Tomassoni, L. Silvestri, M. Bozzi, L. Perregrini, and A. Ghiotto, "A Dual-Mode Quasi-Elliptic Filter in Air-Filled Substrate Integrated Waveguide Technology," *47th European Microwave Conference (EuMC2017)*, Nuremberg, Germany, Oct. 8–13, 2017.

[18] M. Bozzi, N. Delmonte, L. Silvestri, C. Tomassoni, and L. Perregrini, "Compact Cavity Resonators in Substrate Integrated Waveguide (SIW) Technology for RFID Applications," *Progress In Electromagnetics Research Symposium (PIERS 2017)*, Singapore, Singapore, 19-22 Nov. 2017 (invited paper).

[19] Y. Zhou, Y. M. Huang, H. Jin, D. Xu, S. Ding, L. Silvestri, M. Bozzi, and L. Perregrini, "Effective Extracting Method for Electromagnetic Parameters of Periodically Loaded Substrate Integrated Waveguide Units," *2018 IEEE MTT-S International Microwave Symposium (IMS2018)*, Philadelphia, PA, USA, 10-15 June 2018.

NATIONAL CONFERENCES

[1] L. Silvestri, E. Massoni, M. Bozzi, L. Perregrini, C. Tomassoni, and A. Coves, "SIW Filters Based on Perforated Dielectric Substrate," *XXI Riunione Nazionale di Elettromagnetismo (XXI RiNEm)*, Parma, Italy, Sept. 12-14, 2016.

[2] E. Massoni, L. Silvestri, S. Moscato, M. Pasian, M. Bozzi, L. Perregrini, "Additive Manufacturing of Substrate Integrated Waveguide Components," *XXI Riunione Nazionale di Elettromagnetismo (XXI RiNEm)*, Parma, Italy, Sept. 12-14, 2016.

[3] L. Silvestri, E. Massoni, C. Tomassoni, A. Coves, M. Bozzi, and L. Perregrini, "Substrate Integrated Waveguide Filters Based on Periodic Perforations of the Dielectric Layer", *XII Iberian Meeting on Computational Electromagnetics (EIEC2018)*, Coimbra, Portugal, 15-18 May 2018.

[4] E. Massoni, L. Silvestri, G. Alaimo, S. Marconi, M. Bozzi, L. Perregrini, and F. Auricchio, "Additive Manufacturing of a Substrate Integrated Slab Waveguide for Single-Mode Bandwidth Enhancement," *XXII Riunione Nazionale di Elettromagnetismo (XXII RINEM)*, Cagliari, Italy, Sept. 3-6, 2018.

[5] C. Tomassoni, L. Silvestri, M. Bozzi, L. Perregrini, and A. Ghiotto, "Novel Class of Dual-Mode Air Filled SIW Filters," *XXII Riunione Nazionale di Elettromagnetismo (XXII RINEM)*, Cagliari, Italy, Sept. 3-6, 2018.

AWARDS

[1] Best Paper Award at 15th Mediterranean Microwave Symposium (*MMS 2015*)

C. Tomassoni, L. Silvestri, M. Bozzi, and L. Perregrini, "Novel Substrate Integrated Waveguide Filter Based on Mushroom Resonators," *15th Mediterranean Microwave Symposium (MMS2015)*, Lecce, Italy, Nov. 30-Dec. 2, 2015.